# Diagnostics of Rotor and Stator Problems in Industrial Induction Motors

by

**Fang Duan**

B.E. (Telecommunication Engineering),
Southwest Jiaotong University, China, 2005

Thesis submitted for the degree of

**Masters of Engineering Science**

in

School of Electrical and Electronic Engineering
The University of Adelaide, Australia

August 2010


ADELAIDE
UNIVERSITY
AUSTRALIA

# Contents

# Abstract

In this project, two kinds of induction motor faults, stator short circuit fault and broken rotor bar fault, are investigated by using motor current signature analysis (MCSA) and zero crossing time (ZCT) method. These methods are based on the detection of sidebands around the supply frequency in the stator current signal.

The thesis starts by a review of these two common faults and two commonly used diagnostic methods. Before the motor stator short circuit faults experiments, baseline analysis is carried out on two same types of healthy motors. Meanwhile, signal processing programs, composed in MATLAB and LABVIEW, are verified to ensure the accurate diagnosis of motor faults. Through a control box, artificial turn to turn fault and phase to phase fault are structured in each test. MCSA and ZCT are utilized to extract broken rotor bar information from recorded stator current signal.

Although an induction motor is highly symmetrical, it may still have a detectable signal component at the fault frequencies due to imperfect manufacture, improper motor installation and so on. The misalignment experiments reveal that improper motor installation could lead to an unexpected frequency peak, which will affect motor fault diagnosis. Furthermore, manufacture tolerance and working environment could also result in disturbing the motor fault diagnosis.

Through both online and offline experiments, MCSA and ZCT methods could detect particular abnormal harmonics related to stator short circuit fault and broken rotor bar fault. Compared with the conventional MCSA method, the ZCT method has the advantage of reduced computational burden.

# Statement of Originality

This work contains no material that has been accepted for the award of any other degree or diploma in any university or other tertiary institution and, to the best of my knowledge and belief, contains no material previously published or written by another person, except where due reference has been made in the text.

I give consent to this copy of the thesis, when deposited in the University Library, being available for loan, photocopying, and dissemination through the library digital thesis collection, subject to the provisions of the Copyright Act 1968.

I also give permission for the digital version of my thesis to be made available on the web, via the University's digital research repository, the Library catalogue, the Australasian Digital Thesis Program (ADTP) and also through web search engines, unless permission has been granted by the University to restrict access for a period of time.

Signed

Date

# Acknowledgments

I would like to gratefully acknowledge my supervisor, Dr Rastko Zivanovic, whose patience and kindness, as well as his academic experience, have been invaluable to me. I also wish to express my appreciation to co-supervisor, Dr Said Al-Sarawi, for his valuable suggestions and constructive advice.

In particular many thanks go to my industrial co-supervisors, Dr Abhisek Ukil and Dr Andrea Andenna in ABB Corporate Research Center in Dättwil, Baden Switzerland for their time commitment and valuated knowledge that allowed me complete this work with the best possible results. Also, I would like to extend my thanks to the scientists and intern students at Integrated Sensor System Group in ABB for their help and support.

Last, but not least, my parents for their continues support emotionally and financially during my postgraduate years, without their support this thesis would not be possible.

# Abbreviations

| | |
|---|---|
| AI | artificial intelligence |
| BRB | broken rotor bars |
| DFT | discrete Fourier Transform |
| DSP | digital signal processor |
| FFT | fast Fourier Transform |
| FT | Fourier Transform |
| ICA | Independent component analysis |
| LV | low voltage |
| MCSA | motor current signature analysis |
| MMF | magnetic motive force |
| PCA | Principal component analysis |
| RPS | reconstructed phase space |
| ZCT | zero crossing times |

# Symbols

| | |
|---|---|
| $f_0$ | fundamental frequency |
| $f_{comp}$ | component frequency |
| $f_r$ | rotor frequency |
| $f_s$ | supply frequency |
| $f_{short}$ | the frequency component that is related to the short circuit |
| $I_p$ | currents in the primary |
| $I_s$ | currents in the secondary |
| $n_p$ | number of turns in the primary |
| $n_s$ | number of turns in the secondary |
| $N$ | number of samples |
| $p$ | number of pole |
| $P$ | number of pole pairs |
| $s$ | slip |
| $S_r$ | rotor speed |
| $T(n)$ | the time when the current is equal to zero |
| $T_{ZC}$ | ZCT signal |
| $\omega_e$ | angular speed of the stator magnetic motive force in electrical radians per second |
| $\omega_r$ | the angular frequency of rotation of the rotor shaft |
| $\omega_{rm}$ | rotor rotating speed |
| $\omega_{sm}$ | the synchronous speed in mechanical radians |

# Publications

## Referred Conference Publications (Full Paper)

[1] F. Duan and R. Zivanovic, "Estimation of DC Offset Parameters based on Global Optimization," *AUPEC'08 - 18th Australasian Universities Power Engineering Conference*, Sydney, Australia, December 14–17 2008.

[2] F. Duan and R. Zivanovic, "Induction motor fault diagnostics using global optimization algorithm," *AUPEC'09 - 19th Australasian Universities Power Engineering Conference: Sustainable Energy Technologies and Systems*, Adelaide, Australia, September 27–30 2009.

# List of Figures

# List of Tables

# Chapter 1

# Introduction

THIS chapter presents background knowledge of three-phase induction motors. Also review two types of common faults that are related to diagnostic methods. There types are broken rotor bar and stator short circuit fault. In addition, the objectives of the research project are summarized in the chapter.

## 1.1 Introduction

Induction motors, also named asynchronous motor, are widely used in manufacturing, transportation, petrochemical, mining, power systems and so on due to their reliability and simplicity of construction, high overload capability and high efficiency. The range size of induction motors are from tiny to over 100,000 horsepower. Compared with direct-current motors, induction motors are more rugged, less expensive and require less maintenance. Therefore, they are the preferred choice for industrial motors.

The induction motors were invented by Nikola Tesla in 1888. Their rotating parts do not require connecting electricity because electromagnetic induction will provide the transfer of energy from stationary parts to the rotating rotating counterpart. The stationary winding named stator can produce a rotating magnetic field, which induces an alternating electromotive force and current in the rotor. The induced rotor-current and the rotating field of the stationary winding interact and produce a motor torque. The characteristic of induction motor torque-speed is related to the resistance and reactance of the rotor. Therefore, with different ratios of rotor resistance to rotor reactance in rotor circuits, it is possible to achieve different torque-speed characteristics [1].

## 1.2 Construction of Three-phase Induction Machines

For three phase induction machines, the stator consists of three wire coils fixed inside a metal frame and spaced 120 electrical degrees apart. The end shields and terminal box are mounted onto the metal frame in order to bolt the frame and for making connections to the power cable. The center of the end shields are the bearing and it can support the shaft of the rotor. The magnetic core of the stator, that accommodates the three distributed stator windings, is formed by stacking thin electrical steel laminations with uniformly spaced slots stamped in the inner circumference [1]. For example, the steel lamination is about 0.5 mm thick for 60 Hz machines. The stator windings are composed by connecting copper or aluminum conductor coils. The coils are insulated from the slot walls. The axes of the stator windings of a P-pole machine are spaced $(2/P)(2\pi/3)$ mechanical radians apart, with each phase belt occupying the same number of slots. The terminals of the three stator phase windings can be wye ($Y$)

or delta-connected (Δ) [2].

The rotor consists of a cylindrical laminated iron core with uniformly spaced peripheral slots for accommodating the rotor winding. The rotor windings of a three-phase induction machine can take two types: wound and squirrel-cage rotor [1]. For a wound rotor machine, rotor windings are wound on a cylindrical laminated core with uniformly spaced slots on the outer periphery and they are similar as the distributed windings on the stator. The terminals of the rotor windings can be brought out via slip rings and brushes. The slip rings are insulated from the shaft and others. In order to acquire higher starting torque or limited control of speed under synchronous speed, the terminals of the rotor windings can be connected to varying external resistance through slip rings and brushes.

NOTE:
This figure is included on page 3 of the print copy of the thesis held in the University of Adelaide Library.

**Figure 1.1.** Squirrel cage motor and rotor winding.
*(Ref: http://www.ieee-kc.org/library/motors/motorslip.htm)*

Figure 1.1 shows the features of a squirrel-cage motor and the rotor winding. The motor consists of copper or aluminum axial bars with uniform spaces that are soldered onto end short-circuit rings at both ends. The rotor core consists of an iron laminations mold with molten aluminum. There is no insulation between the iron and the conductors, and none is needed. In addition, the current, which is induced in the rotor, is

contained within the circuit formed by the conductors and end-ring, also called end-connections. Skewing the rotor slots can help avoid crawling and reduces vibration [2]. Due to simplicity of construction, high overload capability, high efficiency, low maintenance expense and low cost, the squirrel cage motor is widely used in industry.

The transfer of energy from the stator to the rotor, either squirrel cage or wound rotor, is by means of electromagnetic induction. The stator is often referred to as the primary and the rotor as the secondary. Energy is transferred electromagnetically across the air gap between the stator and the rotor windings. A small air gap can help to reduce reluctance. However, the width of the air gap is constrained by allowable core losses as well as manufacturing tolerances and costs. The air gap is typically between 0.35 to 0.50 mm for motors up to 10kW, and between 0.5 to 0.8 mm for motor in the range of 10 to 100 kW [1].

### 1.2.1 Types of Stator Winding Construction

There are two basic types of stator winding structures namely random-wound stators and form-wound stators using multi-turn coils and form-wound stators using Roebel bars. The random-wound stators are usually utilized for no more than several hundred kW of machines. Furthermore, the form-wound stators are used for larger motors and some generators rated up to between 50 MVA and 100MVA. Roebel bar windings are usually used for large generators [3].

**Random-wound Stators**

Random-wound stators are comprised of insulated copper conductors, winding wire or magnet wire, which is round and the wound is continuously through slots in the stator core to form a coil by a winding machine or by hand [1]. In inserting random-wound coils, each turn or loop of winding wire could be placed against any other turn and independent of the voltage level of the turn, as shown in the Figure 1.2. Thus, the windings are called ”random”. During stator winding, the coils are separated using an insulating material that is positioned to clear the inside diameter of the stator. Random windings are used on lower kW machines.

**Form-wound Stator**

NOTE:
This figure is included on page 5 of the print copy of
the thesis held in the University of Adelaide Library.

**Figure 1.2.** Random-wound stator.
*(Ref: http://www.schulzelectric.com/)*

Form-wound stators windings usually consist of an insulated coil that have been pre-formed, such as square or rectangular magnet wire, before they are put in the slots, as shown in the Figure 1.3. The coil winding process begins with looping of the magnet wire. Due to the difficulty of forming wire of high width-to-thickness ratio, several wires in parallel may make one turn [3]. Through careful design and manufacturing process, an individual turn in a coil is arranged in precise location and adjacent to another turn with the smallest possible voltage difference. Usually, each coil includes from two to twelve turns. The insulation of the wire is designed to handle operating turn-to-turn voltages as well as maximum surge or impulse voltages. They are usually operated at 1000V.

### 1.2.2 Stator Winding Insulation System Features

The stator winding insulation system plays an important role in induction motors. A well designed stator winding insulation system can prevent the electrical short [3]. There are several components and features in a stator winding insulation system, such as strand (or subconductor) insulation, turn insulation and groundwall (or ground or earth) insulation. Figures 1.4 and 1.5 show a cross section of a random wound and form-wound coils in a stator slot. The figures illustrate the location of the insulation

NOTE:
This figure is included on page 6 of the print copy of
the thesis held in the University of Adelaide Library.

**Figure 1.3.** Form-wound stator.
*(Ref: http://www.schulzelectric.com/)*

components in the different motors. For example, the turn insulation is used for preventing shorts among the turns in a coil. When a turn short circuit happens, the shorted turn will appear as the secondary winding of an autotransformer [3]. The transformer law is explained as

$$n_p I_p = n_s I_s \tag{1.1}$$

where $n_p$ and $n_s$ are number of turns in the primary and secondary, respectively, $I_p$ and $I_s$ are the currents in the primary and secondary, respectively. Therefore, the overheating will appear when a big value of current flow appears in the shorted turn that will affect the insulation life of other healthy turns and stator winding.

The electrical insulation material decides the lifetime of insulation. For different purposes of insulation in electric equipment, there are several designs and combinations to perform designed functions. The definitions of the thermal identification and classification of insulating materials and insulation system are published by IEEE and IEC [3]. Table 1.1 shows the accepted temperature indices of materials according to IEC 60085. The motors used in the thesis belong to the class F.

NOTE:
This figure is included on page 7 of the print copy of
the thesis held in the University of Adelaide Library.

**Figure 1.4.** Cross section of a random stator winding slot [3].

NOTE:
This figure is included on page 7 of the print copy of
the thesis held in the University of Adelaide Library.

**Figure 1.5.** Cross section of a form-wound stator winding slot [3].

**Table 1.1.** Thermal classification of rotating machine insulation material.

| Numerical Classification | Letter Classification | Temperature (°C) |
|---|---|---|
| 105 | A | 105 |
| 130 | B | 130 |
| 155 | F | 155 |
| 180 | H | 180 |

## 1.3 On-line Motor Condition Monitoring

On-line motor condition monitoring detects and monitors the operating characteristics of a motor while it is running. The major advantage of on-line condition monitoring is that the device's potential problems could be detected early before a serious deterioration or breakdown occurs. Taking petrochemical plants as an example, Figure 1.6 illustrates that mechanical fault is a major part of the various faults [4]. Thus, increasing research has been developed in on-line condition monitoring techniques for mechanical equipment, especially electrical devices, such as induction motors, generators and transformers in power plants.



**Figure 1.6.** Major causes of 100 large accidents in petrochemical plants [4].

An on-line condition monitoring system includes four main parts, which are sensors, data acquisition, fault detection, and fault diagnosis [5]. A typical on-line condition monitoring system process is shown in Figure 1.7.

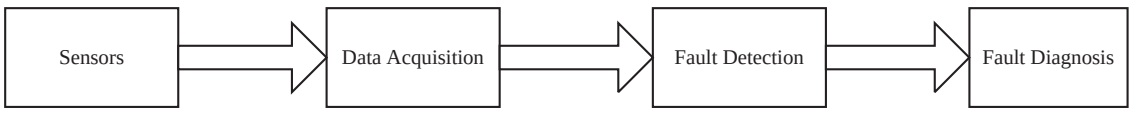


**Figure 1.7.** The on-line condition monitoring process.

Sensors measure physical quantities of the device and convert them into an electrical response to time and to be read by an oscilloscope or other measuring instruments. There are many types of sensors that are utilized in on-line condition monitoring, for example, current sensors, Hall Effect sensors, voltage sensors, flux sensors, vibration sensors, speed sensors and temperature sensors. The selection of a specific sensor type depends on the method of monitoring. The common used monitoring methods are voltage, current, temperature, deviation of magnetic potential vector and asymmetrical magnetic flux distribution, gyration radius, torque and speed fluctuation and so on.

The function of data acquisition is sampling and amplifying the physical signal data acquired from the sensors. Then, the data is converted into feature values that reflect the device's operating condition. A data acquisition system includes three main components, which are physical parameters to electrical signal converter, a signal conditioning circuit and analog to digital signal converter.

The purpose of fault detection is finding out the incipient fault appearing in the machine through processing the acquired data. The signal data which is sensitive of the machine fault is extracted and used for further analysis. The fault detection system includes two different methods, named model-referenced method and feature extraction [5]. The model-referenced method is based on mathematical simulation models or artificial intelligence to compare and analyze measurement results. The feature extraction method extracts information from the processed signal data, such as exceeded thresholds, amplitudes and frequency, and decides whether the machine's operating state is faulty or healthy.

The common machine faults can be broadly divided into two types, stator faults and rotor faults. Figure 1.8 illustrates the faults and related elements [6]. The diagnosis results can clearly indicate the direction of maintenance.

## 1.4 Literature Review of Motor Faults

Motor faults may have only minor symptoms but result in lower efficiency and hence higher energy consumption, poorer performance and long term degradation. Even

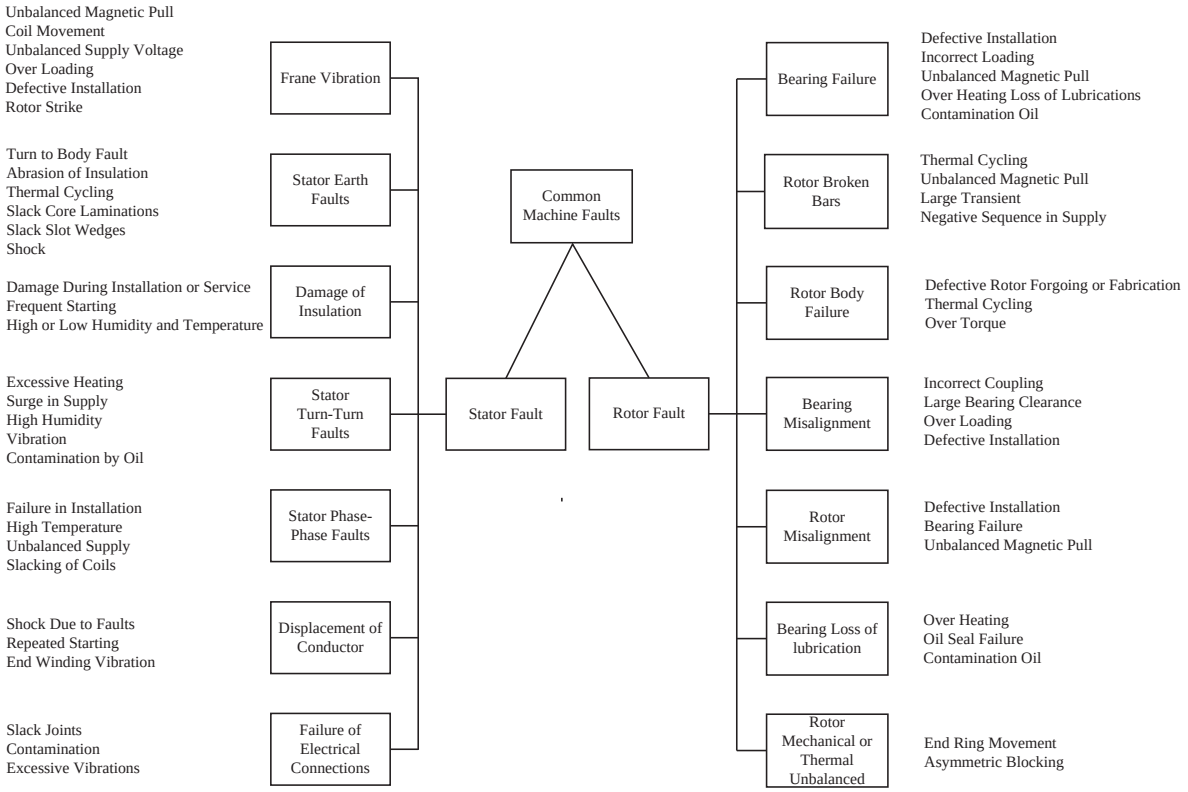


**Figure 1.8.** Motor faults diagram [6].

small faults can cause increased losses such as reducing efficiency, increasing temperature, which will reduce insulation lifetime, and increasing vibration, which may reduce bearing lifetime [7]. They are caused by the operating environment condition and the machines internal factors. Therefore, the diagnosis of induction motor problems is important and prevent expensive maintenance cost. According to published surveys, induction motor failures include bearing related faults (which are responsible for 40% of all faults), short circuits in stator windings (which represent 38% of the reported faults), rotor related faults (which represent 10% of the induction motor faults) and other faults such as end ring faults (which occupy 12% of the reported faults) [8].

Numerous methods of induction motor fault diagnosis were developed in the last decades and many techniques have been proposed [9,10]. The most common approach is motor current signature analysis (MCSA) [11]. Several of induction motor faults detection and identification techniques are based on Fast Fourier Transform spectral signature analysis [12–14]. Other techniques include vibration analysis, temperature measurements, harmonic analysis of speed fluctuations [15,16], vibration monitoring [17],

state and parameters estimation [18], either axial flux or air-gap torque analysis [19], acoustic noise measurement, and magnetic field analysis [20–23]. Currently, more and more new techniques based on artificial intelligence (AI) have been utilized for diagnostic induction motor faults, such as fuzzy logic [24, 25], genetic algorithms [22, 26], neural network [27], Bayesian classifiers [28], and envelope of the three-phase stator current with AI based on Gaussian mixture models and reconstructed phase spaces (RPSs) [29].

The methods used to diagnose broken bars can be broadly categorized into two types, invasive and non-invasive fault diagnosis techniques [30]. The invasive methods diagnose broken bars by monitoring the deviation of the magnetic potential vector and asymmetrical magnetic flux distribution, gyration radius, asymmetrical magnetic flux distribution, torque and speed fluctuation and so on. In these methods, sensors and costly measurement equipments are needed, which will increase the complexity and expense of the diagnostic method. Thus, in this literature review we are only concern with non-invasive fault diagnosis techniques.

### 1.4.1 Broken Rotor Bar Faults

K. R. Cho proposed the use of state and parameter estimation for diagnosing broken rotor bars in induction motors in 1989 [18]. This detection method is based on the hypothesis that rotor resistance of an induction motor will increase when a rotor broken bar occurs. In Cho's experiments, the induction motor working condition is that the apparent rotor resistance should be in the balanced single-phase electrical model when motor operates at constant velocity. During the detection process, the stator voltage, current, excitation frequency, and rotor velocity are measured, which are taken over a small range of velocity. The near-least-square-error estimator was used for the measurements in order to estimate motor states and parameters.

In 2001, Thomson and Fenger diagnosed induction motor faults by using current signature analysis [31]. The authors used a current transformer to measure stator current and a sensor to collect the transformed signal. Then, the signal is transformed to the frequency domain for spectral analysis by using a signal processing box with Discrete Fourier Transform (DFT), low-pass filter and analogue/digital converter. The stator

current spectrum showed abnormal harmonics, which were related to induction motor faults. However, the load of the machine is dynamic, which may lead to changes in current signal frequency. If the frequency is very close to the fundamental frequency, the broken bar fault can not be detected exactly. Therefore, the application of some algorithms to process the spectral signal is required.

In order to overcome the limitations, Çalış and Çaklır in 2007 [32] applied the zero crossing times (ZCT) technique to diagnose the rotor's broken bars. This method only requires the use of a current sensor, which has already been installed in most of motors. The method diagnose broken bars by observing changes in the motor current zero crossing instants. If motor runs at constant speed under balanced supply and stator winding, the spacing between successive zero crossings is equal. The fluctuations in the motor ZCT will appear when broken bar failure occurs. Through an analysis of ZCT data, motor slip and motor status information are estimated. The results show that the method is both sensitive and low cost. The method is based on the assumption that the motor runs at constant speed under balanced supply. However, in real working environment, the conditions are not always satisfied, which may limit its application.

### 1.4.2 Stator Related Faults

In 1978, Bonnett identified that five failure modes in Wye connected stator, as

A) turn-to-turn short circuit fault

B) coil-to-coil short circuit fault

C) open circuit fault

D) phase-to-phase short circuit fault

E) phase-to-ground short circuit fault

In addition, he identified that one of these modes or any combination of them can cause a fault. The turn-to-turn fault is the initial fault, and other faults can be regarded as the

results of it. In the early stage, turn-to-turn fault does not affect motor normal operation because the voltage across the turn insulation is relatively low. However, high substantial transient voltage might cross the insulation when motor is switched on or off. Thus, the destruction of the turn insulation caused by the short circuit may cause a permanent damage. Stator faults typically have the highest rate (38%) amongst the common type of faults in industrial induction motors [31].

In the last decade, several studies of stator winding faults in synchronous and asynchronous motors are developed. The common methods include vibration monitoring, current monitoring, and axial leakage flux monitoring [33]. Recently, new techniques are presented for online motor protection and diagnostics for stator winding faults, such as integrated on-line motor protection system [34] or sensorless online motor diagnostics [35] and so on.

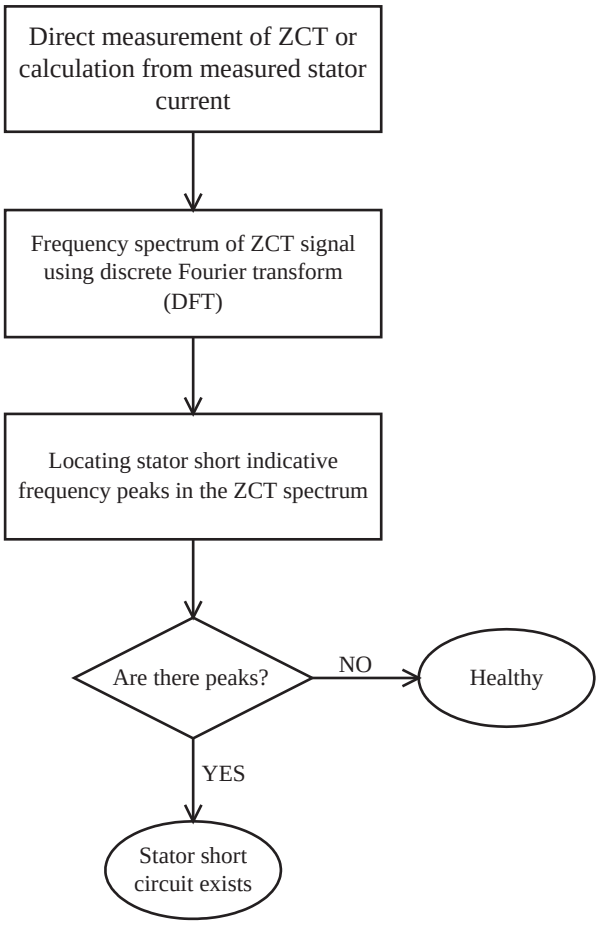


**Figure 1.9.** Flowchart of the stator short circuit detection algorithm using the ZCT signal [36].

Ukil et al. used zero crossing time (ZCT) signal of the stator current to diagnose the stator short circuit faults in 2009 [36]. The algorithm of detecting the stator short circuit is illustrated in the Figure 1.9. Firstly, ZCT signal is acquired form the the measured stator current. Then, the frequency spectrum of ZCT signal is calculated by using FFT. Through the analysis of characteristic fault frequencies, the stator short circuit faults are diagnosed. The work diagnosed stator short circuit without considering the effect of any other problem or mechanical drive characteristic.

Compared with the conventional MCSA method, the method has advantages of low computational requirements by using small numbers of data points without the need for additional sensors. In addition, ZCT can be considered an effective alternative approach for smaller embedded devices for motor fault diagnosis.

## 1.5 Research Objectives

In this thesis, the ZCT signal is acquired by both ABB intelligent sensor and calculating from the measured stator current in order to test ABB intelligent sensor. Furthermore, the motor faults are diagnosed by considering potential effects, such as, improper motor installation, manufacture tolerance and working environment.

The first aim of this project is to build up the background knowledge of induction motor fault diagnose methods and supplementary computer programs. And demonstrate if analysis techniques such as MCSA and ZCT can be used to diagnose stator short circuit faults and broken rotor bar faults. In addition, if it is possible to use such techniques for either off-line and on-line for faults identification.

In order to ensure the accurate diagnosis of motor faults, a comprehensive database of sensor measurements corresponding to a healthy motor will be developed in the baseline study. This is the second aim of this project. Although an induction motor is highly symmetrical, it may still have a detectable signal component at the fault frequencies due to manufacture tolerance, assembling tolerance, working environment

and so on. Therefore, it is important to study motor frequency spectrum characteristics and set threshold levels to distinguish between healthy and faulty motors.

Apart from manufacture defects, improper motor installation can also reduce efficiency, increase current vibration and noise. The current induced by vibration will affect the motor faults diagnosis. Therefore, the third aim is alignment measurement analysis. In the project, the Laser Alignment system, provided by Fixturlaser Company [37], is used to detect and adjust shaft misalignment. Furthermore, the effect of misalignment on motor stator short circuit fault diagnosis will be studied in the experiment.

Fourthly, based on previous work, the motor stator short circuit fault will be experimentally studied by using both off-line and on-line tests. Through a control box, artificial turn-to-turn faults and phase-to-phase faults are simulated in each test. MCSA and ZCT methods are employed to detect the abnormal harmonics in motor current signals.

Lastly, we will investigate whether MCSA and ZCT methods can be utilized to diagnose broken rotor bars fault. The recorded data is provided by the machine laboratory of the Cracow University of Technology. The data includes stator current of a symmetrical motor and motor with broken rotor bars fault.

Chapter 2

# Induction Motor Faults Diagnosis Methods

IN this chapter, motor current signature analysis (MCSA) method and the zero cross time (ZCT) method are reviewed. Compared with MCSA, ZCT has advantages of using less sampling points and reducing computational burden and storage space.

## 2.1 Introduction

Induction motor faults often generate particular frequency components in the current spectrum. The abnormal harmonics contain potential information of motor faults. Therefore, the frequency analysis approach is the most commonly used method to diagnose induction motor faults.

## 2.2 Motor Current Signature Analysis Method

Motor current signature analysis (MCSA) is one of the common methods for diagnosing motor faults due to its low cost and simplicity. The method is based on the detection of sidebands around the supply frequency in the stator current signal [11]. Firstly, the motor faults are simulated to observe the spectrum of stator currents for each fault condition. From the simulation, abnormal harmonics of stator currents are obtained as reference signals. Secondly, the recorded stator current signal is transfered from time domain to frequency domain by using Fourier Transform (FT). Finally, the motor faults could be diagnosed through the comparison of recorded stator current signals and the reference signals in the frequency domain.

In the real applications, the stator current signal is sampled at frequency $f$. So, the Discrete Fourier Transform (DFT) is utilized to transfer the data from the time domain to the frequency domain. The customary formulas exhibiting the DFT of a signal $f[n]$ and its inverse DFT are [38]

$$F(k) = \sum_{n=0}^{N-1} f[n] \exp(-i\frac{2\pi kn}{N}), \qquad k = 0, 1, 2, \cdots, N-1, \tag{2.1}$$

$$f[n] = \frac{1}{N} \sum_{k=0}^{N-1} F(k) \exp(i\frac{2\pi kn}{N}), \qquad n = 0, 1, 2, \cdots, N-1, \tag{2.2}$$

where $N$ is the number of samples of $f[n]$.

According to equation (2.1), a calculation of an $N$-point DFT requires $(N-1)^2$ multiplications and $N(N-1)$ additions, i.e. $O(N^2)$ operations. Numerous Fast Fourier transform (FFT) algorithms with $O(N \log N)$ operations, such as Cooley-Tukey FFT algorithm, Prime-factor FFT algorithm, Bruun's FFT algorithm, Rader's FFT algorithm

and Bluestein's FFT algorithm [38], are put forward to compute the FFT and its inverse. In our study, the stator current signal is transferred from the time domain to frequency domain by using FFT functions (based on Cooley-Tukey FFT algorithm) in MATLAB.

Thomson and Fenger reviewed the application of MCSA in diagnosing broken rotor bars, shorted turns in low voltage (LV) stator windings and airgap eccentricity in three-phase induction motor drives [31]. However, there are some handicaps which may degrade performance and accuracy of this fault diagnosis. The first limitation comes from the stator current sampling and FFT, for example, noisy sensor signals, finite number of samples and finite frequency interval in the FFT. Secondly, the current could be sampled only after the motor reaches steady state. In other words, the variation of the motor may result in fluctuation in stator current frequency spectrum. Last but not least, other unexpected factors could induce ambiguous harmonic frequencies, which will affect the judgment of abnormal harmonics. In light of the shortcomings of MCSA, a considerable amount of research work has been based on advanced signal-processing techniques [39, 40].

## 2.3 Zero Crossing Time (ZCT) Method

The zero crossing time (ZCT) method was firstly put forward by Wang in his PhD thesis [35]. Through monitoring successive zero crossing times, the method has been successfully applied in speed measurement and fault detection. Recently, Çalış and Çaklır [32] applied the ZCT technique to diagnose rotor broken bars. In their experiments, only a current sensor is required, which has already been installed in most of the motors. Thus, it reduced the experimental cost and complexity.

The method diagnoses broken bars by observing the changes in the motor current zero crossing instants. The ZCT signal is defined as the time interval between two successive zero crossing points of the stator current, given by [35]

$$T_{ZC}(n) = T(n) - T(n-1), \tag{2.3}$$

where $T_{ZC}$ is the ZCT signal, $T(n)$ is the time when the current sample is equal to zero. If the motor runs at constant speed under balanced supply and stator winding,

the spacing between successive zero crossings is equal. The ideal stator current of a three phase motor is plotted in the Figure 2.1. The supply frequency is 50 Hz and the sampling frequency of the current signal is 1 kHz. In a real application, it is impossible to find the time that the current is exactly equal to zero due to the discrete sampling. Thus, Fig. 2.2 illustrate the algorithm for calculating approximate zero points [36]. Assume that the current is linear in a small time interval (i.e. sampling time). At the sampling time $n-1$ and $n$, $I(n-1) \times I(n) < 0$. Based on this assumption, the following equation is given by

$$\frac{I(n)-0}{I(n)-I(n-1)} = \frac{t(n)-T(k)}{t(n)-t(n-1)}. \tag{2.4}$$

Then, the approximate time $T(k)$ can be calculated by

$$T(k) = t(n) - \frac{I(n)[t(n)-t(n-1)]}{I(n)-I(n-1)}. \tag{2.5}$$

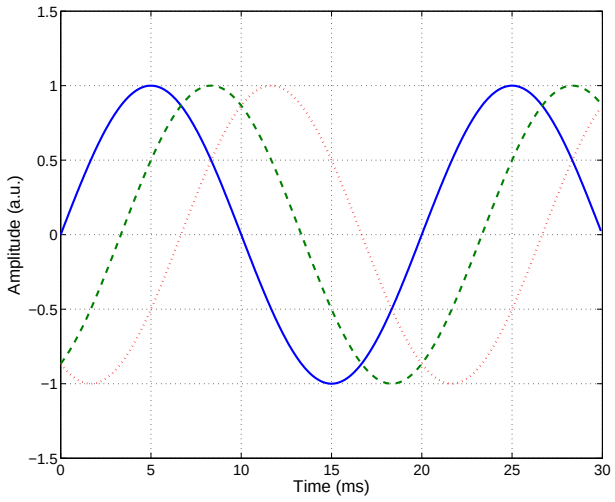


**Figure 2.1.** Ideal stator current of a three phase motor.

Rotor unbalance, such as broken bars, results in positive and negative sequence rotor currents. The positive sequence rotor current produces positive sequence emfs and positive sequence currents on the stator of angular frequency

$$\omega_r + s\omega = \omega(1-s) + s\omega = \omega. \tag{2.6}$$

On the contrary, negative sequence rotor current results in emfs and currents of frequency in the stator,

$$\omega_r - s\omega = \omega(1-s) - s\omega = (1-2s)\omega, \tag{2.7}$$

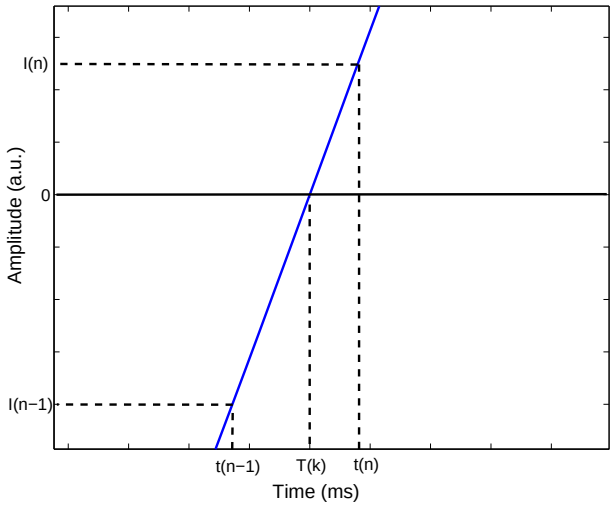


**Figure 2.2.** Method of calculating approximate zero points.

where $s$ is the slip, $\omega_r(rad/s)$ is the angular frequency of rotation of the rotor shaft [32].

The spacing between successive zero crossings is unequal when the motor runs under abnormal conditions. The spectrum of the ZCT signal contains a $2sf$ frequency component, which is influenced only by the negative sequence current in the rotor and its harmonics at $2ks\omega, k = 2, 3, ...$ as frequencies of the broken bar [32]. The amplitude of the harmonic component decreases as the value of $k$ increases. Furthermore, the amplitude of this spectral component rises when the the degree of rotor asymmetry becomes serious. The motor running condition can be inspected by monitoring the $2sf$ component in the ZCT spectrum.

In this thesis, both off-line and on-line tests are utilized to diagnose induction faults. In the off-line test, the time domain current signal is recorded by an oscilloscope. Based on equation (2.5), the ZCT signal is calculated by using MATLAB. Then, the fast Fourier transform (FFT) algorithm is employed to analyze the ZCT signal frequency components with sampling frequency 1000 Hz and window length 1024. In the on-line test, the time domain ZCT signal is acquired by an ABB Intelligent Sensor. Then, time domain and frequency domain ZCT signals are recorded and analyzed using LABVIEW.

Compared with conventional MCSA, the ZCT method uses less sampling points. For instance, if the supply frequency is 50Hz and the sampling frequency of the current signal is 1 kHz, there are 201 current sampling points in one period. On the contrary, the ZCT method gets rid of many unnecessary points. Thus, ZCT could reduce the

computational burden in the FFT. Furthermore, ZCT needs small data storage room. This advantage is obvious in portable devices, which always is limited by less powerful digital signal processors (DSPs) and limited amount of memory and storage. In addition, the ZCT method does not need high a sampling rate [36].

## 2.4 Summary

Two induction motor fault detection methods, conventional MCSA and ZCT, are described in this chapter. Although the MCSA technique is the commonly used method for diagnosing motor faults due to sensorless, low cost and simple experimental setup, there are some shorting comings that limit the application of this method. The ZCT method diagnoses motor faults by monitoring successive zero crossing times. The method uses less sampling points and hence reduces computational burden and storage space.

In our experiments, both conventional MCSA and ZCT were employed to diagnose broken rotor bar faults and stator short circuit faults. The detailed analysis of particular abnormal harmonics related to motor faults and the experimental setup are discussed in chapter 3, 4, 5 and 6.

# Chapter 3

# Baseline Analysis of Induction Motor

THE aim of this chapter is to present the baseline study for the stator short circuit fault diagnosis. The baseline data of the stator short circuit fault were acquired from the ABB Dättwill motor lab. In addition, the behaviours of baseline under different load conditions are analyzed.

## 3.1 Introduction

Baseline analysis plays an important role in the induction motor study. Through the baseline analysis, problematic characteristics of a healthy induction motor can be detected. Although an induction motor is highly symmetrical, there is likelihood of faults in the motor and in the fault diagnosis system [41]. For example, there may be a problem of motor manufacturing or motor installation. Either of them will disturb symmetry and influence the induction motor fault diagnosis. These problems will introduce various frequency components or influence the amplitude of the motor fault frequency. Consequently, determination and classification of a fault becomes difficult. Therefore, analysis of the baseline signal can find a potential fault early and ensure the condition monitoring reliability.

## 3.2 Baseline Study

In the laboratory, two new ABB motors are used and the motor parameters are tabulated in Table 3.1. There are no any artificial faults created for them. In this experiment, the device that does the ZCT signal conversion is used directly to record and analyze the spectrum of the ZCT signal from the induction motor. Although the two motors are of the same type, there are slight differences in the testing results. The rotor frequency as an example is used to illustrate the difference between the Motor I and Motor II testing results.

The rotor frequencies of two motors both with and without load were studied. In the following figures, the time domain ZCT signals are acquired directly from ZCT signal converter and the frequency domain ZCT signals are converted by using FFT in MATLAB. Figure 3.1 shows the operating behavior of motor I without load. For the the reduction of computation complexity, equation (2.3) was modified as [36]

$$T_{ZC}(n) = T(n) - T(n-1) - T_{ref}, \tag{3.1}$$

where $T_{ref}$ is the natural reference time of the ZCT signal. The Y-axis of Figure 3.1 (i) represents the difference between recorded zero crossing time and natural reference time. The rotor frequency is 24.9 Hz and the amplitude is -35.57 dB. As shown in Figure 3.2, when Motor II operates without load, the rotor frequency is 24.9 Hz and amplitude

**Table 3.1.** ABB induction motor parameters.

| Parameter | Value |
|---|---|
| Active power [kW] | 2.2 |
| Nominal voltage [V] | 380-420 |
| Nominal current [A] | 4.9 |
| Nominal frequency [Hz] | 50 |
| Nominal power factor $\cos\varphi_N$ [-] | 0.81 |
| Rotor speed [rpm] | 1430 |
| Winding connection | $Y$ |
| Number of poles per phase winding p [-] | 4 |
| Insulation Classification | $F^*$ |

is -33.09 dB. In theory, the peak values of the two motors should not have much difference in light of the same detection system and the same type of motor. However, the amplitude value of Motor I is smaller than that of Motor II. Therefore, there may be some potential problems in Motor II. Figure 3.3 and 3.4 illustrate the performance of Motor I and II with low load level, respectively. Although the two motors have the same rotor frequencies, the amplitude of Motor I is still smaller than that of Motor II. In addition, the rotor frequency of both Motor I and II decreases from 24.9 Hz to 24.46 Hz when the load increases to 80% current load level.

Motor I and Motor II operating at high load level were also tested. The two motors running under different load levels are compared in Figure 3.5 to 3.10. From these figures, we can conclude that both the rotor frequency and the amplitude of Motor I were smaller than Motor II at the same load level. The difference between the two motors is tabulated in Table 3.2. In addition, for Motors I and II, the amplitude of rotation frequency decreases when the load level increases. In all cases, the load level shown was measured as a percentage of the nominal current.

According to the rotor frequency values which were detected directly by the ABB detection system, the rotor speed $S_r$ and slip $s$ can be computed by

$$S_r = f_r \times 60, \tag{3.2}$$

$$s = (1500 - S_r)/1500, \tag{3.3}$$

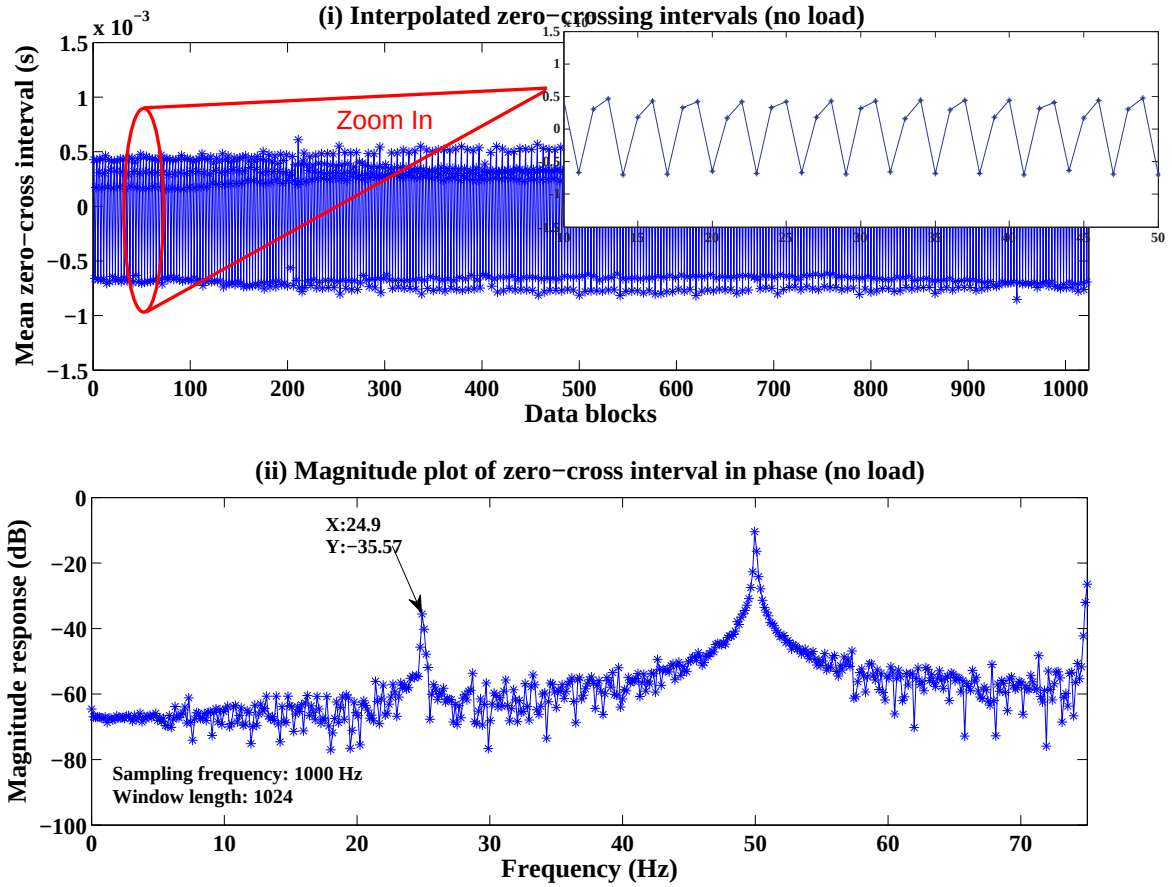


**Figure 3.1.** Healthy induction Motor I without load.

From Table 3.3, the rotor frequency of Motor I with 83.57% load is 24.47 Hz and the $S_r = 24.47 \times 60 = 1468.2\ rpm$. The motor has 4 poles and supplied by 50 Hz. Therefore, the $s = 0.0212$ and $2fs = 2.12$. Tables 3.3 and 3.4 show online testing results for Motor I and Motor II, respectively. In addition, Figures 3.11 and 3.12 illustrate the evolution of slip with the increasing current value.

The amplitude variation of rotor frequency is plotted in Figure 3.13. As the load increases to 80%, the amplitude of the two motors' rotor frequencies increases. However, the amplitudes decline sharply after a load level higher than 80%. The difference is more than 15 dB between zero load and 185% load.

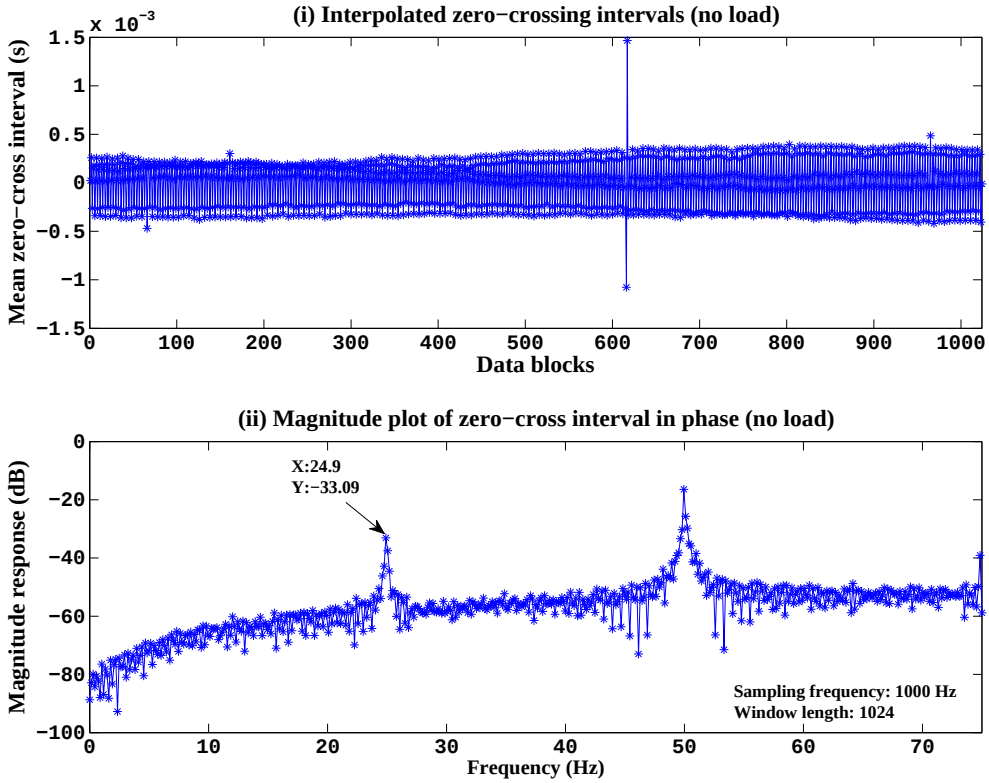


Figure 3.2. Healthy induction Motor II without load.

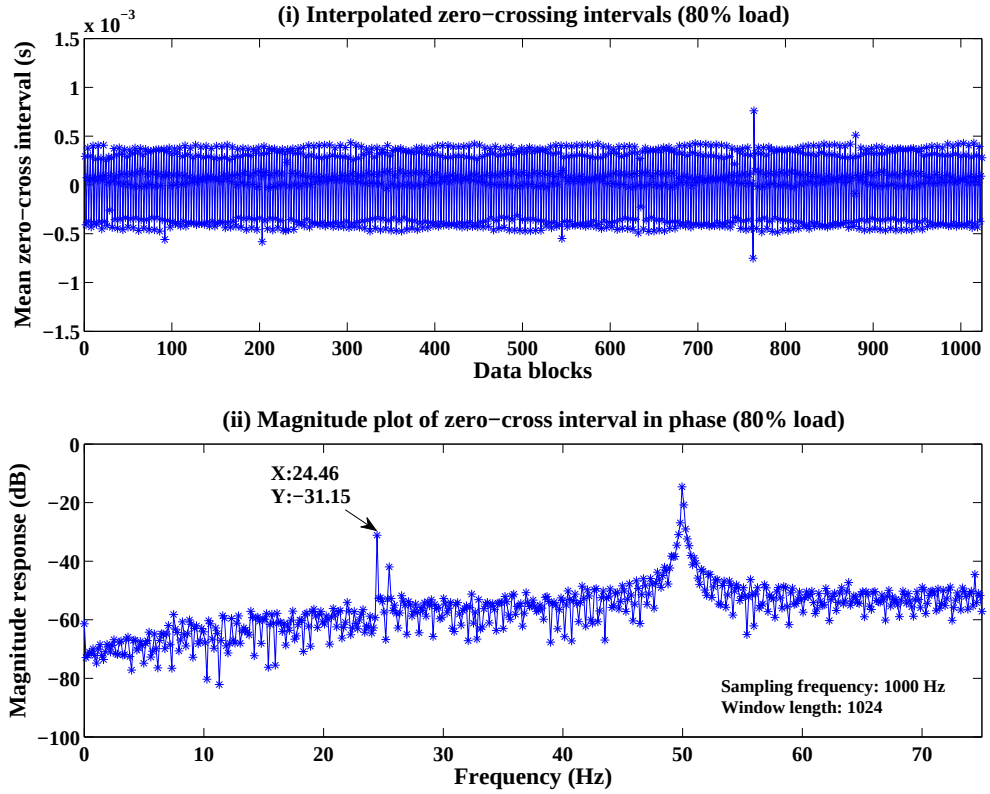


Figure 3.3. Healthy induction Motor I with 80% load.

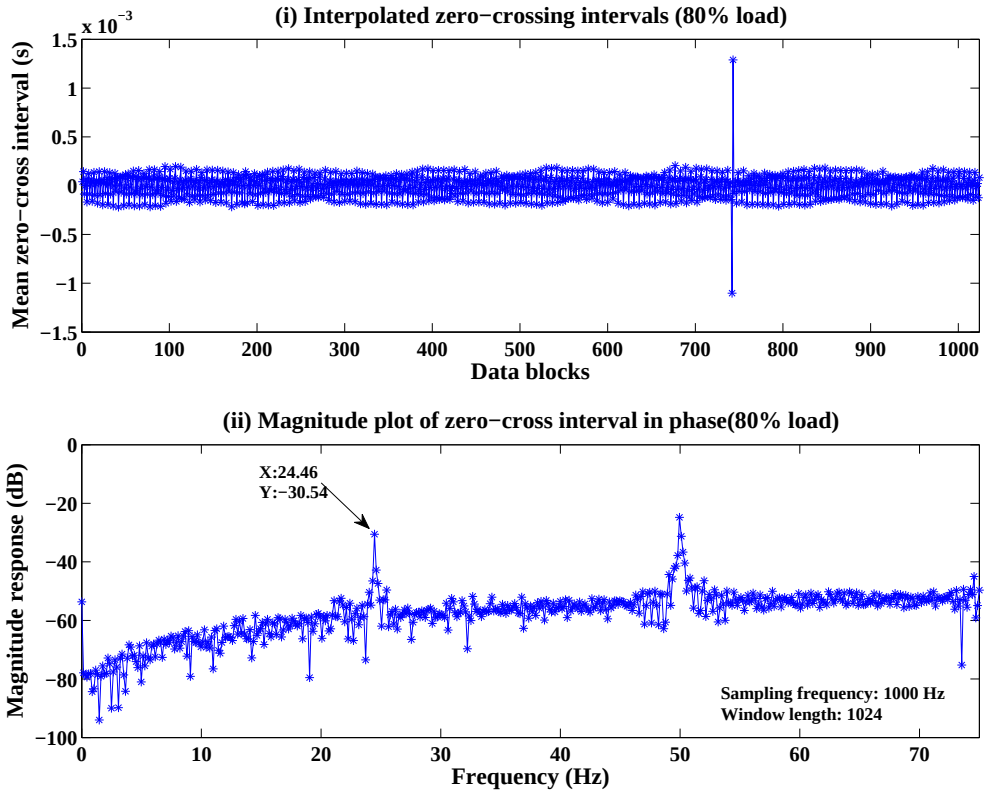


Figure 3.4. Healthy induction Motor II with 80% load.

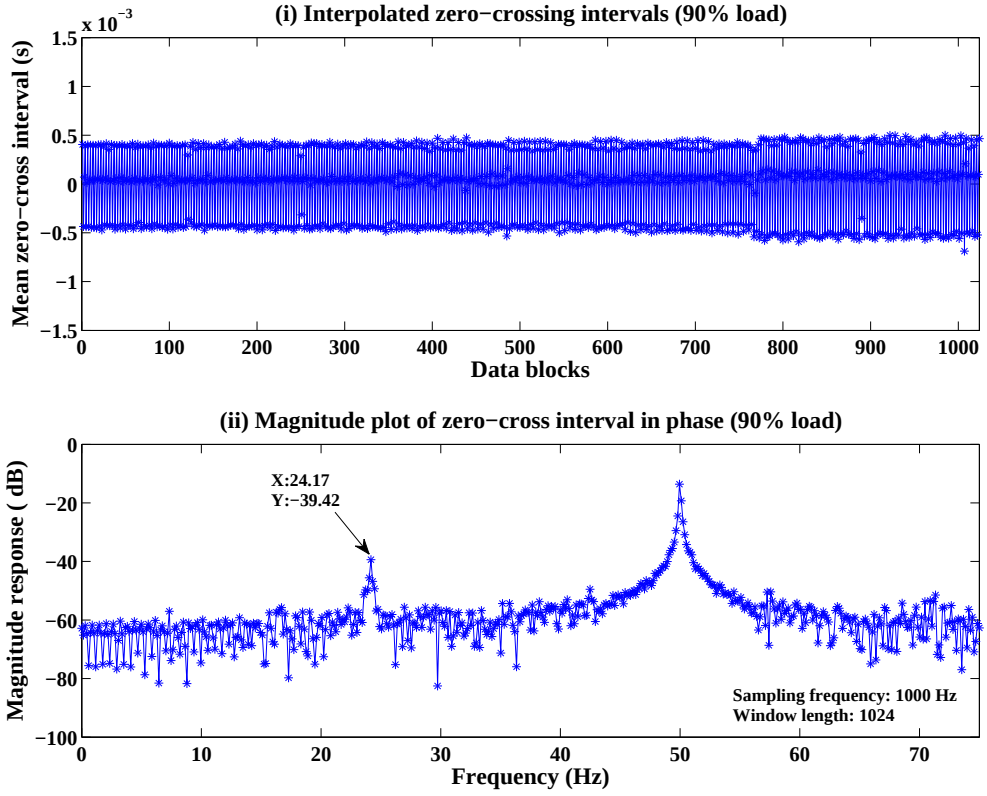


Figure 3.5. Healthy induction Motor I with 90% load.

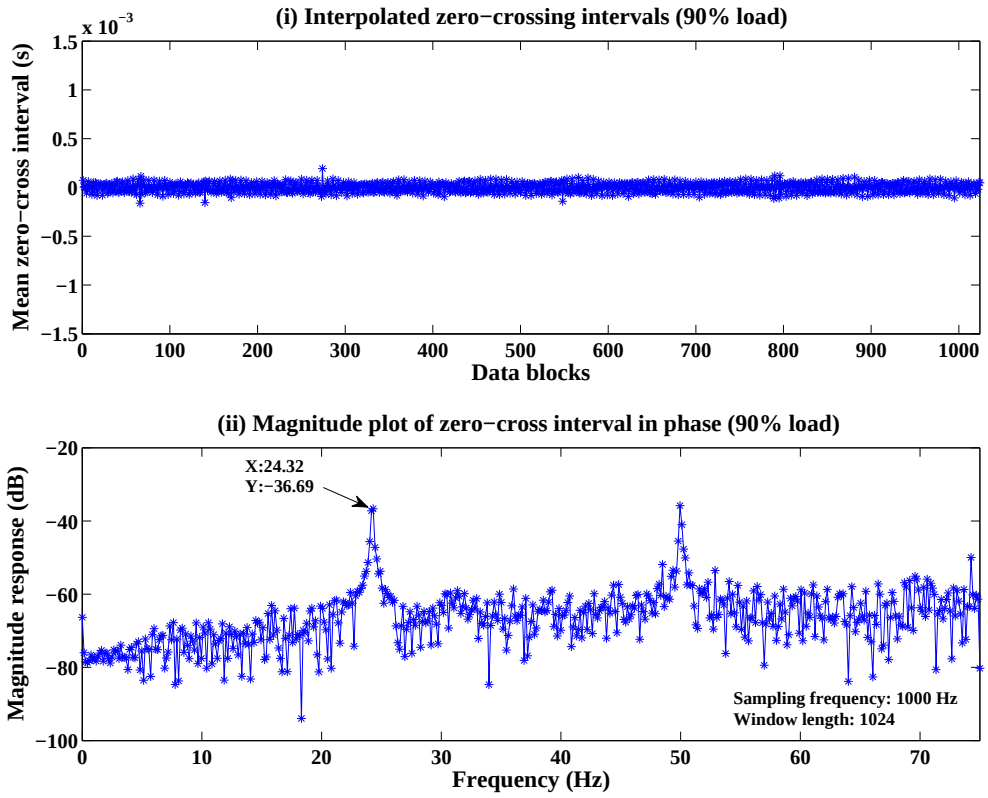


**Figure 3.6.** Healthy induction Motor II with 90% load.

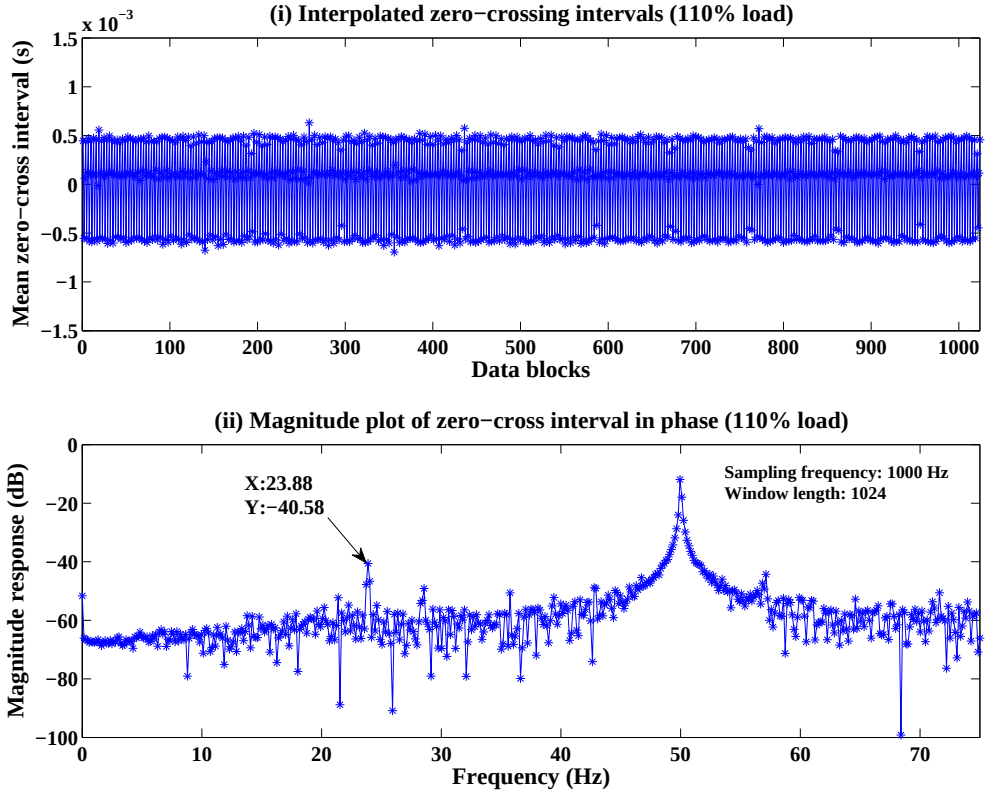


**Figure 3.7.** Healthy induction Motor I with 110% load.

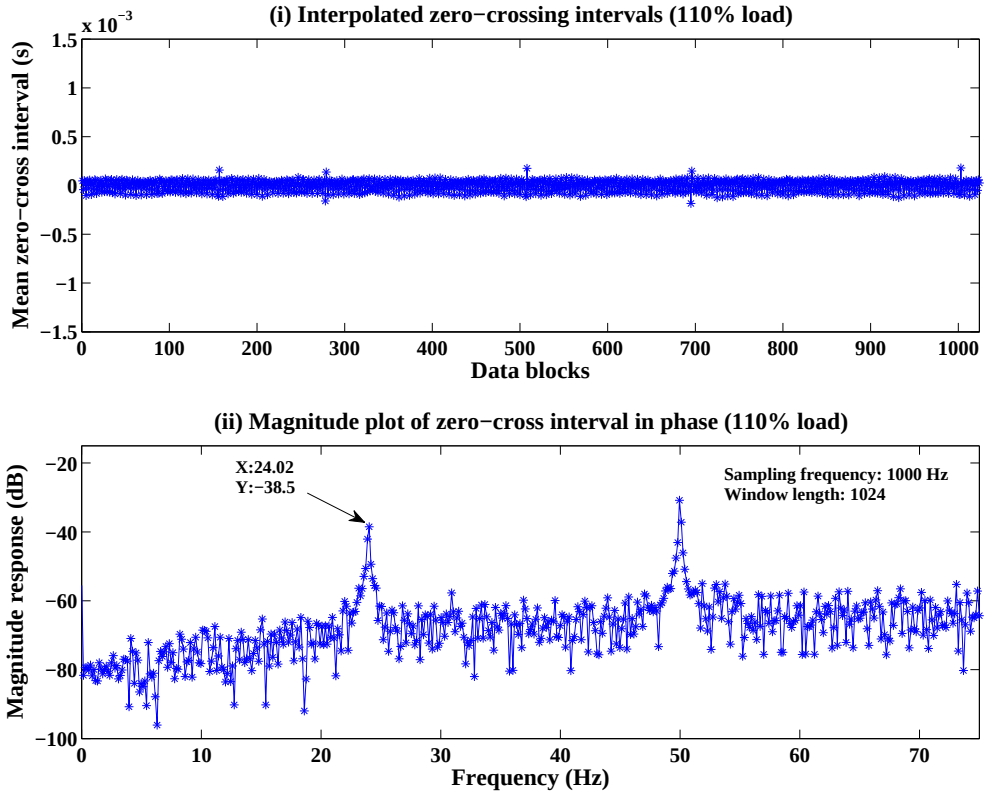


**Figure 3.8.** Healthy induction Motor II with 110% load.

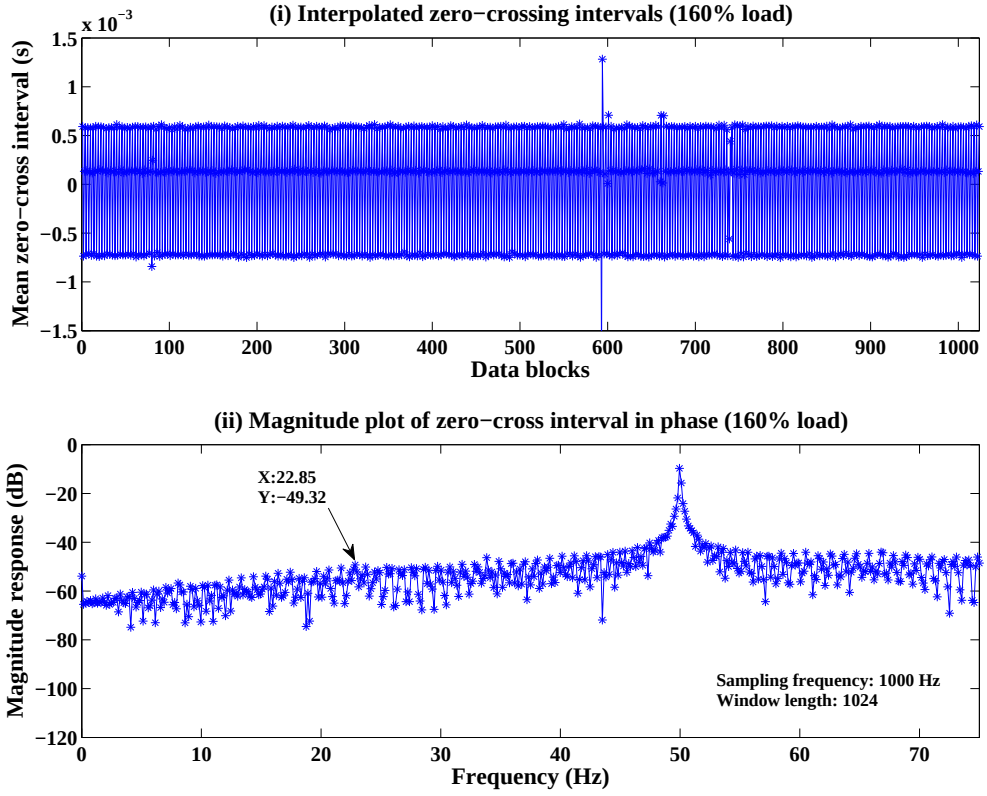


**Figure 3.9.** Healthy induction Motor I with 160% load.

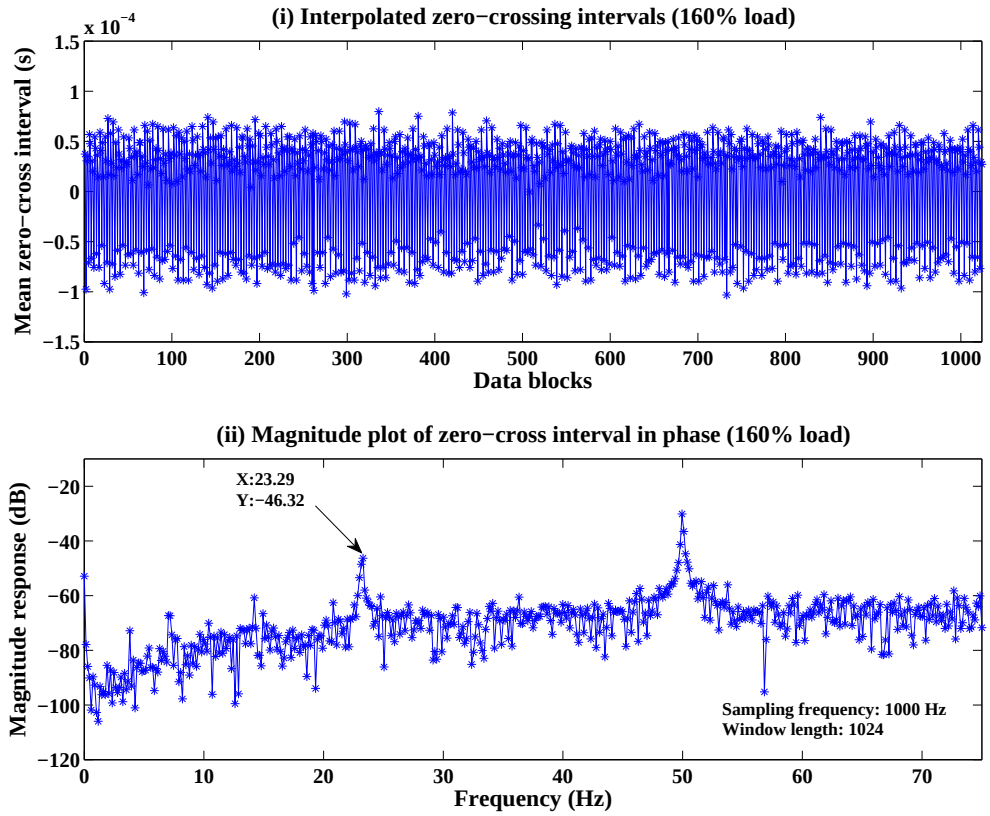


**Figure 3.10.** Healthy induction Motor II with 160% load.

**Table 3.2.** Difference between Motor I and Motor II.

| Load level | Difference of component frequency between Motor I and II (Hz) | Difference of amplitude between Motor I and II (dB) |
|---|---|---|
| 80% | 0.15 | 2.73 |
| 90% | 0.14 | 2.08 |
| 110% | 0.44 | 3 |

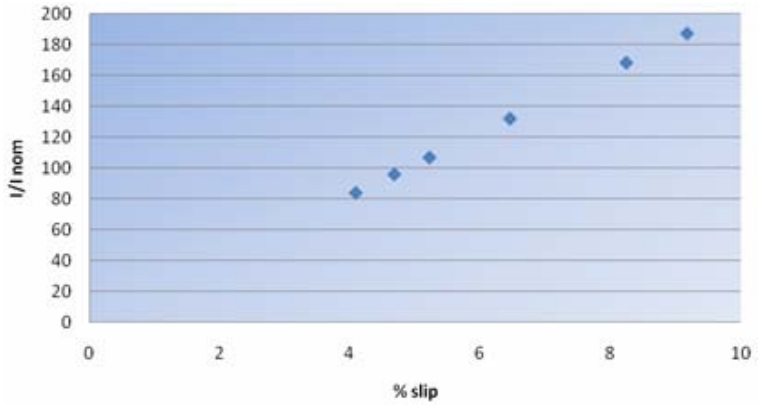


**Figure 3.11.** Computed slip vs. $I/I_{nom}$ for Motor I.

**Table 3.3.** Online testing results for Motor I (recording directly by LabVIEW).

| Current (A) (measured by device) | Rotor frequency (Hz) (20-30) | Amplitude (dB) (20-30) | Computed speed (rpm) (from rotor peak) | Slip (%) (from computed speed) | Load level (%) |
|---|---|---|---|---|---|
| | 24.95 | -27.84 | 1496.86 | 0.2092 | |
| 4.090 | 24.47 | -25.06 | 1468.20 | 2.1012 | 83.57 |
| 4.685 | 24.22 | -28.60 | 1453.20 | 3.1216 | 95.61 |
| 5.224 | 23.94 | -35.00 | 1436.40 | 4.2260 | 106.61 |
| 6.459 | 23.50 | -40.00 | 1410.00 | 6.0024 | 131.82 |
| 8.243 | 22.96 | -40.40 | 1377.60 | 8.1800 | 168.22 |
| 9.174 | 22.55 | -41.30 | 1353.00 | 9.8000 | 187.22 |

**Table 3.4.** Online testing results for Motor II (recording directly by LabVIEW).

| Current (A) (measured by device) | Rotor frequency (Hz) (20-30) | Amplitude (dB) (20-30) | Computed speed (rpm) (from rotor peak) | Slip (%) (from computed speed) | Load level (%) |
|---|---|---|---|---|---|
| | 24.967 | -27.637 | 1498.0 | 0.13 | |
| 4.11 | 24.496 | -24.308 | 1469.7 | 2.02 | 83.878 |
| 4.87 | 24.248 | -27.964 | 1454.9 | 3.01 | 99.388 |
| 5.82 | 23.969 | -31.106 | 1438.1 | 4.12 | 118.78 |
| 6.95 | 23.653 | -38.666 | 1419.2 | 5.39 | 141.84 |
| 8.16 | 23.239 | -37.436 | 1394.4 | 7.04 | 166.53 |
| 9.65 | 22.680 | -40.991 | 1360.8 | 9.28 | 196.94 |

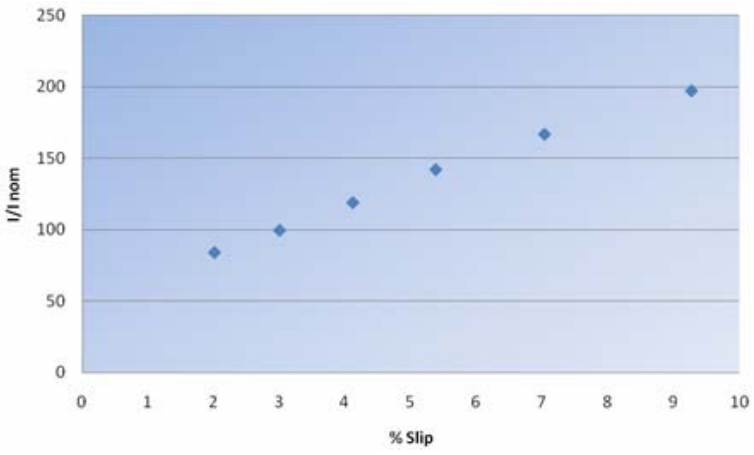


**Figure 3.12.** Computed slip vs. $I/I_{nom}$ for Motor II.

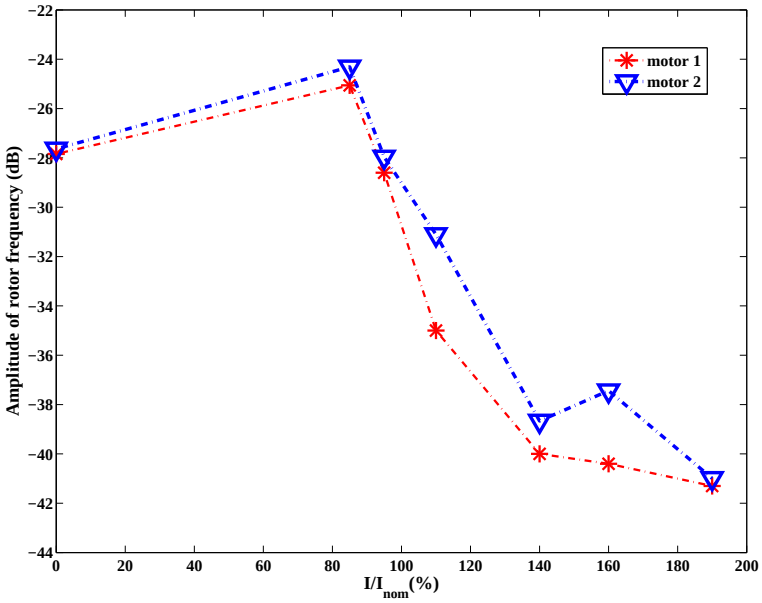


**Figure 3.13.** Amplitude of rotor frequency vs. $I/I_{nom}$.

## 3.3 Summary

In this chapter, two healthy motors were utilized for the baseline analysis. Although a healthy induction motor is highly symmetrical, any potential fault will alter its symmetrical property. These potential faults, which may result from manufacturing or installation, will produce characteristic fault frequencies. Such fault frequencies can be used for diagnosing broken rotor bar and stator short circuit faults. Thus, baseline analysis is important to eliminate other potential faults and understand frequency components of nominally healthy motors. Furthermore, the experiments show the behavior of the characteristic fault frequency components of two healthy motors as a function of load levels.

In summary, through the comparison, even though there is not any artificial fault setting for the two motors, the peak values of Motor I rotor frequency are less than that of Motor II at same load level. Therefore, might a possible misalignment or another potential faults in Motor II.

# Chapter 4

# Alignment Measurement Analysis

IN this chapter, the possibility of motor alignment is studied and if effect on the motor characteristics are investigated through experimentation. The motor alignment is adjusted by using a laser alignment system. The experiments show that motor misalignment influences the fault frequency of a stator short circuit fault at low load levels.

## 4.1 Introduction

A correct alignment of an industrial motor can increase the operating lifetime of rotating machinery and ensure smooth and efficient power transfer from the motor to the driven equipment. A misalignment will cause shaft fracture, bearing failures and vibrations due to the increased stress. These faults will lead to plant breakdowns, energy loss and other potential faults [34].

Misalignment may occur at the motor or shaft [34]. A motor misalignment results in an imbalance among the motor feet. For example, Figure 4.1 shows a motor feet with a vertical misalignment. The motor misalignment is considered as one of the main reasons that the devices waste energy because it can result in an increased friction on the shaft. This kind of friction will result in unnecessary increase of energy consumption.

NOTE:
This figure is included on page 36 of the print copy of the thesis held in the University of Adelaide Library.

**Figure 4.1.** Motor feet misalignment [42].

On the other hand, shaft misalignment is an imbalance between the coupled rotating plant machinery, such as motors, generators and pumps [43]. The aim of the shaft alignment is to ensure the coupled rotating machine works at a perfect rotational center line. The misalignment between two machines will lead to two shafts rotating the deviation of the rotational centre line, which increases the stresses on the shaft and coupling. Then, the friction on bearings will increase the chance of a plant breakdown.

Motor misalignment can be broadly categorized into three types [37]. Firstly, angular misalignment occurs when there is different angles of the horizontal plane between

two parallel shafts [44]. Some driven equipment and motor faults are caused by angular misalignment. The second type is parallel misalignment. The parallel misalignment occurs when the two parallel shafts' centerlines are not in the same line. The offset can be catalogued as either a horizontal or vertical offset. The parallel misalignment can cause an imbalance of the current signal and bring several potential problems for online condition monitoring. Finally, combined misalignment is the most common when the motor's shaft suffers from angular misalignment and parallel misalignment at the same time.

The Laser Alignment system, provided by Fixturlaser Company [37], was utilized to detect motor and shaft misalignment in our lab. The specialist technology ensures a high quality measurement. The Laser Alignment system consists of a display unit (Figure 4.2), measurement unit and shaft bracket, including rods and chain (Figure 4.3).

NOTE:
This figure is included on page 37 of the print copy of the thesis held in the University of Adelaide Library.

**Figure 4.2.** Fixturlaser [37].

The measurement process of the Laser Alignment system is described as follows. Two of the measurement units are fixed on the two shafts. When the detectors receive a laser beam from the transmitters, the two lights on the screen turn to green. Then, the distances between each component need to be measured and entered manually into the system, as shown in Figure 4.4. The measurement will be implemented at three

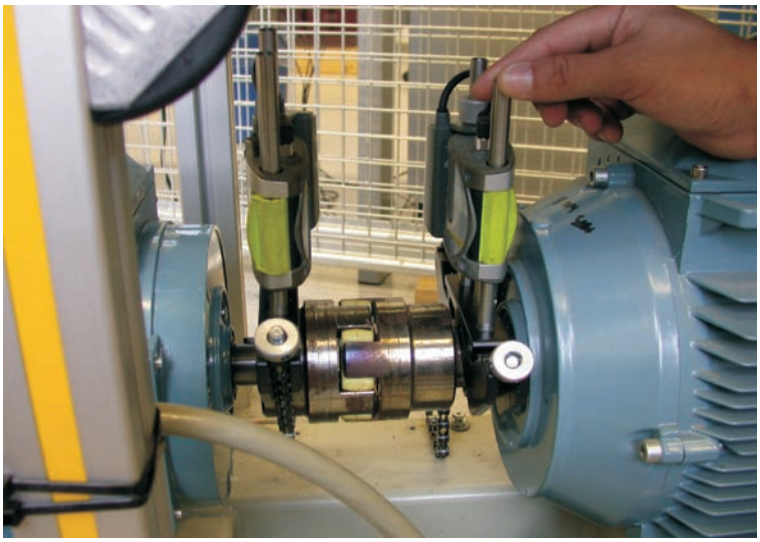

**Figure 4.3.** Measurement unit.

different points. The distance between these points should be at least 60 degrees to improve the accuracy. Finally, the measurement data are analyzed and results are displayed on the screen [37].

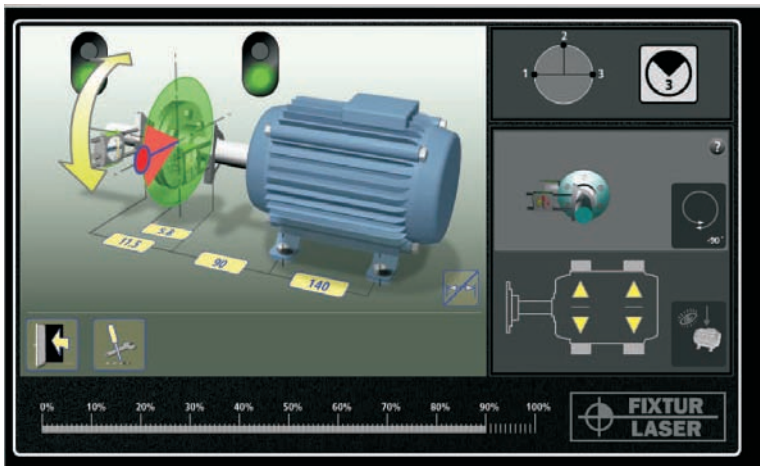


**Figure 4.4.** Measurement process.

## 4.2 Alignment Measurement

Three motors have been installed in our laboratory. The motor parameters are listed in Table 3.1. The alignment measurements of Motor II and Motor III were illustrated as examples. The measurement results of Motor II are shown in Figure 4.5(a). The

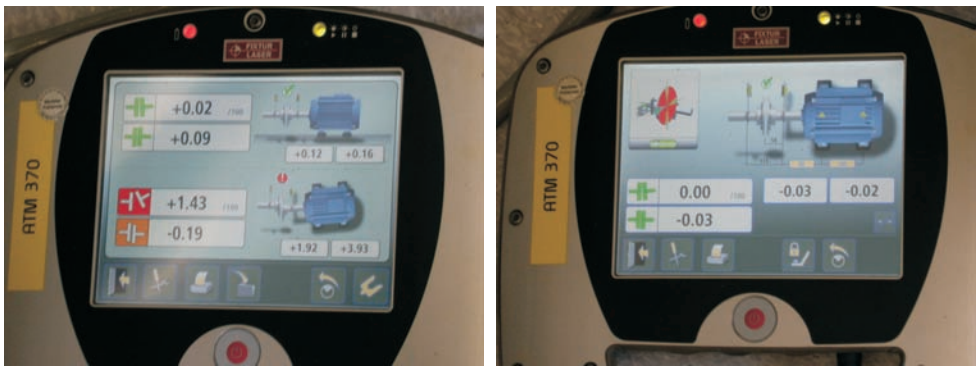


(a) Measurement result

(b) Measurement result after adjustment

**Figure 4.5.** Measurement results of the Motor II.

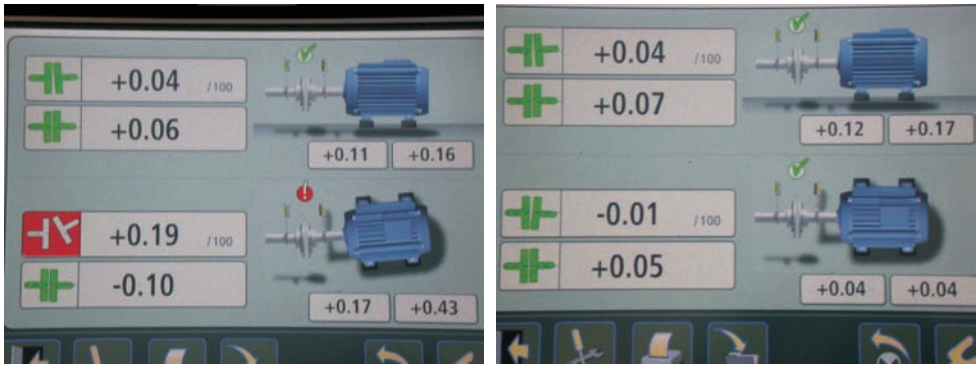


(a) Measurement result

(b) Measurement result after adjustment

**Figure 4.6.** Measurement results of the Motor III.

misalignments are shown in both number and color codes. For example, the red color indicates out of tolerance, the orange means near the tolerance and the green means acceptable. The results denote that the motor suffers from combined misalignment, i.e. both angular and parallel misalignment. Figure 4.5(b) shows the alignment of the adjusted motor. The initial and adjusted alignments of Motor III are shown in Figure 4.6(a) and 4.6(b), respectively.

## 4.3 Comparison of the On-line Condition Monitoring Testing Results

### 4.3.1 Healthy Motor Testing

Through the analysis of motor current signal in the frequency domain, the condition of under-tested motor can be diagnosed to find potential faults, which might result from manufacturing defects and installation problems. Figure 4.7 shows the ZCT signal of Motor III in both time and frequency domains. In frequency domain, there is a frequency peak (-29.7 dB) at 24.46 Hz, which indicated the existence of other faults. After a through inspection, a gap (Figure 4.8) between two the shafts was found. After the gap was reduced, the frequency component decreased by 3.7 dB, as shown in Figure 4.9.

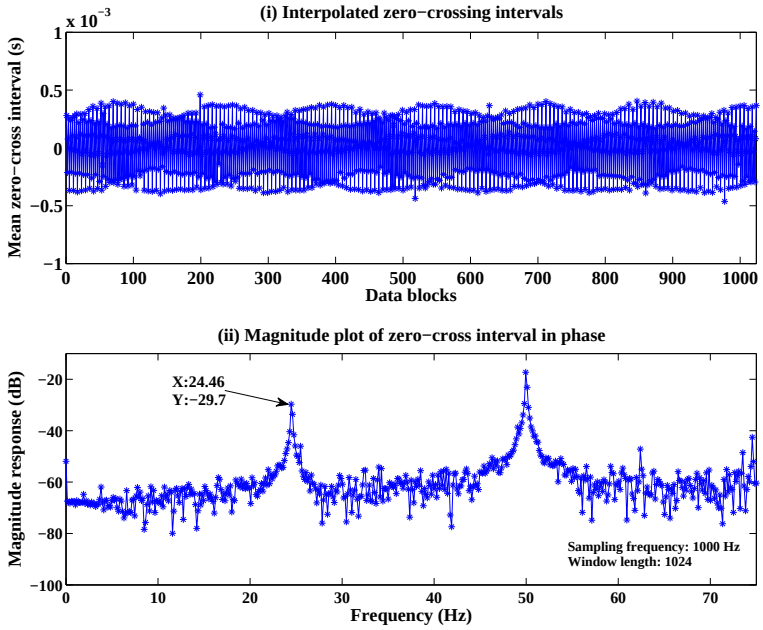


**Figure 4.7.** ZCT signal of Motor III.

The motor was tested with different torque levels resulting from changing the load level. The torque level corresponding to the current load level is shown in the table 4.1. Figure 4.10 reveals that when there is a misalignment, the rotation frequency amplitude of the motor with a coupling gap is higher than without a gap at lower load level. However, the amplitude will be influenced by the noise produced by the high load level. Compared with other graphs which are shown in Figure 4.10, the graph of

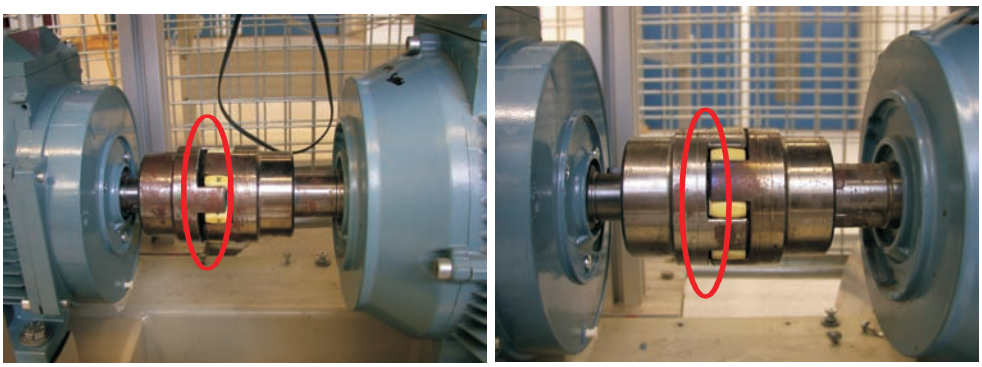

(a) Coupling with gap (b) Coupling state after adjustment

**Figure 4.8.** Coupling adjustment.

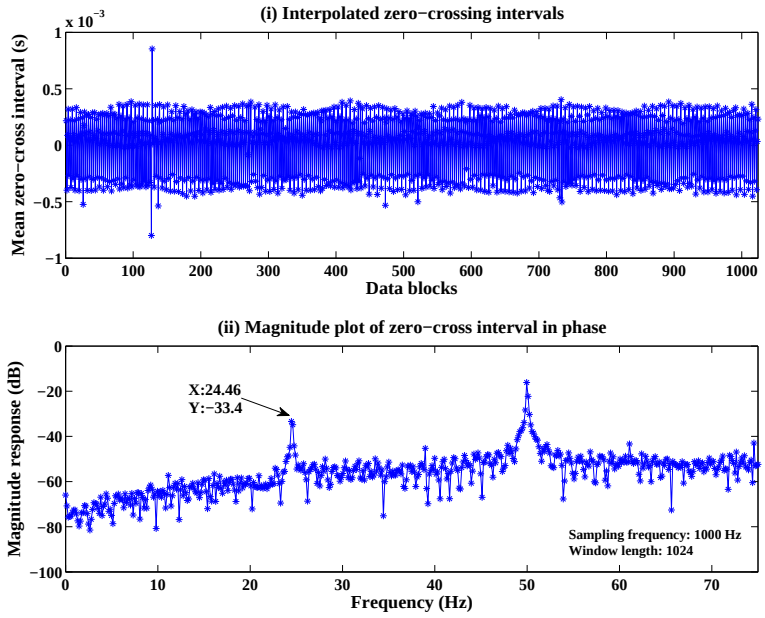


**Figure 4.9.** ZCT signal of Motor III (after coupling adjustment).

**Table 4.1.** Torque levels corresponding current load (Motor III).

| Torque Level | Load Level |
|---|---|
| 10% | $> 70\%$ |
| 20% | $> 80\%$ |
| 30% | $> 98\%$ |
| 40% | $> 117\%$ |
| 50% | $> 140\%$ |
| 60% | $> 165\%$ |
| 70% | $> 196\%$ |

the motor with only a misalignment trend is different than the others. The amplitude reduces when the torque level is 90%. When the motor runs without load, the amplitude of the motor without misalignment is the lowest.

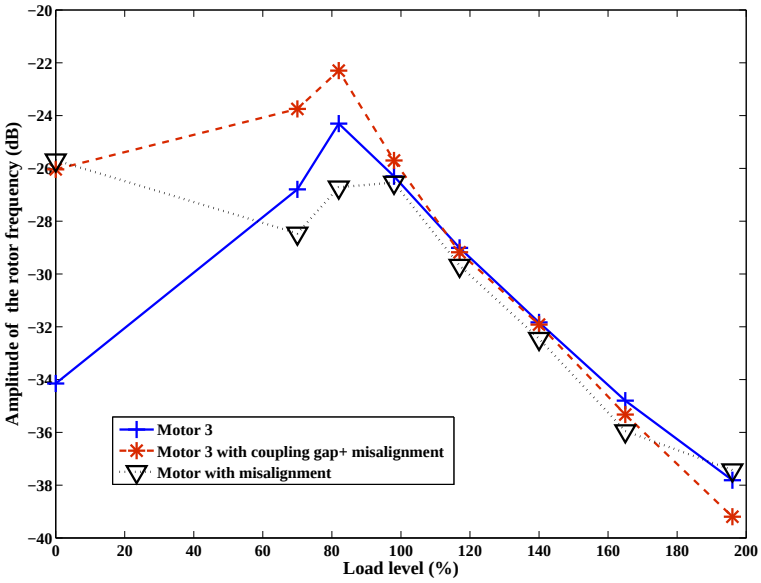


**Figure 4.10.** The test results of Motor III.

### 4.3.2 The Misalignment Influence on Stator Short Circuit Detection

The effect of misalignment for stator short circuit testing is also studied in our lab. There are two types of the testing according to the two kinds of stator short circuits, which are stator short circuit directly and stator short circuit with resistance. The testing was also carried out under different torque levels. The torque levels corresponding to the current load level is shown in the table 4.2.

Figure 4.11 shows the testing results of a motor with three different conditions, a motor with misalignment, a motor with misalignment and turn-to-turn stator short circuit without resistance and a motor without misalignment and turn-to-turn stator short circuit without resistance. The figure clearly shows that all peaks of red line, which represents the motor running with misalignment and turn-to-turn stator short circuit, is higher than the blue line's, which represents healthy motor running with misalignment. The reason is that the value of the fault frequency amplitude increases instantly

**Table 4.2.** Torque levels corresponding current load (Motor II).

| Torque Level | Load Level |
|---|---|
| 10% | $> 72\%$ |
| 20% | $> 83\%$ |
| 30% | $> 98\%$ |
| 40% | $> 117\%$ |
| 50% | $> 140\%$ |
| 60% | $> 165\%$ |
| 70% | $> 193\%$ |

when the stator short circuit fault happens. The influence of the amplitude by misalignment is also shown in Figure 4.11. When the motor runs at the low torque level, the peaks of the black line, which denotes the motor short circuit without resistance, are lower than the red line's peak values. Therefore, the misalignment can increase the amplitude of the fault frequency. However, a high load level will produce large amounts of noise and the peaks of the black line is slightly higher than that of the red's. The test results of the turn-to-turn stator short circuit fault with resistance are shown in Figure 4.12, which shows that misalignment can lead to an increase in amplitude of fault frequency as well.

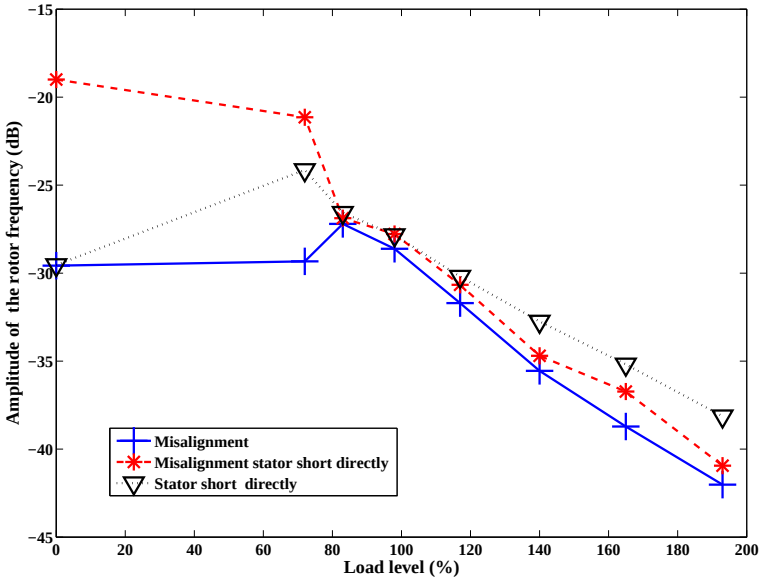


**Figure 4.11.** Misalignment effect for turn-to-turn stator short circuit directly.

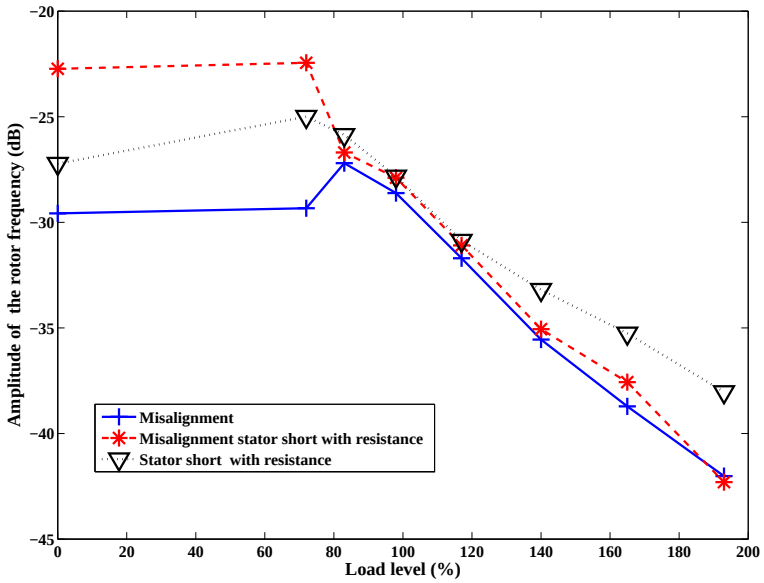


**Figure 4.12.** Misalignment effect for turn-to-turn stator short circuit with resistance.

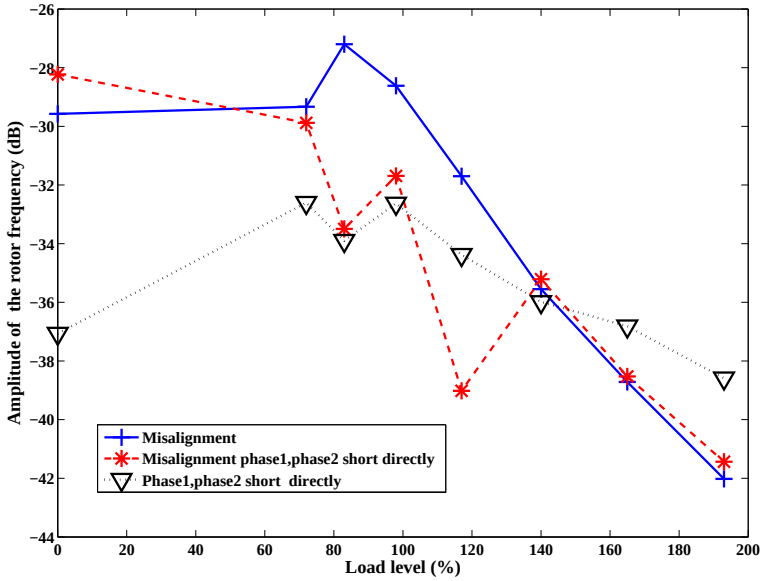


**Figure 4.13.** Misalignment effect for phase-to-phase stator short circuit directly.

The misalignment influence for a phase-to-phase stator short circuit with and without resistance is demonstrated in Figure 4.13 and 4.14. When the motor operates under misalignment and the stator short circuit without resistance, the amplitude value of the fault frequency fluctuates. Compared with Figures 4.13 and 4.14, the resistance will not affect the amplitude of rotor frequency of phase-to-phase stator short circuit at higher load levels (more than 140%). On the contrary, the amplitude of rotor frequency of phase-to-phase stator short circuit without resistance is lower than that of

stator short circuit with resistance.

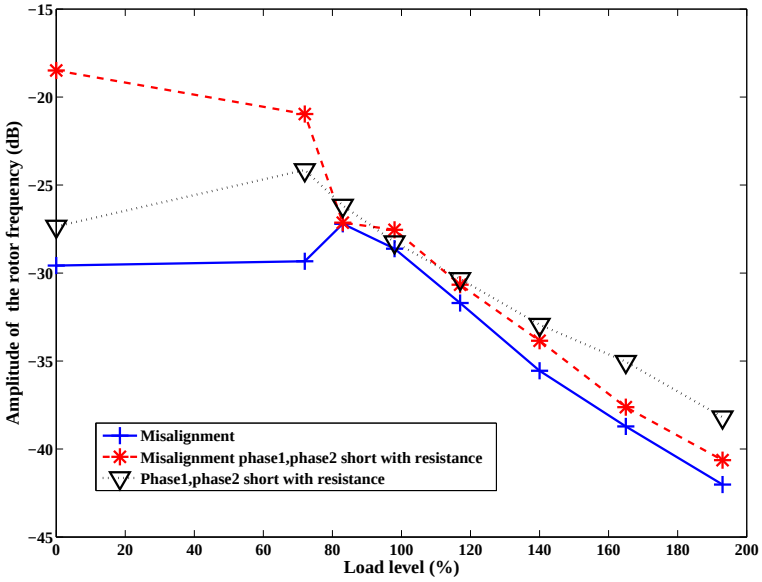


**Figure 4.14.** Misalignment influence for phase-to-phase stator short circuit with resistance.

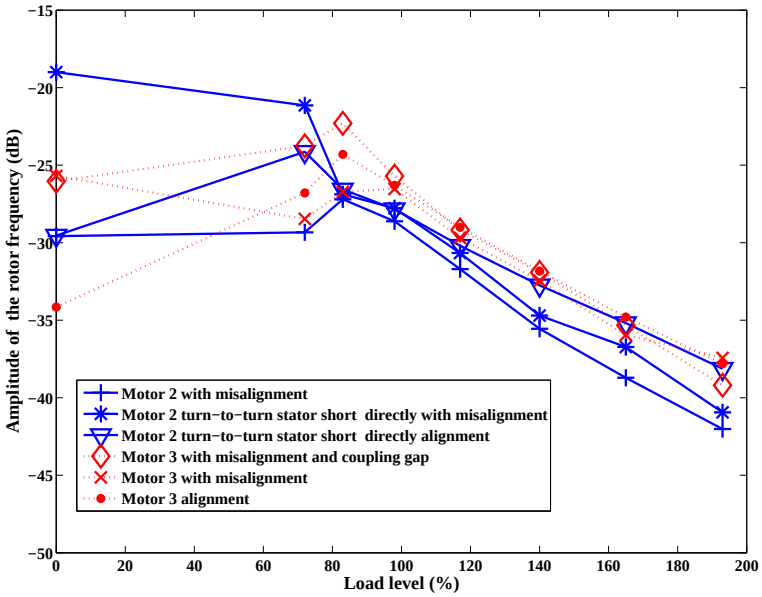


**Figure 4.15.** Comparison of misalignment measurement testing results.

In order to compare Motor II and Motor III, the test results are plotted in the Figure 4.15. Although the type of motor is the same, there is a distinction between the testing results. The amplitude of Motor III with misalignment is higher than Motor II. There may be some potential problems and they will be diagnosed in our future research. In addition, Figure 4.15 demonstrates that the stator short circuit is the primary reason for

increasing the fault frequency amplitude. When the motor operates at low load levels with a stator short circuit, the amplitude of the stator short circuit is higher than that of the other fault amplitudes even if there is a gap in the coupling. This could be because of the whole assembly of shaft bending, and/or an existing manufacturing defect.

## 4.4 Summary

In this chapter, motor misalignment is varied and adjusted by using the Laser Alignment system. Based on the measurements, we also found that a coupling gap can lead to an unexpected frequency peak. At a low load level, misalignment will increase the amplitude of the fault frequency in a stator short circuit fault. While, misalignment has little effect on the amplitude when running under high load conditions.

# Chapter 5

# Stator Short Circuit Fault

IN this chapter, stator short circuit faults are studied by using both off-line and on-line tests. Through a control box, artificial turn-to-turn faults and phase-to-phase faults are simulated. In addition, the experiments consider different load levels.

## 5.1 Introduction

A stator short circuit in winding is considered as one of the main faults in an induction motor. There are four types of stator short circuit faults, turn-to-turn short circuits within a coil, short circuits between coils of the same phase, phase-to-phase shorts and phase to earth short circuits [45]. Figure 5.1 shows the pattern of short circuit faults in a stator winding. Although a stator short circuit fault does not affect the normal operation in the early stage, it will reduce the efficiency of a motor and even damage it when the fault becomes severe. Therefore, early diagnosis of the stator short circuit fault in operation is important before it becomes a catastrophic failure to induction motors. In addition, it will help to eliminate costly damages in terms of lost production time and avoid expensive cost for maintenance and repair [46].

NOTE:
This figure is included on page 48 of the print copy of the thesis held in the University of Adelaide Library.

**Figure 5.1.** Wye connected stator showing possible short circuit faults [45].

A stator short circuit in winding is influenced by the quality of the insulation between the turns and phases of the coils inside a motor [3]. Mechanical stress is generated by stator coils moving during the operation of a motor. When the motor starts, the current in the coils will reach its highest value and it will result in a high magnetic force. This magnetic force will cause the coils to vibrate at two times than line frequency. This

vibration could damage the stator and other motor components. Another fault consequence is electrical stress [3]. Electrical failures are common failures in the induction motor windings. Most of them are caused by over-voltage, current overload and so on. It can cause some faults in the circuit during testing or operation. In addition, thermal stress is also one of the major reasons for a stator short circuit. It results from the insulation deterioration due to the motor working temperature being higher than the designed temperature. The insulation life will be reduced by half when the temperature increases every 10°C above designed temperature [3]. Thermal stress can also reduce the life of a motor when operating at higher than rated voltage and overloaded. Furthermore, the environmental stress cannot be neglected. Contamination, such as dust, oil and moisture, will enter into the motor and cause environmental stress. The contaminations influence the stator insulation lifetime and result in winding faults in the motor.

## 5.2 Detection of Stator Short Circuit

The diagnosis of shorted turns in stator windings of an induction motor using the motor current signature analysis (MCSA) is based on detecting the frequency components given by equation (5.1) [31]

$$f_{short} = f_s \left[ k \pm \frac{n}{P}(1-s) \right], \tag{5.1}$$

where,
$f_{short}$ is the frequency component that is a function of the short circuit,
$f_s$ is the supply frequency,
$P$ is the number of pole pairs,
$n$ and $k$ are two parameters, $n = 1, 2, 3...$ and $k = 1, 2, 3...$

The slip speed $s$ is defined as

$$s = \frac{\omega_{sm} - \omega_{rm}}{\omega_{sm}}, \tag{5.2}$$

where $\omega_{sm} = 2\omega_e/P$ is the synchronous speed in mechanical radians, $\omega_e$ is angular speed of the stator Magnetic Motive Force (MMF) in electrical radians per second and $\omega_{rm}$ is the rotor rotating speed.

When $k = 1$ in equation (5.1), the component frequency, induced in the spectrum of the stator current, superimposed on the fundamental current, will be illustrated by the following formula

$$f_{comp} = f_s \left[\frac{n}{P}(1-s)\right]. \tag{5.3}$$

For two pole motors $(p = 2)$ in first instance, the equation (5.3) will be a whole series of components:

$$f_{comp} = \begin{cases} f_s(1-s) & n = 1 \\ 2f_s(1-s) & n = 2 \\ 3f_s(1-s) & n = 3 \end{cases}$$

For four pole motors $(p = 4)$, the equation (5.3) will be revealed the following series of components:

$$f_{comp} = \begin{cases} (1/2)f_s(1-s) & n = 1 \\ f_s(1-s) & n = 2 \\ (3/2)f_s(1-s) & n = 3 \end{cases}$$

These components are visible in the frequency spectrum of the stator current (as sidebands to the fundamental peak). This will affect the normal ZCT spacing, causing the indicative frequency components to appear at locations given by equation (5.3) in the spectrum of the ZCT signal as well [31]. Since this stator fault component in the ZCT spectrum is independent of the motor's inertia, it can be used as a good indicator of the stator short circuit fault. However, putting $n = 1$ in equation (5.3), we can get

$$f_{comp} = f_s \left[\frac{1-s}{p}\right]. \tag{5.4}$$

Equation (5.4) expresses the relationship between the component frequency and rotor frequency. When $n = 1$, it is difficult to judge the frequency peak due to stator fault or rotor frequency in the ZCT spectrum. Therefore, we utilize values of $n > 1$ .

## 5.3 Experiment Setup for Stator Short Circuit Faults Diagnosis

The off-line and on-line test system sketches are shown in Figures 5.2(a) and 5.2(b). Two of the same type of motors, Motor I and Motor II, are employed in off-line and

on-line test, respectively. The motor parameters are listed in Table 3.1. For the off-line test, an oscilloscope is used to show and capture the current signal. Then, the signal is processed by using MATLAB. On the other hand, during the on-line test, the ZCT signal is acquired by the device that does the ZCT signal conversion and LabVIEW is employed to plot and analyze the signal.

Another motor wass utilized as a load and the load level was varied through the AC drives to change the load level. The setup of the experiment is illustrated in Figure 5.3. Some turns from one slot were selected and scraped off their insulation layer and soldered them with different wires labeled with numbers. There are several combinations of the wires for the stator short circuit. In addition, in order to test the phase-to-phase stator short circuit, Some turns from another slot were selected and also soldered with a different wires labels. Finally, the wires are connected to a switch box to control the stator short circuit.

## 5.4 Off-line Test of Stator Short Circuit Faults

A turn-to-turn fault is the initial fault in the induction motor. It will cause other faults such as phase-to-phase, phase to earth fault or even more serious faults like motor damage. Therefore, turn-to-turn faults detection is important to prevent potential catastrophic faults.

In this section, turn-to-turn faults are studies in both off-line and on-line tests. The off-line testing was utilized to analyze the motor's current signal when the motor is operated at different load levels. The magnitude variation of the fault frequency amplitude was estimated. Compared with off-line testing, on-line testing is using the current ZCT signal and it can monitor and diagnose motor faults immediately when the motor is running.

### 5.4.1 Analysis of Turn-to-turn Fault of Motor I

In this section, the frequency components in the current signal, when $n = 1$, $P = 2$ and $k = 1$ in equation (5.1), are investigated and analyzed. In addition, two types of

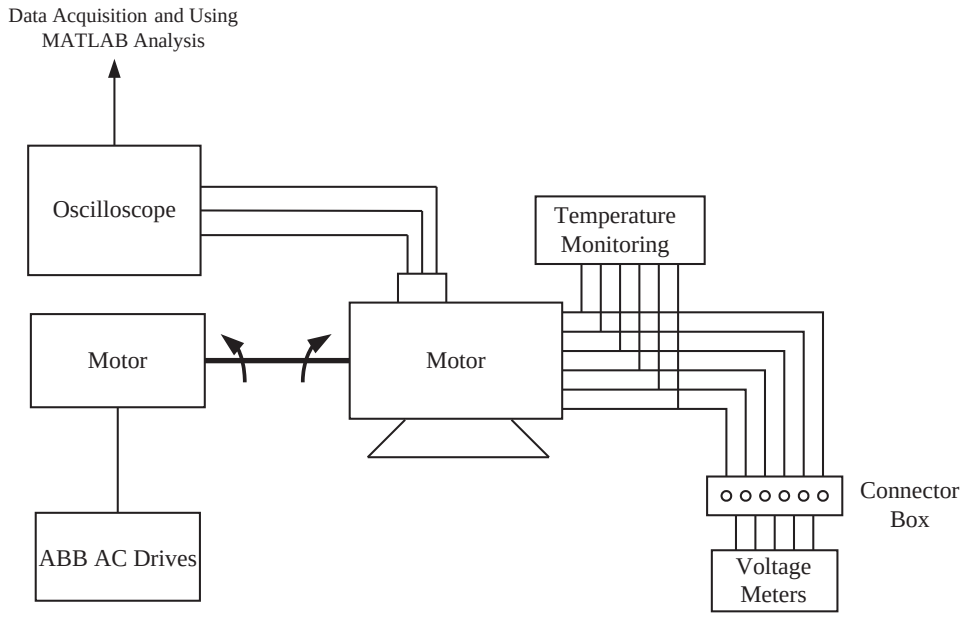


(a) Off-line detection structure diagram

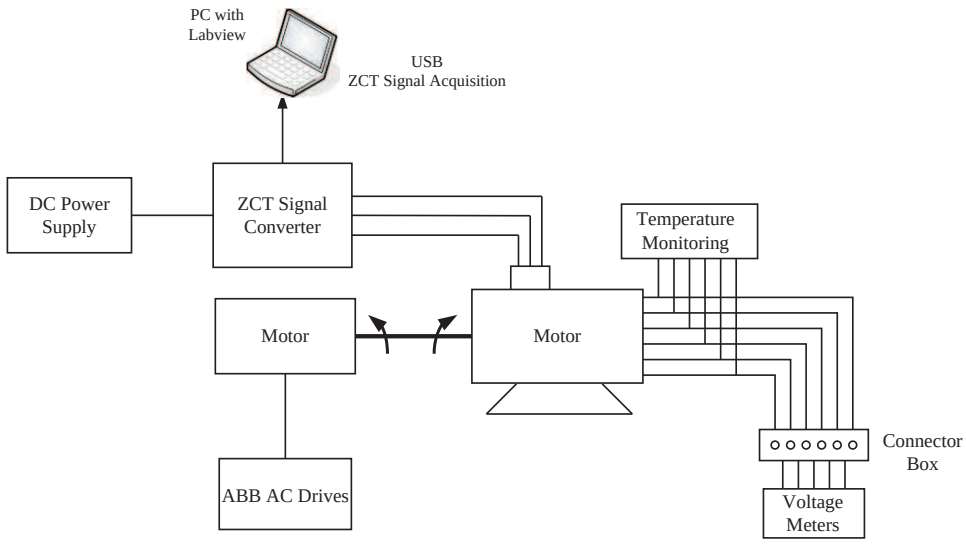


(b) On-line detection structure diagram

**Figure 5.2.** Off-line and on-line detection structure diagram.

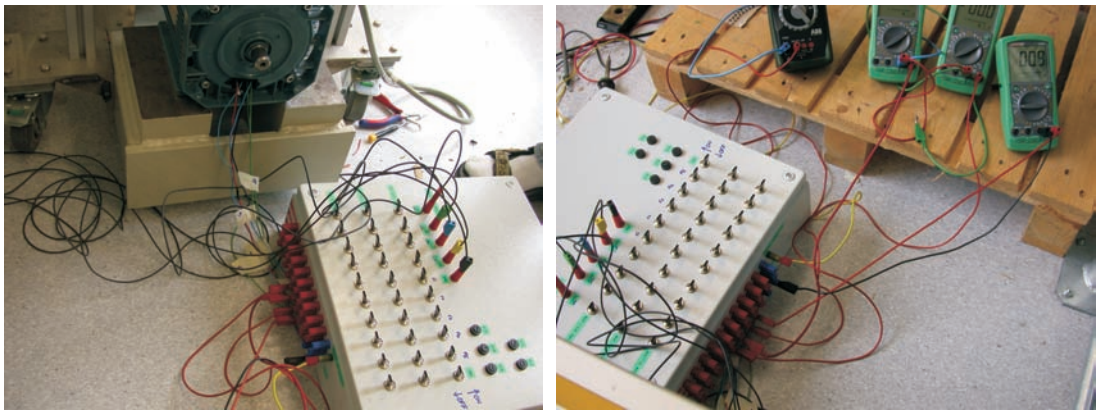

(a) (b)

**Figure 5.3.** The laboratory setup for induction motor stator short circuit experiments.

turn-to-turn faults are tested: two turns short circuit and five turns short circuit.

When a healthy motor is under 80% load, the measured rotor speed is 1471 *rpm*. Therefore, the slip, $s = (1500 - 1471)/1500 \approx 0.019$, and the fault component frequency can be computed $f_{comp} = 1/2 \times 50 \times (1 - s) \approx 24.5$ Hz. When $k = 1$, according to equation (5.1), the fault frequency is $f_{short} = |24.5 \pm 50|$ Hz. Thus, the left and right hand short frequency are $f_{short_L} = |24.5 - 50| = 25.5$ Hz and $f_{short_R} = |24.5 + 50| = 74.5$ Hz, respectively. Figure 5.4 illustrates the testing current data and ZCT signal. In Figure 5.4, the fault frequencies can be found and the corresponding amplitudes are -8.613 dB (25.5 Hz) and -6.947 dB (74.5 Hz). In addition, the healthy motor with high load levels was also tested. The load level with 140%, as an example, can verify the reliability of the experiment setup. When the healthy motor operates under 140% load level, the measured rotor speed is 1421 *rpm*. Thus, the slip can be calculated as $s = (1500 - 1421)/1500 \approx 0.053$ and the component frequency can be computed $f_{comp} = 1/2 \times 50 \times (1 - s) = 23.675$ Hz. The the left and right hand short frequency are $f_{short} = |23.675 \pm 50|$ Hz, i.e. 26.325 Hz and 73.675 Hz. However, there are slight differences between the computed fault frequencies and the fault frequencies, which are showed in Figure 5.5. The reason could be due to error in the rotor speed measurement or a computation error in MATLAB. In spite of the small error, the experiment setup is considered as reliable. In addition, Figure 5.5 shows the corresponding amplitude of the fault frequencies as -11.63 dB (26.35 Hz), -10.88 dB (73.65 Hz). Compared with Figure 5.5 and 5.6, the fault frequencies are close to the rotor fundamental frequency

and the amplitudes of the fault frequencies decrease when the load level increases.

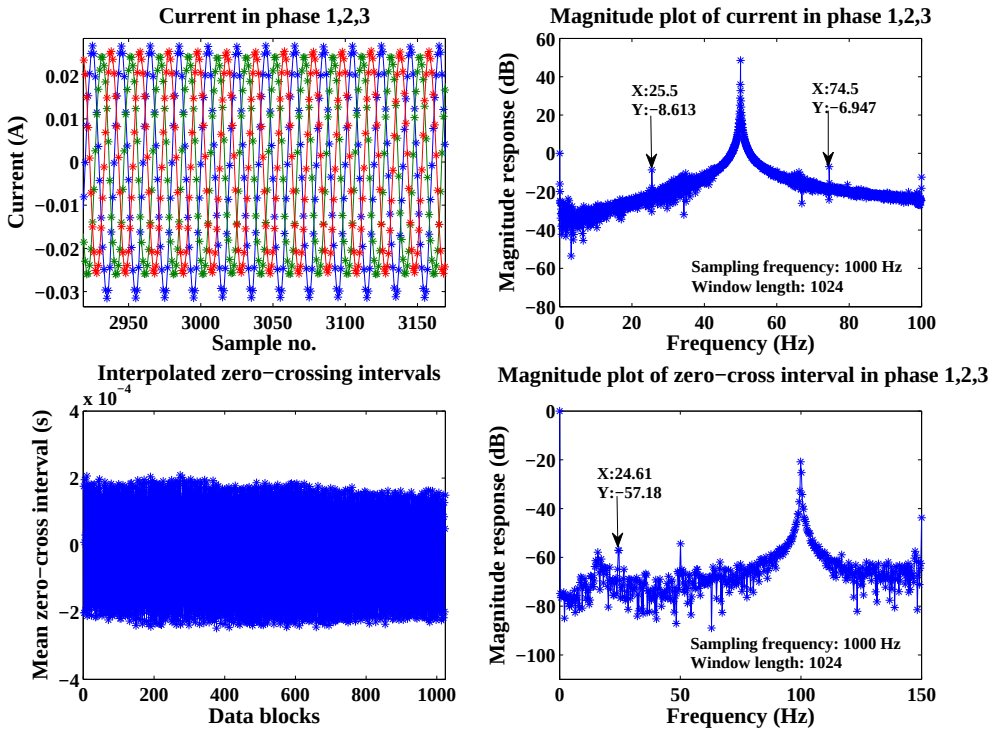


**Figure 5.4.** Healthy motor with 80% load level.

When a turn-to-turn fault happens, the variations in the current signal are revealed in Figures 5.6 and 5.7. They are the test results for two turns short circuit in the same slot. Figure 5.6 shows that the amplitudes of frequencies are higher than the amplitudes which are presented in Figure 5.4. Although there is a slight difference with the frequencies presented in Figure 5.4, the error is within tolerance because the difference is produced by the noise of the load level. Comparing Figure 5.5 with 5.7, the magnitude at fault frequency (23.44 Hz) increases as high as 4 dB when a turn-to-turn short circuit occurs. Therefore, we can conclude that when the motor operates with a turn-to-turn fault, the amplitude of specific fault frequencies will increase as we expected.

By using the switch box, different turns shorts in the same slot are realized. The test results for two and five turn-to-turn faults are listed in Tables 5.1 and 5.2, respectively. In each test, the harmonic frequencies and the corresponding amplitudes are recorded at different loading conditions. In addition, the slip values are computed and the variations are plotted in Figure 5.8.

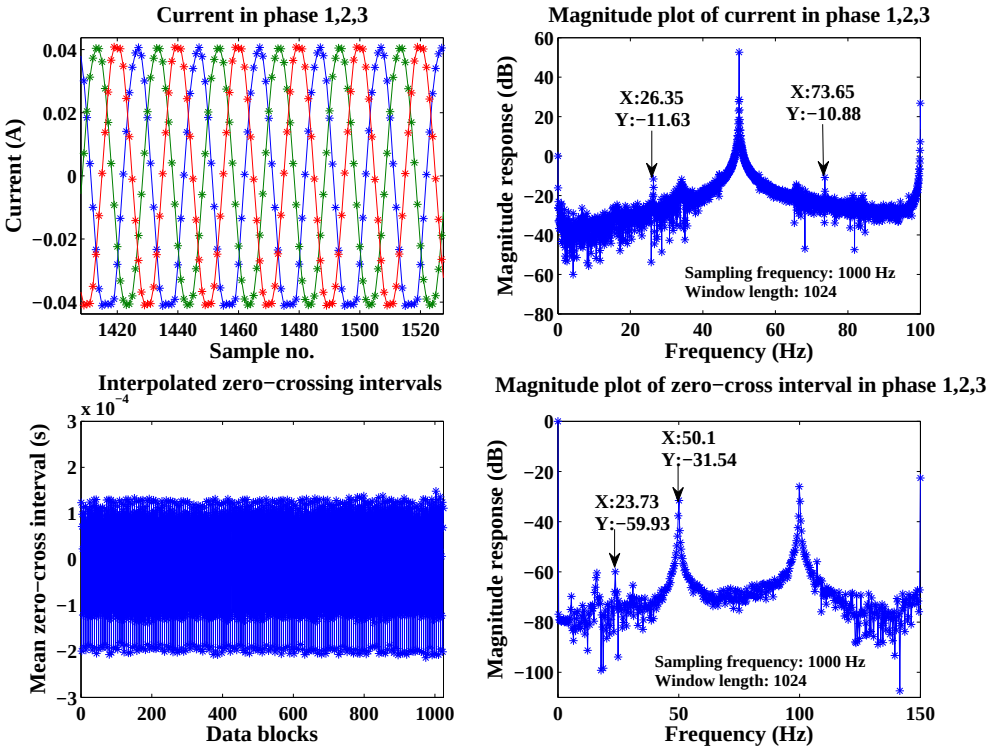


**Figure 5.5.** Healthy motor with 140% load level.

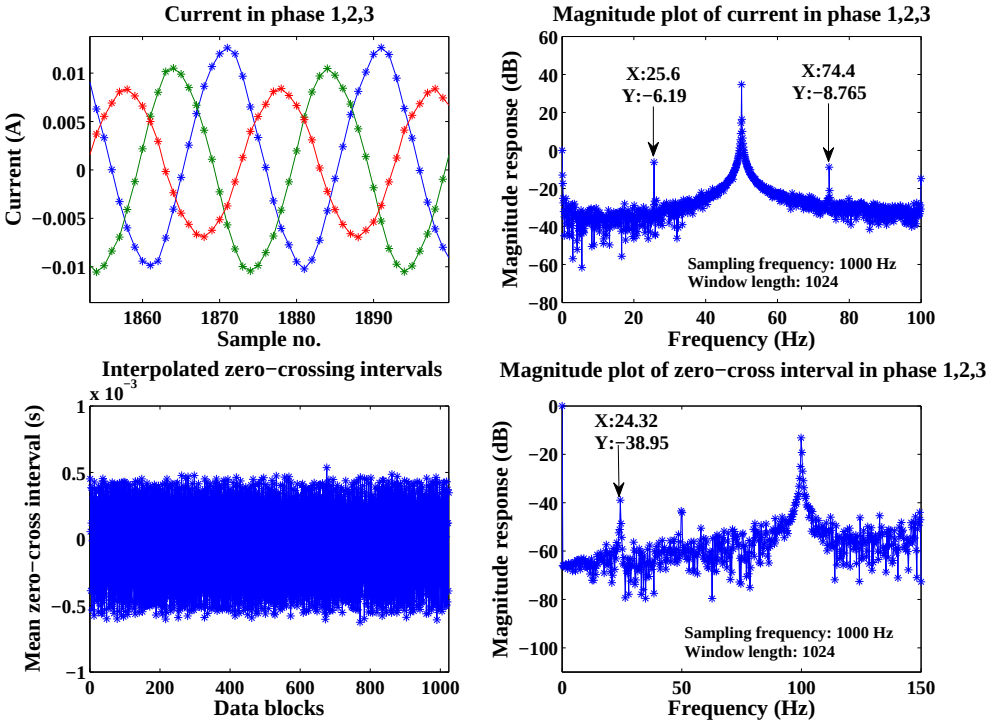


**Figure 5.6.** Turn-to-turn short circuit with 80% loading level.

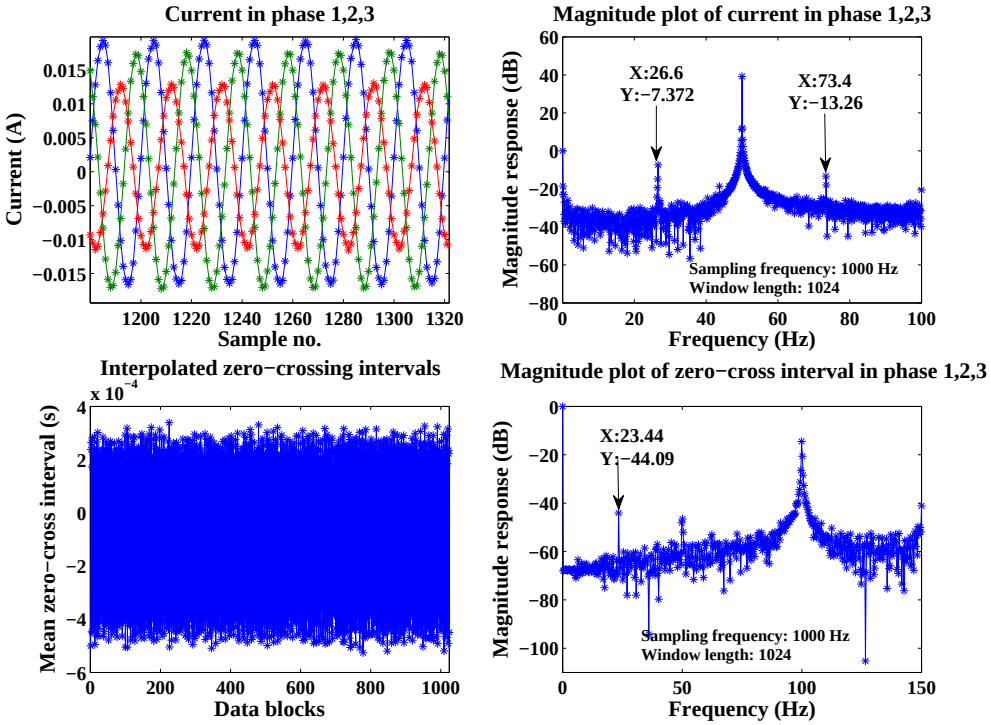


**Figure 5.7.** Turn-to-turn short circuit with 140% loading level.

**Table 5.1.** Turn-to-turn fault (two turns).

| Load Level (%) | Fault Component Frequency (n=1 k=+1) | Amplitude of frequency component (n=1 k=+1) | Fault component frequency (n=1 k=-1) | Amplitude of frequency component (n=1 k=-1) | Slip (%) |
|---|---|---|---|---|---|
| 0 | 25 | -21.5 | 75 | -18.4 | |
| 80 | 25.6 | -6.19 | 74.4 | -8.765 | 2.4 |
| 90 | 25.9 | -6.315 | 74.1 | -9.391 | 3.6 |
| 110 | 26.2 | -5.135 | 73.8 | -10.03 | 4.8 |
| 140 | 26.6 | -7.372 | 73.4 | -13.26 | 6.4 |

**Table 5.2.** Turn-to-turn fault (five turns).

| Load Level (%) | Fault Component Frequency (n=1 k=+1) | Amplitude of frequency component (n=1 k=+1) | Fault component frequency (n=1 k=-1) | Amplitude of frequency component (n=1 k=-1) | Slip (%) |
|---|---|---|---|---|---|
| 0 | 25 | -17.81 | 75 | -13.3 | |
| 80 | 25.5 | -18.34 | 74.5 | 18.6 | 2 |
| 90 | 25.8 | -18.34 | 74.2 | -18.6 | 3.2 |
| 110 | 26.2 | -20.07 | 73.9 | -14.3 | 4.4 |
| 140 | 26.4 | -17.8 | 73.6 | -17.7 | 5.6 |

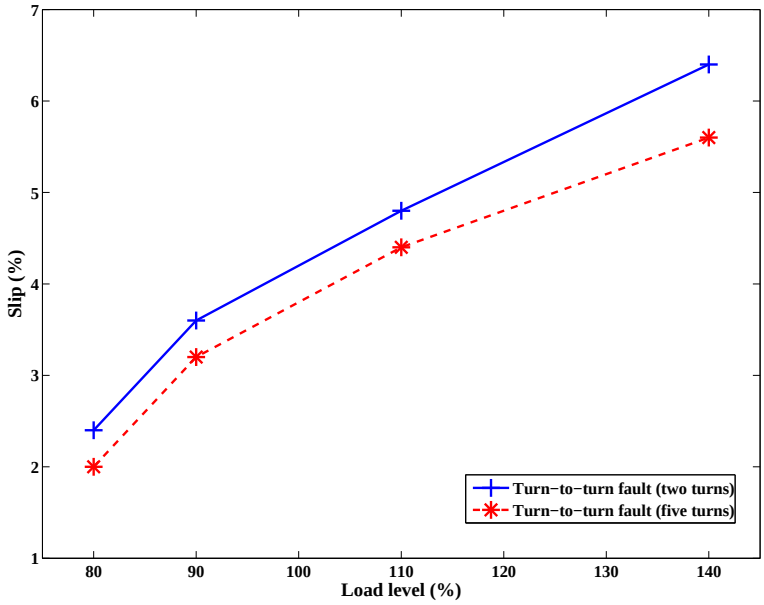


**Figure 5.8.** Slip with two and five turns faults.

Figure 5.8 illustrates the variation of the motor slip value for different turn-to-turn short circuits. The slip value rises while the load level increases. At the same load level, the slip value for five turn fault is smaller than the value of two turn fault. In addition, the difference in slip values between the different levels also increases as load level increase.

Figure 5.9 shows the fault frequencies amplitudes of a healthy motor, a slight turn-to-turn fault (2 turns fault) and a motor with a serious turn-to-turn fault (5 turns fault). When the motors operate without load, the fault frequency amplitude of the healthy

motor is the lowest, as expected, and the amplitude of the serious turn-to-turn fault frequency is the highest. The amplitudes of the frequencies of the two turns fault are always higher than the values of the healthy motor under different load levels. However, the load levels affect the variation of rotor frequency amplitude when there is a serious fault. The rotor frequency amplitude of a serious fault has small changes under the different load levels.

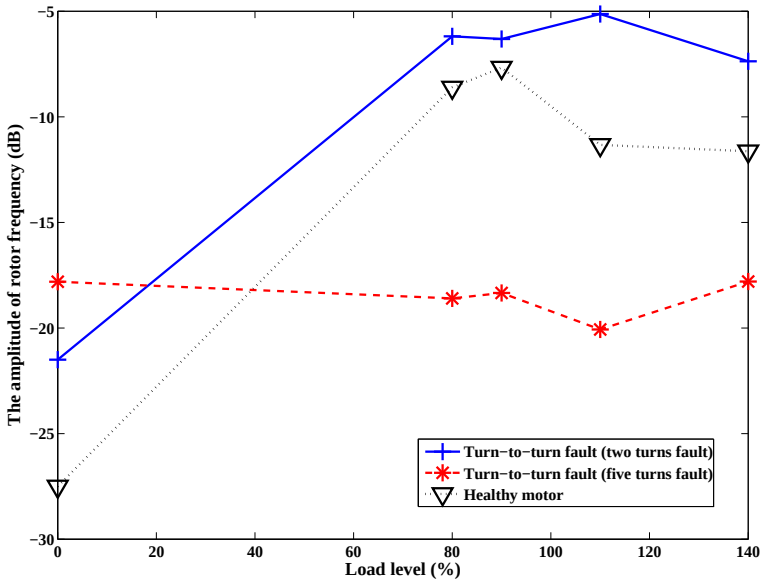


**Figure 5.9.** The amplitude of rotor frequency under different load levels.

### 5.4.2 Analysis of Phase-to-phase Fault in Motor I

The phase-to-phase fault is the short circuit between two turns in different slots. It is expected to have a similar influence as the turn-to-turn faults on the amplitude of the rotor frequency. Under this assumption, the turn-to-turn fault detection method can also detect phase-to-phase faults. Like turn-to-turn fault detection, when $n = 1$, $p = 2$ and $k = \pm 1$ in equation (5.1).

The phase-to-phase short circuit is more serious than turn-to-turn fault because a higher voltage difference between two phases make this fault accelerate very quickly. If the fault is left unattended, it can lead to rapid deterioration of the winding, and potentially destroy the motor. The magnitude of the fault frequency amplitude variation is

higher than that for a turn-to-turn fault. Figures 5.10 and 5.11 show the detection results of a phase-to-phase short circuit when the machine operates under 80% load and 140% load. Comparing Figure 5.6 with 5.10, we can conclude that the amplitude of the fault frequencies of the phase-to-phase short circuit is much higher than that of the turn-to-turn short circuit. While the load level grows up to 140%, the amplitude of the fault frequency increases to 0.2273 dB (when $k = -1$).

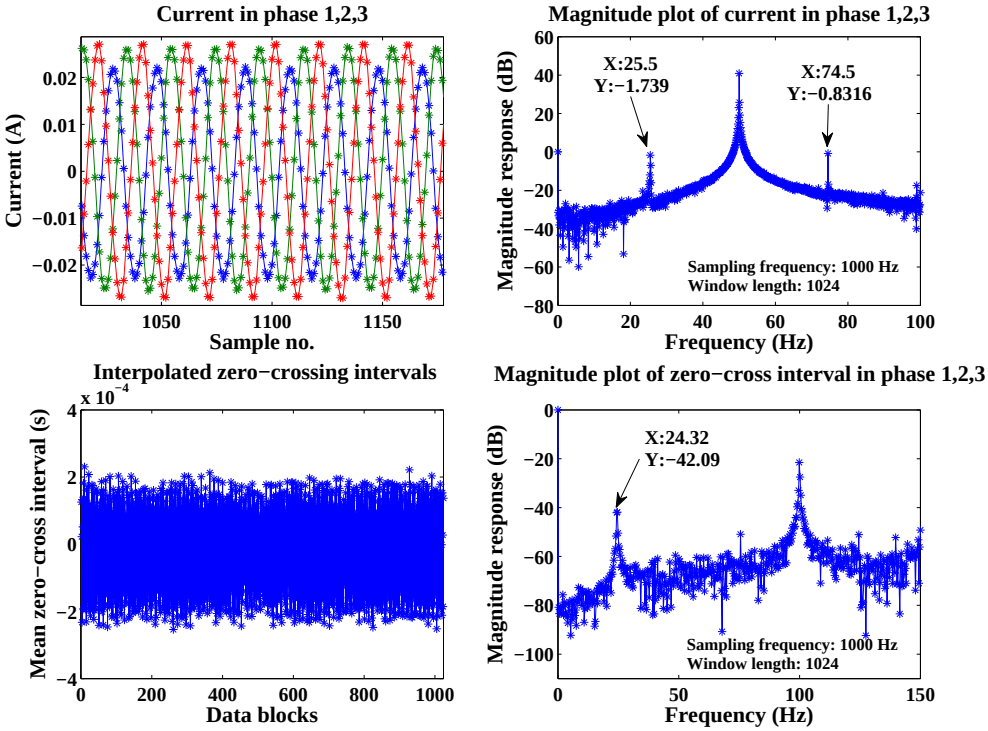


**Figure 5.10.** Phase-to-phase fault with 80% loading level.

The FFT result for the phase-to-phase fault is summarized in Table 5.3. A more serious condition, both a phase-to-phase fault and a turn-to-turn short circuit fault, is also tested and listed in Table 5.4. The tables state the frequencies and corresponding amplitudes when the motor was tested with different loading levels. The motor slip is computed and listed in the tables too.

The slip variations for a phase-to-phase short circuit and phase-to-phase short circuit combined with a turn-to-turn fault are illustrated in Figure 5.12. The slip values of both faults rise quickly while the load level increases. In addition, under different load levels, the slip value of a phase-to-phase short circuit fault is always higher than that

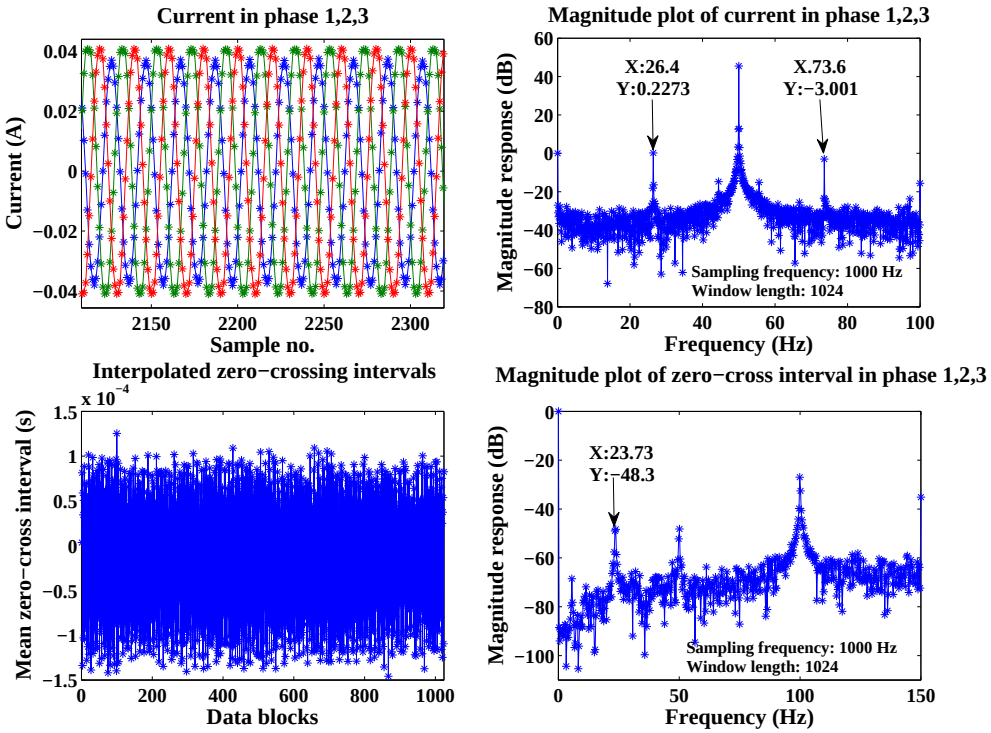


**Figure 5.11.** Phase-to-phase fault with 140% loading level.

**Table 5.3.** Phase-to-phase fault.

| Load Level (%) | Fault Component Frequency (n=1 k=+1) | Amplitude of frequency component (n=1 k=+1) | Fault component frequency (n=1 k=-1) | Amplitude of frequency component (n=1 k=-1) | Slip (%) |
|---|---|---|---|---|---|
| 0 | 25 | -13.11 | 75 | -16.63 | |
| 80 | 25.5 | -1.739 | 74.5 | -0.8316 | 2 |
| 90 | 25.8 | -0.3755 | 74.2 | -3.423 | 3.2 |
| 110 | 26.1 | -0.2722 | 74 | -6.349 | 4 |
| 140 | 26.4 | 0.2273 | 73.6 | -3.001 | 5.6 |

**Table 5.4.** Phase-to-phase fault plus turn-to-turn fault.

| Load Level (%) | Fault Component Frequency (n=1 k=+1) | Amplitude of frequency component (n=1 k=+1) | Fault component frequency (n=1 k=-1) | Amplitude of frequency component (n=1 k=-1) | Slip (%) |
|---|---|---|---|---|---|
| 0 | 25.1 | -14.75 | 74.9 | -8.727 | |
| 80 | 25.6 | -11.05 | 74.3 | -20.47 | 2.8 |
| 90 | 25.9 | -5.132 | 74.1 | -12.94 | 3.6 |
| 110 | 26.2 | -11.37 | 73.7 | -16.47 | 5.2 |
| 140 | 26.6 | -14.57 | 73.4 | -18.37 | 6.4 |

for the motor with a phase-to-phase fault plus a turn-to-turn fault.

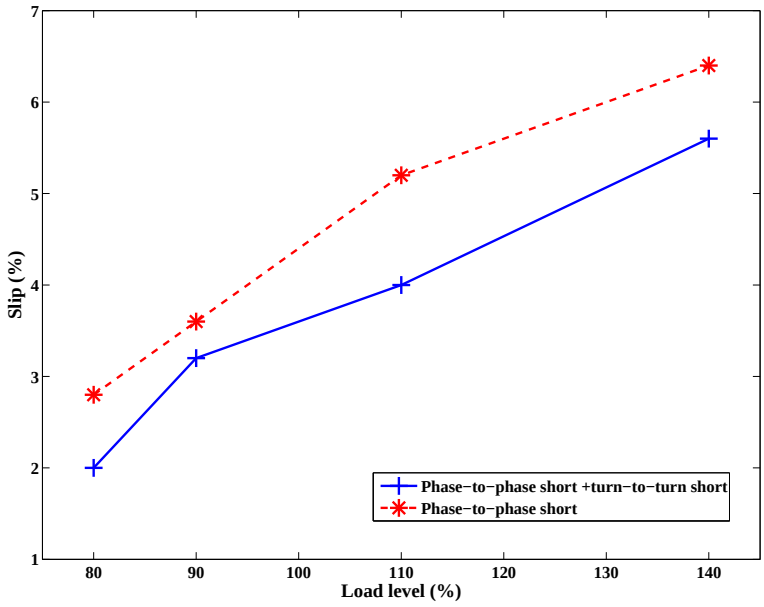


**Figure 5.12.** Slip of phase-to-phase short circuit and turn-to-turn short circuit under different load level.

The slip variations of the healthy motor, the motor with a phase-to-phase fault and the motor with a serious fault (phase-to-phase fault combined with turn-to-turn fault), are plotted in Figure 5.13. In general, the slip values of a serious fault are higher than the slip for only a phase-to-phase fault. However, this does not appear as expected in Figure 5.13. On the contrary, the slip values of a serious fault are lower than those of a phase-to-phase fault. The possible reason is that there are some reverse voltages due to the addition of a turn-to-turn fault. Especially, when the motor runs at 80% load level,

the slip for a serious fault is lower than that of a healthy motor.

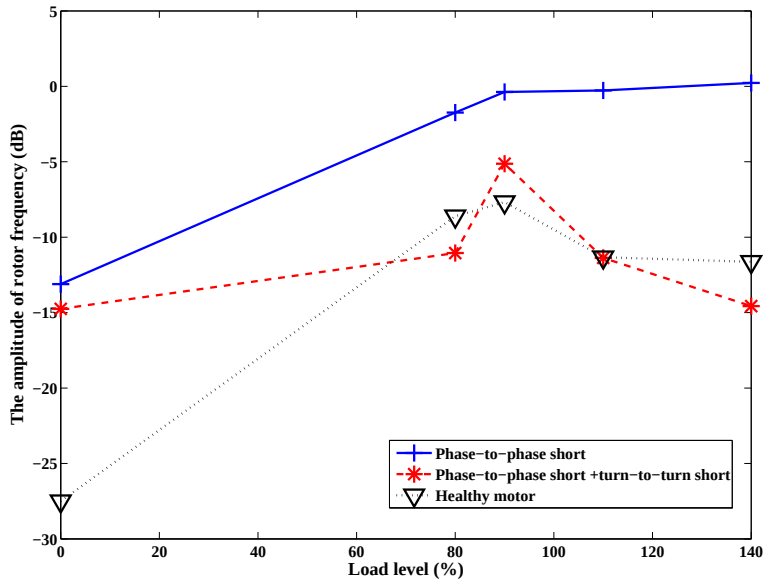


**Figure 5.13.** The amplitude of rotor frequency under different load levels.

The comparison of a turn-to-turn fault and a phase-to-phase fault test results are presented in Figure 5.14. As expected in theory, the amplitude of the fault frequency (when $k = 1$ in equation (5.1)) of a phase-to-phase short circuit is higher than that for a turn-to-turn fault even when the motor runs with high load level. In addition, the amplitudes of the fault frequencies climb significantly in these three conditions. However, there are slight fluctuations when the healthy motor and the motor with a turn-to-turn short circuit fault run between 90% and 110% load level.

The two kinds of serious faults' testing results are also compared in Figure 5.15. The amplitudes of the fault frequencies (when $k = 1$ in equation (5.1)) of a serious phase-to-phase short circuit fault are higher than those of a serious turn-to-turn short circuit fault. When the motor operates without load, the amplitude of the fault frequency of the healthy motor is the lowest. The amplitude of frequency of the serious phase-to-phase short circuit is higher than that for the healthy motor when the motor operates below 70% of the full load level.

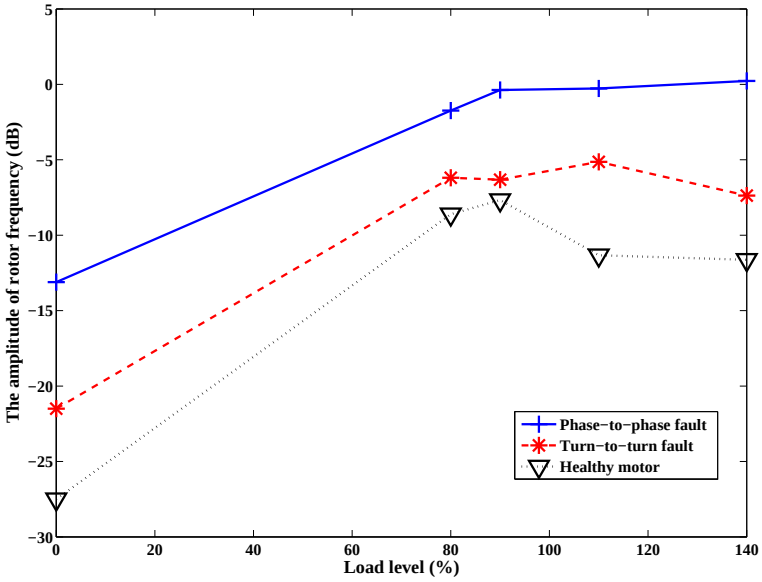


**Figure 5.14.** The amplitude of rotor frequency of phase-to-phase fault and turn-to-turn fault under different load levels.

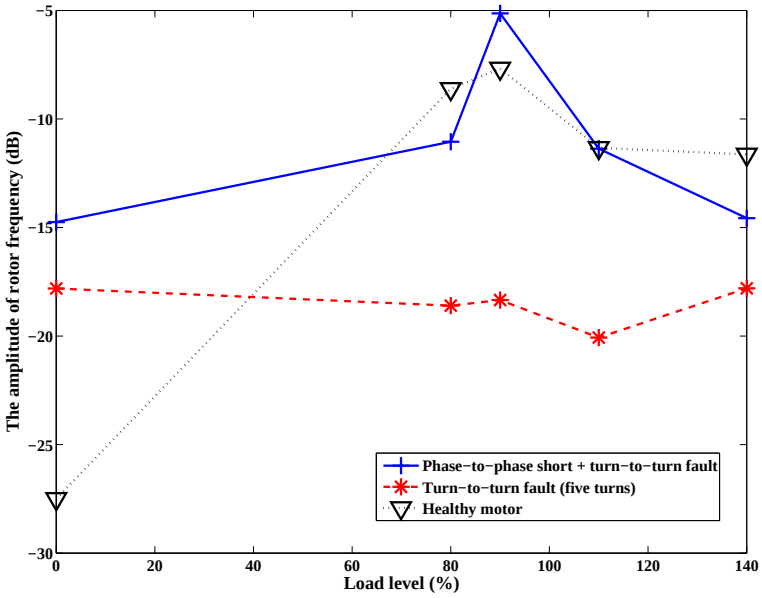


**Figure 5.15.** The amplitude of rotor frequency of serious faults under different load level.

## 5.5 On-line Test of Stator Short Circuit Faults

The on-line testing system is described in the section 5.2. During the test, the motor operating parameters are recorded by the ZCT signal converter device and processed by Labview.

### 5.5.1 Analysis of Turn-to-turn Fault of Motor II

For the turn-to-turn short circuit experiment, the insulation of three points in two adjacent turns of the same coil is scratched. Then, three wires are soldered to these three points. Through a control box, artificial turn-to-turn faults are simulated. Figure 5.16 and 5.17 show the results for wires shorted directly and wires connected via a 5.88 kΩ resistance. Figure 5.16 reveals that when the torque level is equal to zero, the amplitude of the no fault motor is the lowest and the amplitude of wire 1 and wire 3 short circuit without resistance is the highest. Due to the noise caused by a high load level, there is obvious fluctuation for the amplitude of the stator short circuit without resistance except or the wire 1 and wire 2 short circuit and wire 1 and wire 3 short circuit. Furthermore, for all fault condition the amplitude values go down after fluctuation as the load level increases. In addition, when the load level is zero, the resistance, added in the stator short circuit, decreases the amplitude of the wire 1 and wire 3 short circuit by nearly 10 dB. However, the amplitude of the wire 2 and wire 3 short circuit is still higher than the wire 1 and wire 2 short circuit.

The amplitude fluctuation is obvious in the phase-phase stator short circuit without resistance, as shown in Figure 5.18. In Figure 5.19, the amplitude of the no fault motor is lower than the two conditions of stator short circuit even at high torque level. The amplitude of the phase 1-2 and phase 2-1 short circuit is lower than that for the phase 1-1 and phase 2-1 short circuit except when the torque level is at zero. Comparing Figure 5.18 with 5.19, we can conclude that the resistance effect on the phase-to-phase stator short circuit is more significant in Motor II.

Temperature monitoring is another effective method to monitor the motor operating state. Increased temperature could be related to overload, high environment temperature or motor faults, such as a stator short circuit. The high temperature in a motor

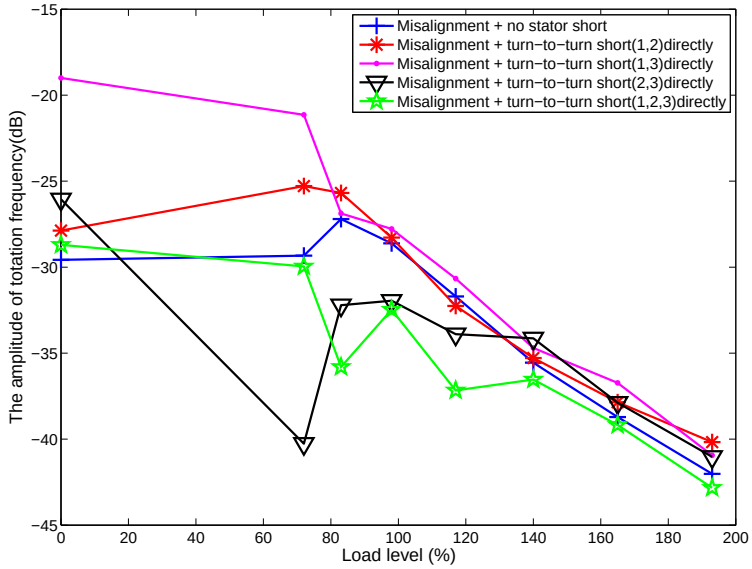


**Figure 5.16.** Comparison of testing results of turn-to-turn stator short circuit without resistance.

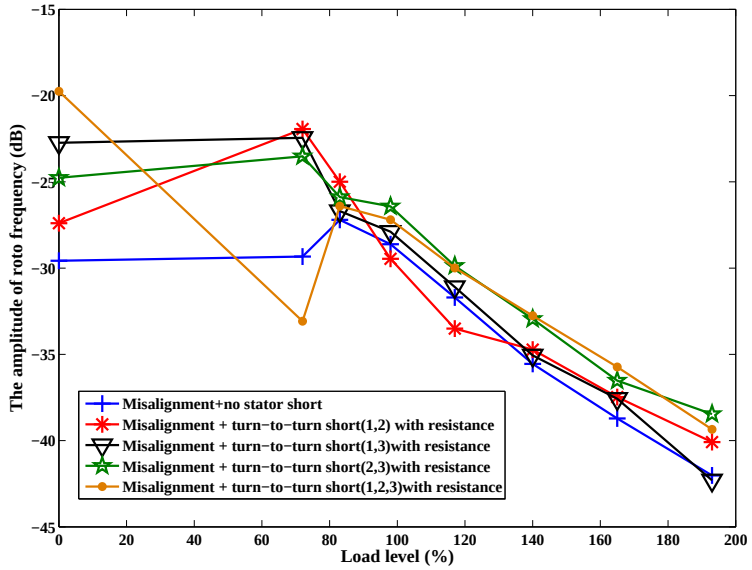


**Figure 5.17.** Comparison of testing results of turn-to-turn stator short circuit with resistance.

could also reduce the insulation life and result in a permanent failure.

Figure 5.20 illustrates the motor temperature during a stator turn-to-turn short circuit fault without resistance. The temperature with the 82.24% load increases more sharply compared to the motor without load. The temperature with 82.84% load arrived at 95°C in 13 min. For the motor in our lab, the temperature tolerance is 150°C. If the temperature exceeds 150°C, the insulation could be damaged.

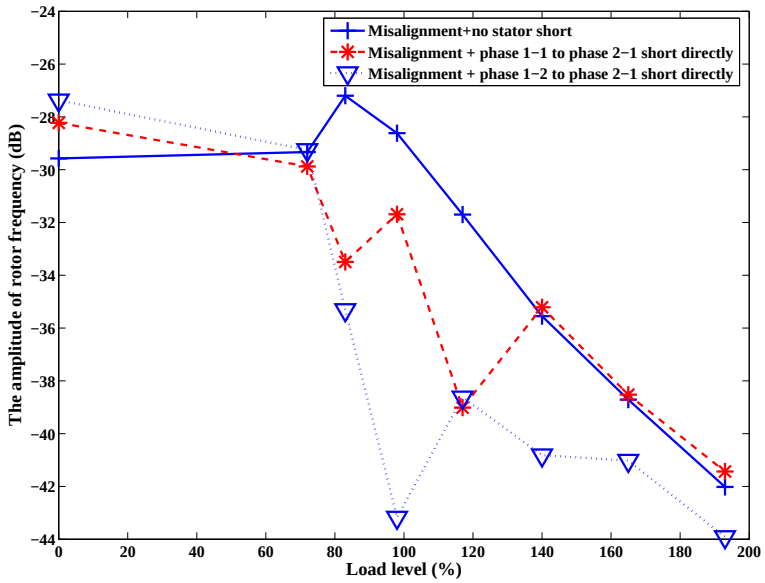


**Figure 5.18.** Comparison of testing results of phase-to-phase stator short circuit without resistance.

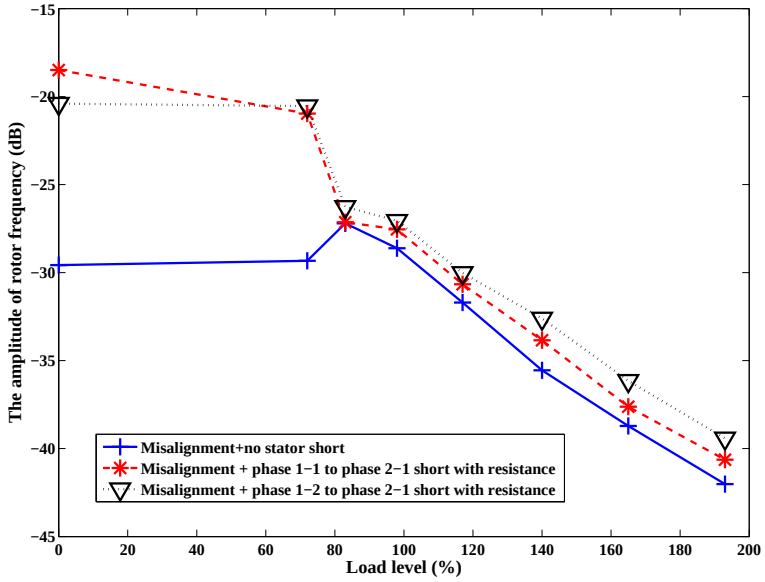


**Figure 5.19.** Comparison of testing results of phase-to-phase stator short circuit with resistance.

## 5.6 Summary

The experimental results are in good agreement with the theoretical calculations. Through the analysis of the current or the ZCT signal, a stator short circuit fault can be detected in both the off-line and on-line test. In addition, temperature monitoring can also be considered as a supplementary method to monitor the motor operating condition.

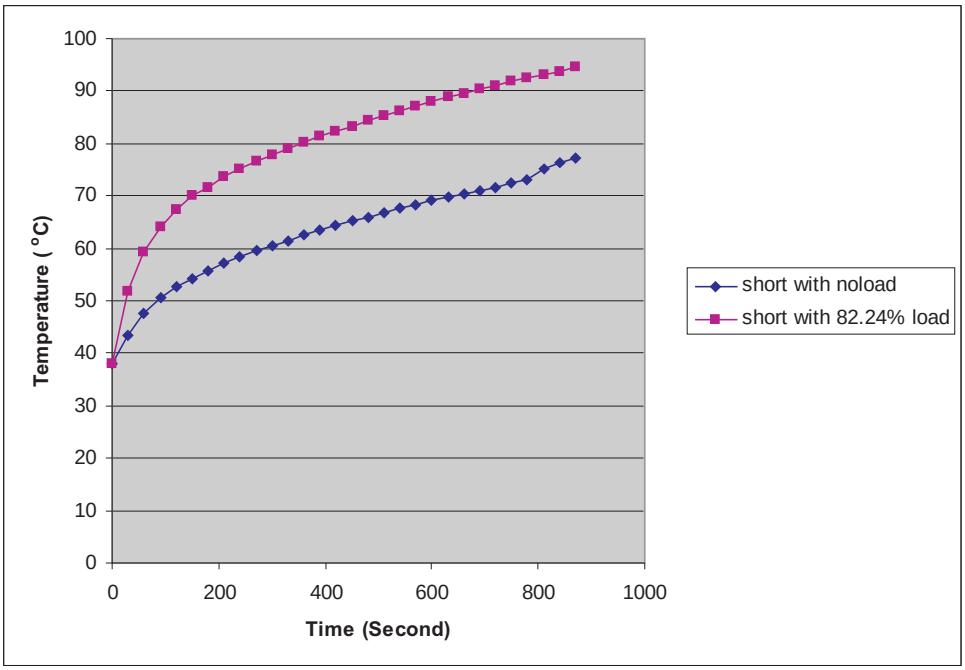


**Figure 5.20.** Temperature of turn-to-turn short circuit fault.

# Chapter 6

# Broken Rotor Bar Fault

TWO techniques, MCSA and ZCT are implemented to diagnose induction motor broken rotor bar faults. Through comparison of their results, the ZCT method is verified as an effective approach.

## 6.1 Introduction

Rotor bar faults occupy about 10% of overall fault conditions in an induction motor. It is usually caused by the poor operating conditions such as high temperatures, high mechanical loading especially in the starting time [32]. In addition, the problems of the manufacturing process, like defective casting, or poor jointing can also cause rotor broken bars. Initially, these problems were presented as an increase of resistance and temperature. Then they progressed as cracking or small holes in the rotor bars. The rotor bars which are near the cage end rings are vulnerable.

In this section, the data of a symmetrical motor and a motor with a broken rotor bars fault were provided by laboratory of the Cracow University of Technology. The motor parameters and the test data are shown in Appendices D and E, respectively.

## 6.2 Broken Rotor Bar Fault Detection Techniques

The frequency components that are related to a broken rotor bar $(BRB)$ condition for slip $s$ [10] are

$$f_{BRB} = (1 \pm 2ks) f_0 \tag{6.1}$$

where $k = 1, 2, 3, 4, ....$

Dominant $BRB$ frequencies $(k = 1)$ are very close to the fundamental frequency $f_0$, and this combined with low signal to noise ratio makes the task of detecting a $BRB$ condition difficult. If the load is time-varying the spectral estimation should be done using a very short data window. Methods based on the Discrete Fourier Transform $(DFT)$ are not able to detect frequencies close to the fundamental when using a very short data window. By monitoring spacing between successive zero crossings, the ZCT method could increase the detection accuracy.

## 6.3 Analysis of Broken Rotor Bars

The detection for the following cases with different load levels are carried out:

**Table 6.1.** Motor parameters.

| Parameter | Value |
|---|---|
| Active power $P_N[kW]$ | 0.8 |
| Nominal voltage $UN[V]$ | 380 |
| Nominal current $[A]$ | 2.2 |
| Nominal power factor $\cos\varphi$ | 0.74 |
| Rotor speed $[rpm]$ | 1400 |
| No load speed $[rpm]$ | 1497 |
| Winding connection | Y |
| Number of poles per phase winding $p$ | 2 |
| Nominal frequency $[Hz]$ | 50 |
| Number of rotor bars | 22 |
| Number of stator slots | 24 |
| Rotor inertia $[kg * m^2]$ | 0.0025 |
| Coil number per phase | 4 |
| Turn number of coil | 90 |

A) symmetrical motor

B) one broken rotor bar

C) two broken rotor bars

D) three broken rotor bars

The parameters of the motor, which is used in the laboratory are listed in the Table 6.1.

Current and ZCT signals are recorded for the symmetrical motor with a 81.36% load level. The FFT results are shown in Figures 6.1 and 6.2. The current signal and its spectra are presented on the top of Figure 6.1. The ZCT signals of the current signals are computed by MATLAB and plotted in the bottom of Figure 6.1. The synchronous speed is 1500 $rpm$. For the rotor measurement speed of 1450 $rpm$, the slip can be calculated as $s = (1500 - 1450)/1500 = 0.033$. The peak is presented in ZCT spectra of Figure 6.1 and the amplitude of this peak is very low. Figure 6.2 shows the ZCT signal, which is acquired directly in the monitoring process. According to Figures 6.1 and 6.2, there are no obvious peaks appearing at sideband frequencies $(1 \pm 2s)f_0$. Therefore,

we can regard this motor is running under normal conditions.

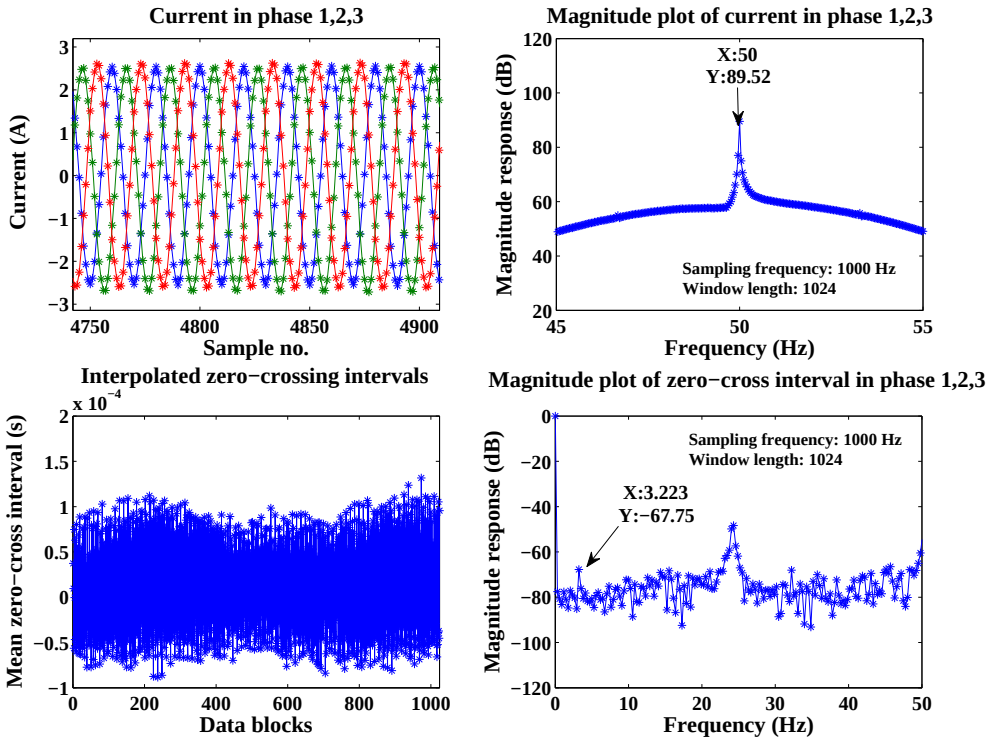


**Figure 6.1.** Current and ZCT signal from healthy motor (81.36% load level).

Figure 6.3 shows the symmetrical motor detection results when the load current is at 2.23 A (101.36% load level). The current data and ZCT signal spectra are computed by MATLAB. When the load current of the symmetrical motor is 2.23 A, the rotor speed is measured as 1419 $rpm$. The slip can be calculated as $s = (1500 - 1419)/1500 = 0.054$. The $2sf$ peak is revealed in the ZCT spectra of Figure 6.3. Figure 6.4 shows the analysis from the ZCT signal directly acquired during the test. Although there is no broken bar fault, there are small peaks appearing at sideband frequencies $(1 \pm 2s)f$ in the current spectra of Figure 6.3. The possible reason is that there is a slight crack in the rotor bar.

For the case shown in Figure 6.5, there is one artificial broken rotor bar in the test motor, the measured rotor speed is 1394 $rpm$. Then, the slip value is $s = (1500 - 1394)/1500 = 0.07067$ and the $2sf = 100s = 7.067$ Hz. Figure 6.5 illustrates that peaks appear at sideband frequencies $(1 \pm 2s)f$ in the current spectra and the $2sf$ peak is showed in the ZCT spectra, corresponding to the computed $2sf$. The $2sf$ peak appears in the directly recorded ZCT signal in Figure 6.6 the same as in the computed ZCT in Figure 6.5. The

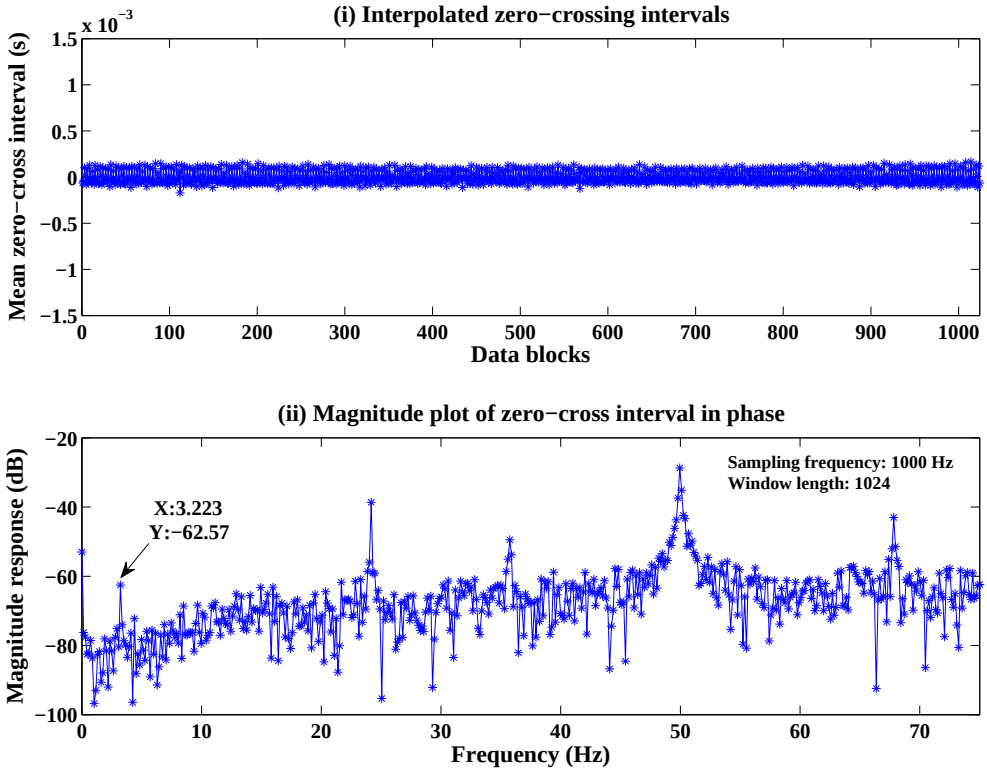


**Figure 6.2.** Direct recorded ZCT signal from healthy motor (81.36% load level).

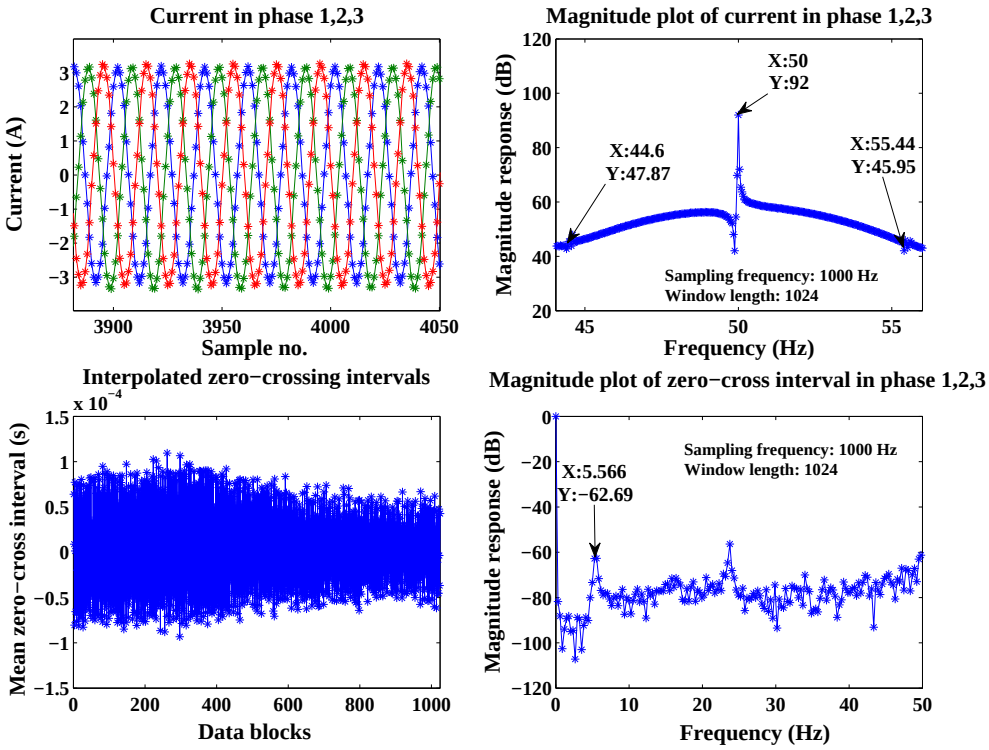


**Figure 6.3.** Current and ZCT signal from healthy motor (101.36% load level).

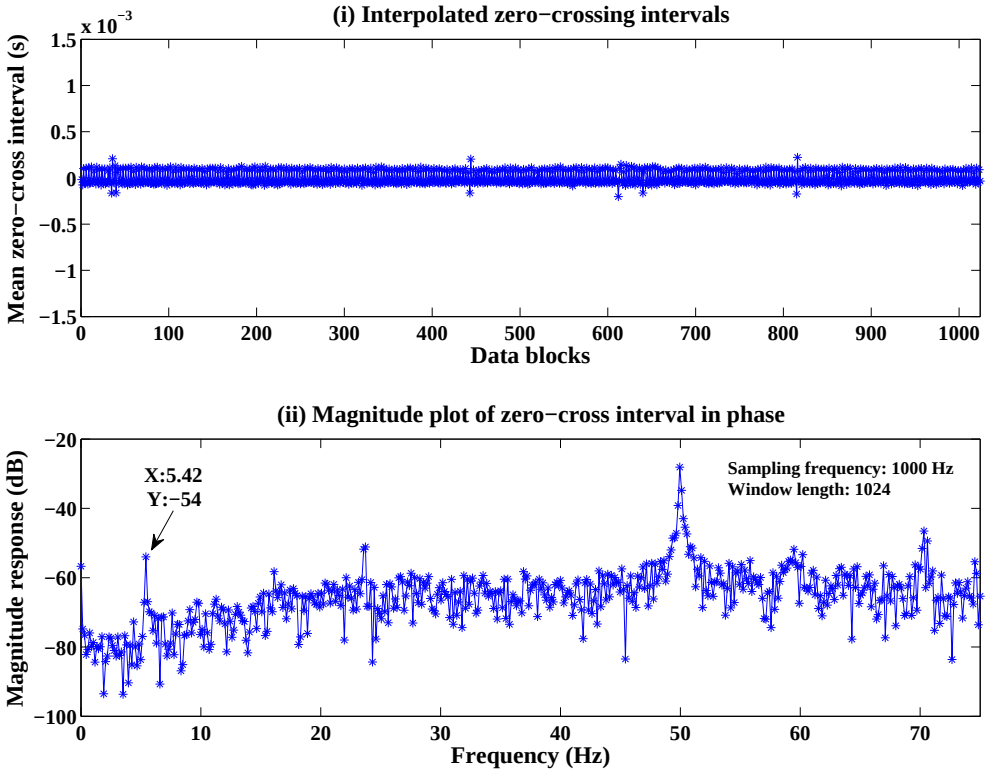


**Figure 6.4.** Direct recorded ZCT signal from healthy motor (101.36% load level).

magnitude of $2sf$ of the directly recorded ZCT signal is 4 dB higher than that of the calculated ZCT signal under the same sampling frequency (1000 Hz) and window length (1024). The second harmonic $2sf$ could also be observed in Figure 6.6. There are a few glitches in the ZCT measurement in the top plot of Figure 6.6. This may result from the small interruption during the measurement. However, these do not affect the $2sf$ peak detection.

The test results of the two artificial broken rotor bars fault are illustrated in Figure 6.7 and 6.8. The rotor speed is 1415 $rpm$. According to equation ( 6.1), the computed slip is 0.0567. Thus, $2sf$ is equal to 5.67 Hz. In Figure 6.7, the two peaks of the sideband frequencies $(1 \pm 2s)f$ are showed in the current spectra and the $2sf$ peak is showed in the ZCT spectra. The $2sf$ peak and second harmonic peak of the directly recorded ZCT signal are also observed in Figure 6.8.

The signals acquired directly from the ZCT signal converter are summarized in the following tables. Table 6.2 illustrates the measurement results of the symmetrical motor with different load levels. Tables 6.3, 6.4 and 6.5 present the measurement results of the

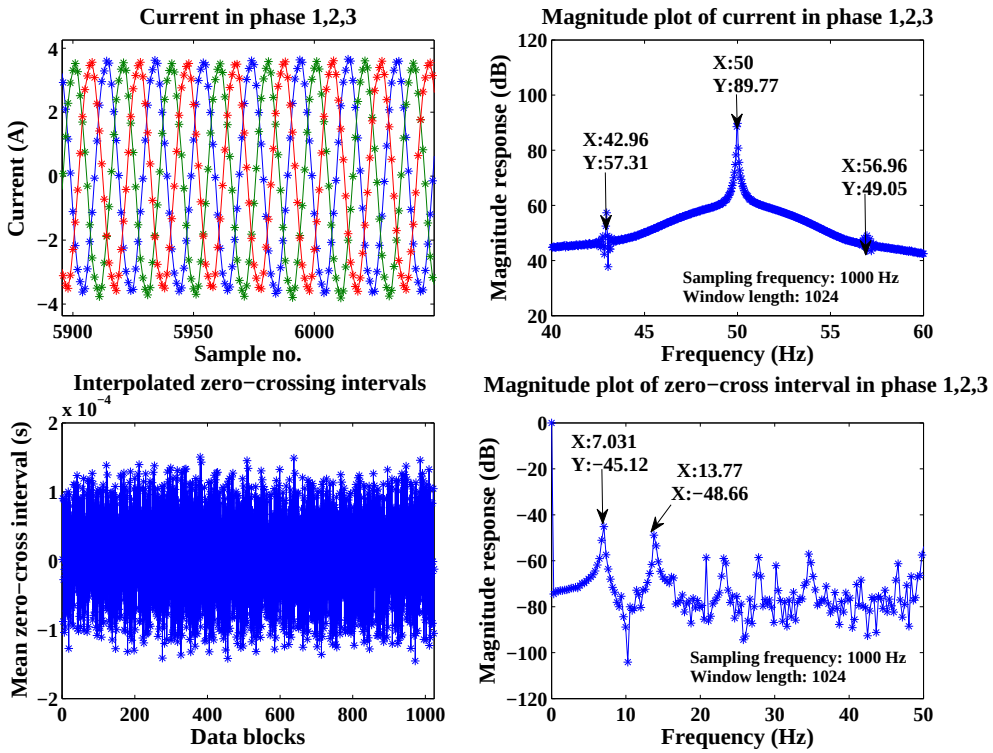


**Figure 6.5.** Current and ZCT signal from motor with one $BRB$.

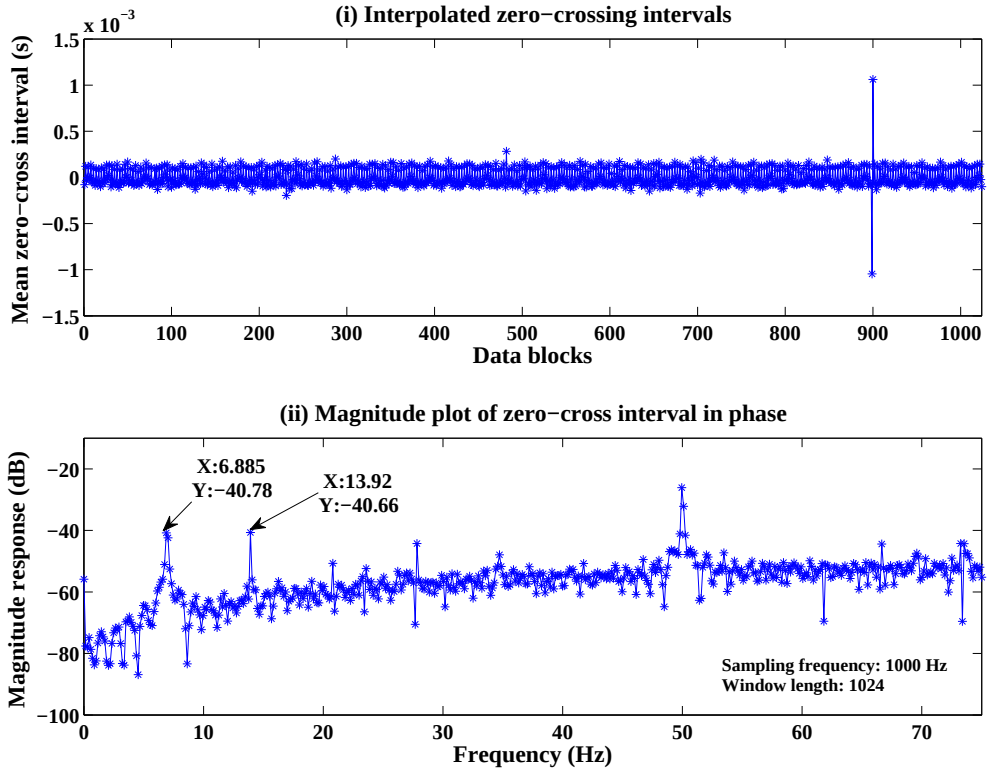


**Figure 6.6.** Direct recorded ZCT signal from motor with one $BRB$.

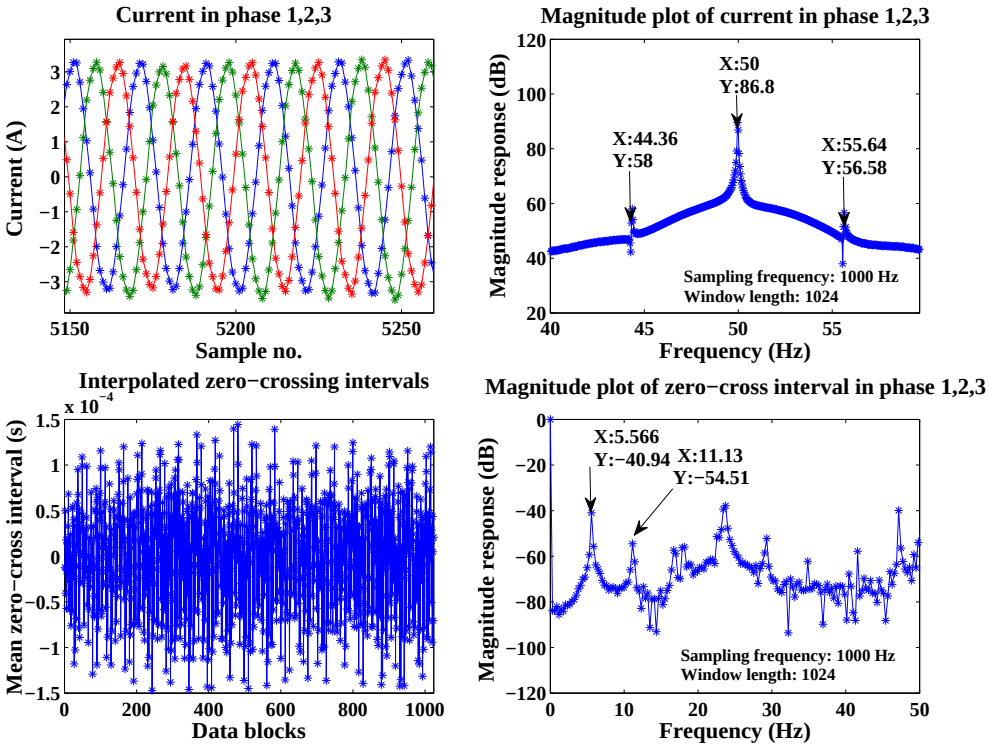


**Figure 6.7.** Current and ZCT signal from motor with two $BRB$.

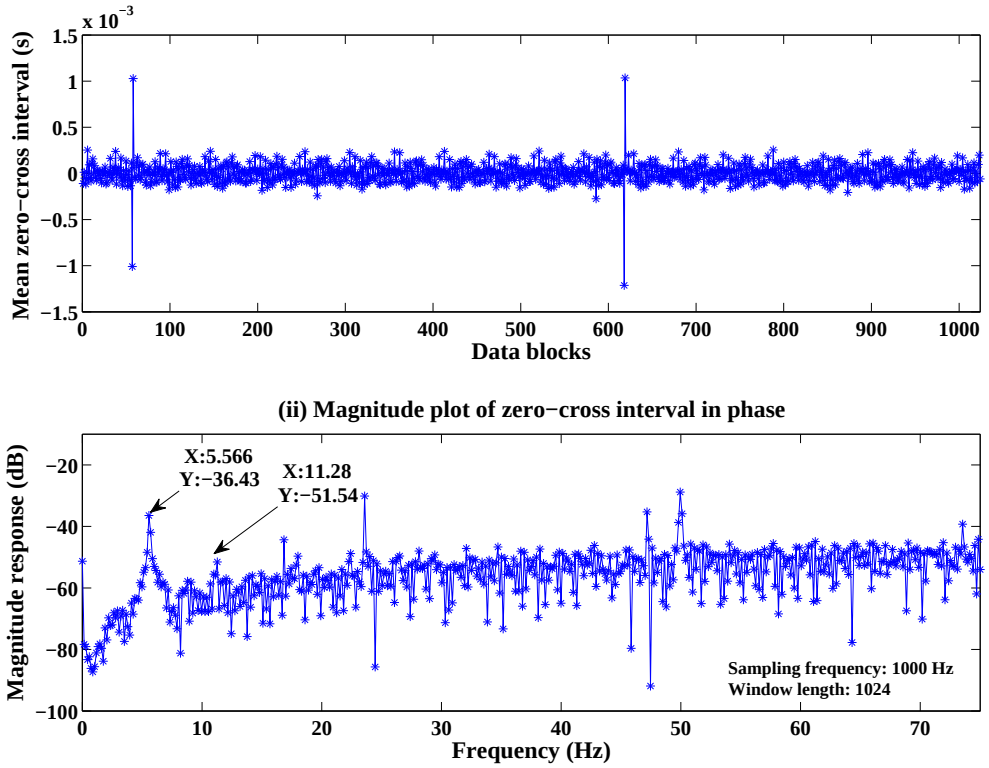


**Figure 6.8.** Direct recorded ZCT signal from motor with two $BRB$.

**Table 6.2.** Symmetrical motor measurement results.

| Measured data file Name | Slip | Loading (%) | 2sf (Hz) | Peak value (Hz) (ZCT extraction) | Peak value (dB) (ZCT extraction) | Peak value (Hz) (ZCT acquired directly) | Peak value (dB) (ZCT acquired directly) | Average rotor speed ($rpm$) |
|---|---|---|---|---|---|---|---|---|
| S1_002.dat | 0.03333 | 81.3636 | 3.333 | 3.2227 | -67.7536 | 3.2227 | -62.5701 | 1450 |
| S1_003.dat | 0.04333 | 90.9091 | 4.333 | 4.3945 | -66.5511 | 4.248 | -58.8159 | 1435 |
| S1_004.dat | 0.054 | 101.3636 | 5.4 | 5.5664 | -62.6907 | 5.4199 | -54.0002 | 1419 |
| S1_005.dat | 0.066 | 112.7273 | 6.6 | 6.4453 | -60.4214 | 6.5918 | -51.6884 | 1401 |

**Table 6.3.** One broken rotor bar fault measurement results.

| Measured data file Name | Slip | Loading (%) | 2sf (Hz) | Peak value (Hz) (ZCT extraction) | Peak value (dB) (ZCT extraction) | Peak value (Hz) (ZCT acquired directly) | Peak value (dB) (ZCT acquired directly) | Average rotor speed ($rpm$) |
|---|---|---|---|---|---|---|---|---|
| S1_007.dat | 0.03267 | 82.2727 | 3.267 | 3.2227 | -56.4234 | 6.4453 | -49.9055 | 1451 |
| S1_008.dat | 0.048 | 95.4545 | 4.8 | 4.6875 | -49.8731 | 4.6875 | -44.4785 | 1428 |
| S1_009.dat | 0.058 | 105 | 5.8 | 5.859 | -47.61 | 5.8594 | -40.6925 | 1413 |
| S1_010.dat | 0.07067 | 115.9091 | 7.067 | 7.031 | -39.32 | 6.8848 | -40.7818 | 1394 |

motor with one $BRB$, two $BRB$s and three $BRB$s at different load levels, respectively. From the tables, we can find that there is not a big difference between the extracted ZCT signal from current signal by MATLAB and the directly acquired ZCT signal. The amplitude of $2sf$ increases in these four states when the load level rises.

The slip variation of the symmetric motor and the motor with one, two and three $BRB$ faults is represented in Figure 6.9. Under these four conditions, the value of the slip increases with an increase in the load level. In theory, the more broken bars appear, the larger slip will be observed. However, the slip of one broken rotor bar fault is bigger than that of two broken rotor bars when the load level is bigger than 85% load level. Furthermore, the slip of one broken rotor bar fault should be bigger than that of a healthy motor. On the contrary, the smallest slip value of one broken rotor bar fault

**Table 6.4.** Two broken rotor bar fault measurement results.

| Measured data file Name | Slip | Loading (%) | 2sf (Hz) | Peak value (Hz) (ZCT extraction) | Peak value (dB) (ZCT extraction) | Peak value (Hz) (ZCT acquired directly) | Peak value (dB) (ZCT acquired directly) | Average rotor speed $(rpm)$ |
|---|---|---|---|---|---|---|---|---|
| S1_012.dat | 0.03467 | 85 | 3.467 | 3.5156 | -53.234 | 3.3692 | -44.4412 | 1448 |
| S1_013.dat | 0.046 | 95 | 4.6 | 4.3945 | -48.6896 | 4.541 | -38.3987 | 1431 |
| S1_014.dat | 0.05667 | 105 | 5.667 | 5.5664 | -40.937 | 5.5664 | -36.4333 | 1415 |
| S1_015.dat | 0.068 | 115.9091 | 6.8 | 6.7383 | -38.0139 | 6.7383 | -33.2382 | 1398 |

**Table 6.5.** Three broken rotor bar fault measurement results.

| Measured data file Name | Slip | Loading (%) | 2sf (Hz) | Peak value (Hz) (ZCT extraction) | Peak value (dB) (ZCT extraction) | Peak value (Hz) (ZCT acquired directly) | Peak value (dB) (ZCT acquired directly) | Average rotor speed $(rpm)$ |
|---|---|---|---|---|---|---|---|---|
| S1_017.dat | 0.036 | 82.2727 | 3.6 | 3.5156 | -54.5292 | 3.51565 | -50.3325 | 1446 |
| S1_018.dat | 0.05067 | 95 | 5.067 | 4.9805 | -44.55 | 4.98045 | -41.9625 | 1424 |
| S1_019.dat | 0.06 | 103.1818 | 6 | 5.8594 | -46.6981 | 6.00585 | -40.86 | 1410 |
| S1_020.dat | 0.07267 | 114.0909 | 7.267 | 7.3242 | -45.502 | 7.17775 | -36.7028 | 1391 |

is obtained under 80% load level. The abnormal behavior of one broken rotor bar slip illustrates there might be some problems in the rotor speed measurement.

Figure 6.10 represents a comparison of the variation of the $2sf$ peaks magnitude when the motor runs in the different fault conditions at several load levels. The increasing load level leads to an increase in frequency amplitude at $2sf$ peaks under all motor running conditions. According to Figure 6.10, the rotor broken bars fault could be diagnosed by monitoring the $2sf$ peaks amplitude [47].

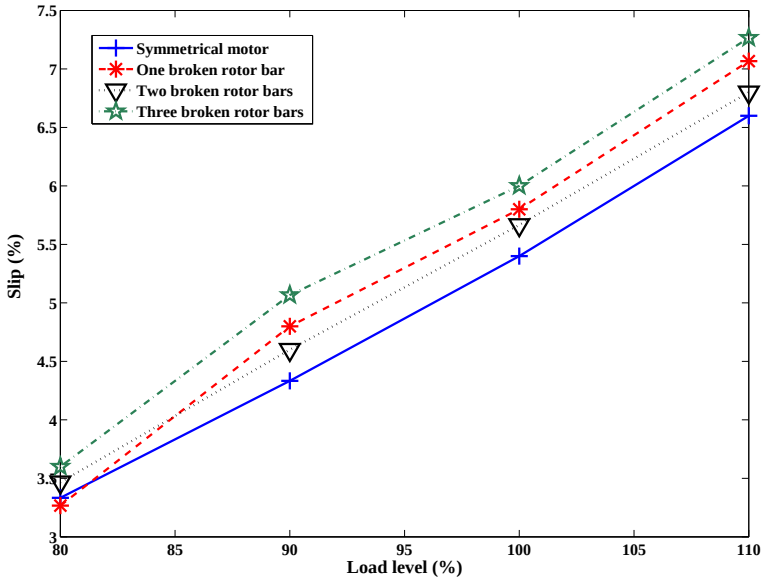


**Figure 6.9.** The relationship between slip and load level.

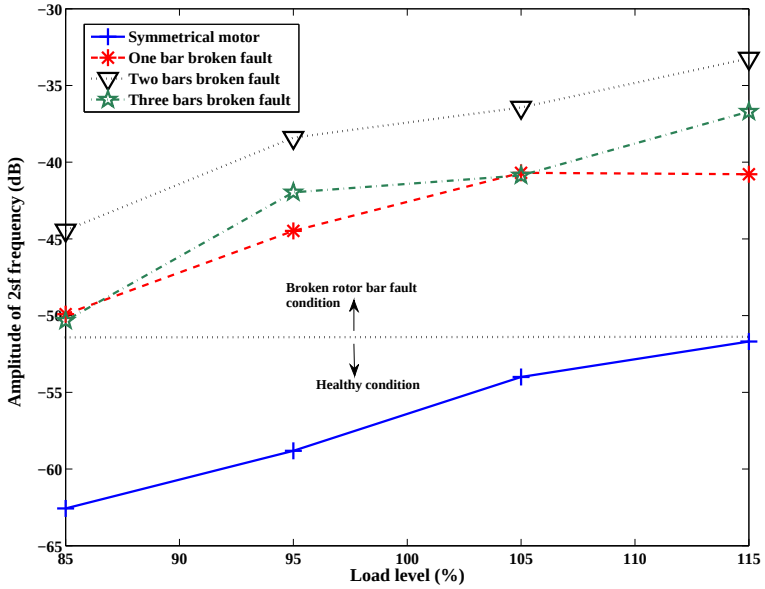


**Figure 6.10.** The relationship between the amplitude of rotor frequency and load level.

## 6.4 Summary

Different numbers of rotor broken bars are studied with several load levels. The faults are analyzed and diagnosed by using the current signal and two ZCT signals, one computed by MATLAB from the current signal and another acquired directly from the ZCT signal converter device. The peaks of the $(1 \pm 2s)f$ sideband frequencies are very close to the fundamental frequency and difficult to be represented in the current spectra. In

contrast, the ZCT method, which diagnoses $BRB$ by monitoring the $2sf$ peak, is an effective approach. Even if there is a small fault, the $2sf$ peaks are represented in the zero crossing time signal. In our experiments, the magnitude of $2sf$ of the directly acquired ZCT signal was higher than that of the calculated ZCT signal.

# Chapter 7

# Thesis Summary and Recommendation for Future Work

## 7.1 Thesis Summary

Two steady-state fault detection methods, MCSA and ZCT, have been utilized to diagnose stator short circuit faults and broken rotor bar faults. After a literature review of these two common faults and two commonly used diagnosis methods, the baseline analysis was performed using two healthy motors. Through the baseline study, signal processing programs, using MATLAB and LabVIEW, the motor healthy states are verified to ensure the accurate diagnosis of motor faults.

Motor misalignment is tested and adjusted by using the Laser Alignment system. The experimental results show that improper motor installation will affect motor fault diagnosis. For example, a coupling gap can lead to an unexpected frequency peak; misalignment will increase the amplitude of the fault frequency in a stator short circuit fault at low load levels. Improper motor installation, combined with manufacture tolerance and working environment, may lead to an unexpected difference in motors of the same type. This will decrease the accuracy of motor faults diagnosis.

Based on these preparations, motor stator short circuit faults are comprehensively studied by using both off-line and on-line tests. Through a control box, artificial turn-to-turn faults and phase-to-phase faults are simulated. Furthermore, the experiments are implemented under different load levels. The experimental results are in good agreement with the theoretical calculations. Compared with the conventional MCSA

method, the ZCT method has the advantages of lower sampling rate and lower computational burden. In the experiments, the ZCT method shows frequency components, which are related to motor faults. In others words, the accuracy of the ZCT method is comparable to the conventional MCSA.

In addition, these two method are also used to analysis recorded stator current data provided by the machine laboratory of the Cracow University of Technology. The data includes stator current of a symmetrical motor and motor with broken rotor bars fault. The results show that the ZCT method can be used reliably for detecting broken rotor bars faults.

## 7.2 Future Work

Most work in this thesis is from the experimental point of view. The recorded stator circuit data is analyzed using MCSA and ZCT methods to diagnose stator short circuit faults and broken rotor bar faults. FFT is the main and only type of analysis method used in this work. The study can be expanded further by employing similar or more advanced signal processing techniques such as wavelet transforms. Some parametric spectrum analysis methods as well as that of modern non-parametric techniques might reveal more useful information and enable easier fault diction. These methods might automatically detect faults and allow for better diagnostic of faults. Furthermore, some pattern recognition techniques, such as principal component analysis (PCA) and independent component analysis (ICA), could reveal ”hidden” components of the ZCT signals, which can improve the analysis of motor current signals. Moreover, the investigation can be undertaken different types of induction motors with different ratings. In addition, the further simulation work could enhance the understanding of significant frequencies related to the induction motor faults and improve the overall effectiveness of the fault detection.

# References


[1] C. I. Hubert, *Electric machines: theory, operation, applications, adjustment and control*. Merrill, 1991, ch. 2.

[2] C. Ong, *Dynamic Simulation of Electric Machinery: Using MATLAB/SIMULINK*. Prentice Hall PTR, 1998, ch. 6.

[3] G. C. Stone, E. A. Boulter, I. Culbert, and H. Dhirani, *Electrical Insulation For Rotating Machines-Design, Evaluation, Aging, Testing and Repair*. IEEE Press and A John Wiley & Sons, INC., 2004, ch. 4.

[4] K. Wang, *Intelligent Condition Monitoring And Diagnosis Systems A Computational Intelligence Approach*. IOS Press, 2003, ch. 3.

[5] Y. Han and Y. Song, "Condition monitoring techniques for electrical equipment - a literature survey," *Power Delivery, IEEE Transactions on*, vol. 18, no. 1, pp. 4–13, Jan 2003.

[6] G. Singh and S. A. Kazzaz, "Induction machine drive condition monitoring and diagnostic research - a survey," *Electric Power Systems Research*, vol. 64, pp. 145–158, 2003.

[7] J. Faiz and M. Ojaghi, "Different indexes for eccentricity faults diagnosis in three-phase squirrel-cage induction motors: A review," *Mechatronics*, vol. 19, no. 1, pp. 2–13, 2009.

[8] S. Nandi, H. A. Toliyat, and X. Li, "Condition monitoring and fault diagnosis of electrical motors - a review," *IEEE Transactions on Energy Conversion*, vol. 20, no. 4, pp. 719 – 729, 2005.

[9] W. Deleroi, "Squirrel cage motor with broken bar in the rotor -physical phenomena and their experimental assessment," in *International Conference on Emergency Medicine (ICEM 1982)*, Budapest, Hungary, 1982, pp. 767–770.

[10] N. Elkasabgy, A. Eastham, and G. Dawson, "Detection of broken bars in the cage rotor on an induction machine," *Industry Applications, IEEE Transactions on*, vol. 28, no. 1, pp. 165 –171, Jan. 1992.

[11] J.-H. Jung, J.-J. Lee, and B.-H. Kwon, "Online Diagnosis of Induction Motors Using MCSA," *Industrial Electronics, IEEE Transactions on*, vol. 53, no. 6, pp. 1842 –1852, Dec. 2006.

[12] M. Benbouzid, "A review of induction motors signature analysis as a medium for faults detection," in *Proceedings of the 24th Annual Conference of the IEEE Industrial Electronics Society, 1998. IECON '98*, vol. 4, 1998, pp. 1950 –1955.

[13] G. Kliman, R. Koegl, J. Stein, R. Endicott, and M. Madden, "Noninvasive detection of broken rotor bars in operating induction motors," *IEEE Transactions on Energy Conversion*, vol. 3, no. 4, pp. 873 –879, Dec. 1988.

[14] A. Bellini, F. Filippetti, G. Franceschini, C. Tassoni, and G. Kliman, "Quantitative evaluation of induction motor broken bars by means of electrical signature analysis," *IEEE Transactions on Industry Applications*, vol. 37, pp. 1248 –1255, Sep. 2001.

[15] B. Gaydon, "Instrument to detect induction motor rotor circuit defects by speed fluctuation measurements." in *International Conference on Advances in Medical Signal and Information Processing*, no. 174, 1979, pp. 5 – 8.

[16] F. Filippetti, G. Franceschini, C. Tassoni, and P. Vas, "Ai techniques in induction machines diagnosis including the speed ripple effect," *IEEE Transactions on Industry Applications*, vol. 34, no. 1, pp. 98 –108, Jan. 1998.

[17] A. Sadoughi, M. Ebrahimi, and E. Razaei, "A new approach for induction motor broken bar diagnosis by using vibration spectrum," in *International Joint Conference SICE-ICASE, 2006.*, Oct. 2006, pp. 4715 –4720.

[18] K. Cho, J. Lang, and S. Umans, "Detection of broken rotor bars in induction motors using state and parameter estimation," *IEEE Transactions on Industry Applications*, vol. 28, no. 3, pp. 702 –709, May 1992.

[19] M. G. Melero, M. F. Cabanas, F. R. Faya, C. H. Rojas, and J. Solares, "Electromagnetic torque harmonics for on-line inter turn short circuits detection in squirrel cage induction motors," in *8th European Conf. on Power Electronics and Appl. EPE, Lausanne, Switzerland*, Sep 1999, p. 9.

[20] D. Dorrell, W. Thomson, and S. Roach, "Analysis of airgap flux, current, and vibration signals as a function of the combination of static and dynamic airgap eccentricity in 3-phase induction motors," *IEEE Transactions on Industry Applications*, vol. 33, no. 1, pp. 24 –34, Jan 1997.

[21] S. Fruechtenicht, E. Pittius, and H. Seinsch, "Diagnostic system for three-phase asynchronous machines," in *International Conference on Advances in Medical Signal and Information Processing*, no. 310, 1989, pp. 163 – 171.

[22] A. Siddique, G. Yadava, and B. Singh, "A review of stator fault monitoring techniques of induction motors," *IEEE Transactions on Energy Conversion*, vol. 20, no. 1, pp. 106–114, March 2005.

[23] H. Su and K. T. Chong, "Induction machine condition monitoring using neural network modeling," *IEEE Transactions on Industrial Electronics*, vol. 54, no. 1, pp. 241–249, Feb. 2007.

[24] M. Benbouzid and H. Nejjari, "A simple fuzzy logic approach for induction motors stator condition monitoring," in *IEEE International Electric Machines and Drives Conference, IEMDC*, 2001, pp. 634–639.

[25] B. Ayhan, M.-Y. Chow, and M.-H. Song, "Multiple discriminant analysis and neural-network-based monolith and partition fault-detection schemes for broken rotor bar in induction motors," *IEEE Transactions on Industrial Electronics*, vol. 53, no. 4, pp. 1298 –1308, June 2006.

[26] L. Cristaldi, M. Lazzaroni, A. Monti, F. Ponci, and F. Zocchi, "A genetic algorithm for fault identification in electrical drives: a comparison with neuro-fuzzy computation," in *Proceedings of the 21st IEEE Instrumentation and Measurement Technology Conference, 2004. IMTC 04.*, vol. 2, May 2004, pp. 1454–1459.

[27] F. Filippetti, G. Franceschini, and T. Carla, "Neural networks aided on-line diagnostics of induction motor rotor faults," in *Conference Record - IAS Annual Meeting (IEEE Industry Applications Society)*, vol. 1, 1993, pp. 316 – 323.

[28] M. Haji and H. Toliyat, "Pattern recognition - a technique for induction machines rotor broken bar detection," *IEEE Transactions on Energy Conversion*, vol. 16, no. 4, pp. 312 –317, Dec. 2001.

[29] A. da Silva, R. Povinelli, and N. Demerdash, "Induction machine broken bar and stator short-circuit fault diagnostics based on three-phase stator current envelopes," *IEEE Transactions on Industrial Electronics*, vol. 55, no. 3, pp. 1310 –1318, March 2008.

[30] P. Vas, *Parameter Estimation, Condition Monitoring, and Diagnosis of Electrical Machines*. Clarendron Press Oxfords, 1993, ch. 3.

[31] W. Thomson and M. Fenger, "Current signature analysis to detect induction motor faults," *IEEE Industry Applications Magazine*, vol. 7, no. 4, pp. 26 –34, Jul/Aug 2001.

[32] H. Çalış and A. Çaklır, "Rotor bar fault diagnosis in three phase induction motors by monitoring fluctuations of motor current zero crossing instants," *Electric Power Systems Research*, vol. 77, no. 5-6, pp. 385–392, 2007.

[33] D. Dorrell, W. Thomson, and S. Roach, "Analysis of airgap flux, current, and vibration signals as a function of the combination of static and dynamic airgap eccentricity in 3-phase induction motors," *IEEE Transactions on Industry Applications*, vol. 33, no. 1, pp. 24–34, Jan. 1997.

[34] W. Thomson, "A review of on-line condition monitoring techniques for three phase squirrel cage induction motors-past, present and future," in *SDEMPED'99, Gijon, Spain,*, vol. 33, no. 1, Sep. 1999, pp. 3–18.

[35] Y. Wang, "The ZCT method of induction motor failure prediction and speed monitoring," Ph.D. dissertation, University of Sussex, England, 1997.

[36] A. Ukil, S. Chen, and A. Andenn, "Detection of stator short circuit faults in three-phase induction motors using motor current zero crossing instants," *Electric Power System Research*, 2009, to be published.

[37] Fixturlaser Company. [Online]. Available: www.fixturlaser.com/products-services/fixturlaser-product-range/fixturlaser-xa-2.aspx

[38] R. N. Brancewell, *The Fourier Transform and Its Applications*, 3rd ed. McGraw-Hill, 2000, ch. 2.

[39] H. Razik, M. B. R. Correa, and E. R. C. Da Silva, "An application of genetic algorithm and fuzzy logic for the induction motor diagnosis," in *34th Annual Conference of IEEE Industrial Electronics, 2008. IECON 2008.*, Nov. 2008, pp. 3067–3072.

[40] R. Puche-Panadero, M. Pineda-Sanchez, M. Riera-Guasp, J. Roger-Folch, E. Hurtado-Perez, and J. Perez-Cruz, "Improved resolution of the MCSA method via Hilbert transform, enabling the diagnosis of rotor asymmetries at very low slip," *IEEE Transactions on Energy Conversion*, vol. 24, no. 1, pp. 52 – 59, 2009.

[41] K. Ohyama, G. Asher, and M. Sumner, "Comparative analysis of experimental performance and stability of sensorless induction motor drives," *IEEE Transactions on Industrial Electronics*, vol. 53, no. 1, pp. 178 – 186, Feb. 2005.

[42] *Manual for low Voltage Motors*, ABB, 2004.

[43] S. Chaudhury and S. Gupta, "Online Identification Of AC Motor Misalignment Using Current Signature Analysis and Modified K-Mean Clustering Technique," in *Industrial Technology, 2006. ICIT 2006. IEEE International Conference on*, Dec. 2006, pp. 2331 –2336.

[44] M. E. Brumbach and J. A. Clade, *Industrial Machines*. Thomson Delmar Learning, Inc., 2003, ch. 4.

[45] A. Bonnett and G. Soukup, "Cause and analysis of stator and rotor failures in three-phase squirrel-cage induction motors," *IEEE Transactions on Industry Applications*, vol. 28, no. 4, pp. 921 –937, Jul. 1992.

[46] G. Joksimovic and J. Penman, "The detection of inter-turn short circuits in the stator windings of operating motors," *IEEE Transactions on Industrial Electronics*, vol. 47, no. 5, pp. 1078 –1084, Oct. 2000.

[47] S. Chen, "Induction motor broken rotor bar diagnostics," ABB, Tech. Rep., Sep. 2008.

# Appendix A

# MATLAB Code

## A.1 Data Analysis Algorithm for Broken Rotor Bar Detection (umc100current.m)

```
% ZCT spectral analysis of Uni Krakow new data for broken bar analysis
% with plot, for real data
% can choose 1 or 3 phase analysis. Use this one!!
% data: S1_001 to S1_020  (change last digit 1,2,3,...,20)
%       S2_001 to S2_020  (change last digit 1,2,3,...,20)


clear all

%data=load('C:\test\Krakow_data\S1\S1_043.dat');
data=csvread('04-11-09-50-20.csv');
downsample=10;              % downsampling factor

N_ph = 3;                   %number of phases for analysis

F_rated = 50;               %fundamental frequency
Fs=1/(data(2,1)-data(1,1)); %Sampling frequency
Fs=Fs/downsample;
disp(['Sampling frequency =' ' ' num2str(Fs) ' ' 'Hz'])

%resample properly
if downsample>1
    filterorder=5; %vary between 2-15
 [b,a] = butter(filterorder,1/downsample);
   %[b,a] =cheby1(filterorder,0.5,1/downsample);
    data=filter(b,a,data);
```

```
end

data=data(1:downsample:end,:);

if N_ph==3
    phase=[1 2 3]; % for three phase ZCT analyiss
elseif N_ph==1
        phase = 1;    %should be 1, 2 or 3
end
index=1:size(data,1);
sig=data(index,phase+1); %data(:,1) is samples, so phase+1 gives phase,
                         %choose Fs samples for having 1 second data


if N_ph==3
    [zcount,zindex,zspace]=zcrinterp3phase(sig,Fs,F_rated); %count=zero-cross count,
                        %index and space intervals between contiguous zero-crossings
elseif N_ph==1
    [zcount,zindex,zspace]=zcrinterp(sig,Fs,F_rated); %count=zero-cross count,
                %index and space intervals between contiguous zero-crossings
end


S=fft(sig(:,1));      %FFT of current signal
Smag=abs(S);          % Magnitude  response of current signal
Smag=20*log10(Smag);  %in dB scale
Smag(1)=0;            %DC correction

fftPoints = 2^10; %FFT of ZCTs, 2^9 uses 512 points
%we use the last portion of the data
zspace = zspace(length(zspace) - fftPoints + 1 : length(zspace));
%zspace=zspace+randn(size(zspace))*50*1e-3;    % with added noise
Z=fft(zspace,fftPoints);
Zmag=abs(Z);          % Magnitude  response of zero-cross intervals
Zmag=20*log10(Zmag);  %in dB scale
Zmag(1)=0;            %DC correction


sN=numel(Smag);
sF=[0:round(sN/2)]/sN*Fs; %Frequency range for current signal
zN=numel(Zmag);
zF=[0:round(zN/2)]/zN*2*N_ph*F_rated;
```

```
            %Whole frequency range for ZCT spectrum is N_ph*2*50 Hz

close all
subplot(221),plot(index,sig,'*-'),title(strcat('Current in phase:',...
      num2str(phase),'; ',num2str(Fs),' Hz sampling freq')),...
      ylabel('Current in A'),xlabel('Sample no.')
subplot(223),plot(zspace,'*-'),title('Interpolated zero-crossing intervals'),...
      ylabel('Mean zero-cross interval (no. of samples)'),xlabel('Data blocks')
subplot(222),plot(sF,Smag(1:numel(sF)),'*-'),title(strcat('Magnitude plot of ...
       current in phase:',num2str(phase),'; ',num2str(numel(S)),' samples')),...
       ylabel('Magnitude response in dB'),xlabel('Frequency in Hz'),xlim([0 100])
subplot(224),plot(zF,Zmag(1:numel(zF)),'*-'),title(strcat('Magnitude plot...
       of zero-cross interval in phase:',num2str(phase),'; ',num2str(zcount),...
       ' samples')), ylabel('Magnitude response in dB'),...
       xlabel('Frequency in Hz'),xlim([0 zF(end)])

%Broken Bar analysis based on zero-cross
sf2_range=10;     % slip range of interest (Hz)
n=round(length(Z)*sf2_range/(2*N_ph*F_rated));  % 10Hz is up to n data points
% here only take the first half to calculate threshold
%beware the length of Z is the actual point of fft. Shuold not use zspace
ZZ=Zmag(2:n); %check for max Zmag in the range 0.1-10 Hz
[max_value,max_index]=max(ZZ);
%threshold=mean(ZZ)+2.5*std(ZZ);
threshold=-67;

disp('[MAX peak in 0-10Hz range     Fixed threshold]')
disp([num2str(ZZ(max_index)) '                          '  num2str(threshold)])


if ZZ(max_index)>threshold
    brb = 1;
    disp('--------- There are broken bars ----------')
else
    disp('################ NO broken rotor bars ################')
    sf2 = 0;
    brb = 0;
end

disp('The following estimations are valid only if the peak is significant,...
                    i.e. above the threshold.')
```

```
sf2=max_index*(N_ph*2*F_rated/zN);    % twice slip frequency 2sf
% length(zspace) point FFT, N_ph*2*F_rated Hz sampling freq for zero crossing
slip=sf2/(2*F_rated);                 % slip
rotor_speed=60*F_rated*(1-slip)/2;         % rotor mechanic speed
disp(['slip =' ' ' num2str(slip) ' '])
disp(['twice slip frequency =' ' ' num2str(sf2) ' ' 'Hz'])
disp(['rotor mechanic speed =' ' ' num2str(rotor_speed) ' ' 'rmp'])


result = [0,max_value,0,threshold,0,sf2,0,brb];
```

## A.2 Single-phase Zero Crossing Times Calculation (umc100zc.m)

```
% ZCT spectral analysis of Mikko motor setup data for broken bar analysis
% with plot, for real data
% can choose 1 or 3 phase analysis. Use this one!!
% data: S1_001 to S1_020  (change last digit 1,2,3,...,20)
%       S2_001 to S2_020  (change last digit 1,2,3,...,20)


clear all
clc

N_ph = 3;                    %number of phases for analysis
F_rated = 50;                %fundamental frequency

%data=dlmread('C:\test\Krakow_data\S1\S1_059.log',';');
data=dlmread('2009-08-04_Bunch1_NoShort_Load_20.txt',';');

zspace=[];

%process columnwise to retrive zct signal
signal=[];
for i=1:size(data,1)
    for j=1:3
        signal(end+1)=data(i,j*2); %get col 2, 4 6
    end
end

%take difference
for i=1:numel(signal)-1
```

```
    temp_zspace=signal(i+1)-signal(i);
    if temp_zspace<0
        temp_zspace=temp_zspace+65536;
    end
    zspace(end+1)=temp_zspace;
end

zspace_ref=5833.33;

fftPoints = 2^10; %FFT of ZCTs, 2^9 uses 512 points
% zspace = zspace(length(zspace) - fftPoints + 1 : length(zspace));
%
% zspace=(zspace-zspace_ref)*(8e-6/7); % make zspace to time


figure(2)
plot(zspace,'*-')
```

## A.3 Three-phase Zero Crossing Time Calculation (zcrinterp3phase.m)

```
function [count,index,space]=zcrinterp3phase(x,f_s,f_rated)
% Function zero-crossing count using interpolation
% [count,index,space]=zcrinterp(x,f_s,f_rated)
% Counts the zero crossings of x in count
% Index of the zero values in index
% Spacings of the zero-indeces in space
%
% Analyze the 3-phase ZCT

count=0;
if size(x,1)<size(x,2)          % if rows > columns
    x=x';
end

%If shifted signal adjust by mean centring
for clom=[1:3]
    x(:,clom)=x(:,clom)-mean(x(:,clom));
end
```

```
index=[];          % unit times at each ZC point
                   % /f_foundamental is the real ZC times
id=size(x);         % id = [rows columns]

for i=1:id(1)-1   % rows
    for k=1:id(2) % columns
        if x(i,k)==0
            index(end+1)=i;   % exact zero
            count=count+1;
        elseif (x(i,k)<=0 & x(i+1,k)>=0) | (x(i,k)>0 & x(i+1,k)<=0)
            index(end+1)=i+x(i,k)/(x(i,k)-x(i+1,k));
            count=count+1;
        end
    end
end

index=index/f_s;
space=[];

if ~isempty(index)
    for i=1:numel(index)-1
        %space(end+1)=index(i+1)-index(i);            % calculate the ZCT
        %space(end+1)=index(i+1)-index(i)-f_s/(6*f_rated);
                                    % subtract the fundamental component
        space(end+1)=index(i+1)-index(i)-1/(6*f_rated);
                                    % subtract the fundamental component
    end
end
```

# Appendix B

# Test Results of Stator Short Faults before Misalignment Adjust

**Table B.1.** Healthy motor

| Load Level | Rotor Frequency (Hz) (20-30) | Amplitude (dB) (20-30) | Measured Speed (rpm) (from drives panel) | Computed speed (rpm) (from rotor peak) | % Slip (from measured speed) | % Slip (from computed speed) | Current (A) (measured by device) | % Current /Nominal (4.9 A) |
|---|---|---|---|---|---|---|---|---|
| noload | 24.97 | -29.58 | 1494.80 | 1497.93 | 0.35 | 0.14 | 3.40 | 69.39 |
| 10% | 24.75 | -29.33 | 1485.10 | 1484.72 | 0.99 | 1.02 | 3.59 | 73.27 |
| 20% | 24.47 | -27.20 | 1472.70 | 1468.25 | 1.82 | 2.12 | 4.11 | 83.88 |
| 30% | 24.27 | -28.62 | 1461.80 | 1456.21 | 2.55 | 2.92 | 4.87 | 99.39 |
| 40% | 24.01 | -31.70 | 1446.80 | 1440.51 | 3.55 | 3.97 | 5.79 | 118.16 |
| 50% | 23.70 | -35.55 | 1430.10 | 1422.04 | 4.66 | 5.20 | 6.88 | 140.41 |
| 60% | 23.34 | -38.71 | 1408.40 | 1400.21 | 6.11 | 6.65 | 8.10 | 165.31 |
| 70% | 23.69 | -42.02 | 1379.80 | 1421.41 | 8.01 | 5.24 | 9.53 | 194.49 |

**Table B.2.** 1,2 short directly

| Load Level | Corrected (Hz) (20-30) | Amplitude (dB) (20-30) | Measured Speed (rpm) (from drives panel) | Computed speed (rpm) (from rotor peak) | % Slip (from measured speed) | % Slip (from computed speed) | Current (A) (measured by device) | % Current /Nominal (4.9 A) |
|---|---|---|---|---|---|---|---|---|
| noload | 24.96 | -27.87 | 1495.00 | 1497.85 | 0.33 | 0.14 | 3.40 | 69.39 |
| 10% | 24.72 | -25.29 | 1484.50 | 1483.01 | 1.03 | 1.13 | 3.63 | 74.08 |
| 20% | 24.51 | -25.69 | 1474.10 | 1470.47 | 1.73 | 1.97 | 4.14 | 84.49 |
| 30% | 24.27 | -28.28 | 1460.90 | 1455.94 | 2.61 | 2.94 | 4.88 | 99.59 |
| 40% | 24.00 | -32.25 | 1447.40 | 1440.14 | 3.51 | 3.99 | 5.81 | 118.57 |
| 50% | 23.69 | -35.28 | 1430.40 | 1421.63 | 4.64 | 5.22 | 6.88 | 140.41 |
| 60% | 23.34 | -37.85 | 1409.10 | 1400.14 | 6.06 | 6.66 | 8.10 | 165.31 |
| 70% | 22.84 | -40.17 | 1381.50 | 1370.54 | 7.90 | 8.63 | 9.52 | 194.29 |

**Table B.3.** 1,2 short with resistance

| Load Level | Rotor Frequency (Hz) (20-30) | Amplitude (dB) (20-30) | Measured Speed (rpm) (from drives panel) | Computed speed (rpm) (from rotor peak) | % Slip (from measured speed) | % Slip (from computed speed) | Current (A) (measured by device) | % Current /Nominal (4.9 A) |
|---|---|---|---|---|---|---|---|---|
| Base-line | 25.00 | -33.61 | | | | | 3.35 | 68.37 |
| noload | 24.97 | -27.40 | | | | | 3.40 | 69.39 |
| 10% | 24.71 | -21.94 | 1484.10 | 1482.58 | 1.06 | 1.16 | 3.57 | 72.86 |
| 20% | 24.49 | -24.99 | 1472.70 | 1469.22 | 1.82 | 2.05 | 4.08 | 83.27 |
| 30% | 24.24 | -29.46 | 1460.20 | 1454.42 | 2.65 | 3.04 | 4.85 | 98.98 |
| 40% | 23.96 | -33.51 | 1444.50 | 1437.45 | 3.70 | 4.17 | 5.81 | 118.57 |
| 50% | 23.64 | -34.72 | 1425.60 | 1418.51 | 4.96 | 5.43 | 6.91 | 141.02 |
| 60% | 23.22 | -37.47 | 1401.50 | 1394.06 | 6.57 | 7.06 | 8.20 | 167.35 |
| 70% | 22.64 | -40.08 | 1365.70 | 1358.54 | 8.95 | 9.43 | 9.74 | 198.78 |

**Table B.4.** 1,3 short directly

| Load Level | Rotor Frequency (Hz) (20-30) | Amplitude (dB) (20-30) | Measured Speed (rpm) (from drives panel) | Computed speed (rpm) (from rotor peak) | % Slip (from measured speed) | % Slip (from computed speed) | Current (A) (measured by device) | % Current /Nominal (4.9 A) |
|---|---|---|---|---|---|---|---|---|
| noload | 24.97 | -19.00 | 1494.40 | 1498.25 | 0.37 | 0.12 | 3.32 | 67.76 |
| 10% | 24.72 | -21.14 | 1484.90 | 1483.26 | 1.01 | 1.12 | 3.59 | 73.27 |
| 20% | 24.51 | -26.88 | 1474.30 | 1470.55 | 1.71 | 1.96 | 4.14 | 84.49 |
| 30% | 24.26 | -27.78 | 1461.50 | 1455.61 | 2.57 | 2.96 | 4.94 | 100.82 |
| 40% | 23.99 | -30.66 | 1446.70 | 1439.31 | 3.55 | 4.05 | 5.90 | 120.41 |
| 50% | 23.66 | -34.70 | 1428.30 | 1419.84 | 4.78 | 5.34 | 7.01 | 143.06 |
| 60% | 23.25 | -36.73 | 1403.80 | 1394.73 | 6.41 | 7.02 | 8.27 | 168.78 |
| 70% | 22.70 | -40.94 | 1370.70 | 1361.71 | 8.62 | 9.22 | 9.79 | 199.80 |

**Table B.5.** 1,3 short with resistance

| Load Level | Rotor Frequency (Hz) (20-30) | Amplitude (dB) (20-30) | Measured Speed (rpm) (from drives panel) | Computed speed (rpm) (from rotor peak) | % Slip (from measured speed) | % Slip (from computed speed) | Current (A) (measured by device) | % Current /Nominal (4.9 A) | Voltage (V) |
|---|---|---|---|---|---|---|---|---|---|
| Base-line | 24.97 | -25.35 | | | | | 3.35 | 68.37 | 3.9 |
| noload | 24.95 | -22.73 | 1495.10 | 1496.77 | 0.33 | 0.22 | 3.37 | 68.78 | 3.8 |
| 10% | 24.72 | -22.45 | 1485.70 | 1483.43 | 0.95 | 1.10 | 3.57 | 72.86 | 3.8 |
| 20% | 24.51 | -26.69 | 1474.70 | 1470.73 | 1.69 | 1.95 | 4.10 | 83.67 | 3.8 |
| 30% | 24.27 | -27.89 | 1461.70 | 1456.44 | 2.55 | 2.90 | 4.84 | 98.78 | 3.8 |
| 40% | 24.01 | -31.10 | 1447.50 | 1440.69 | 3.50 | 3.95 | 5.77 | 117.76 | 3.8 |
| 50% | 23.69 | -35.06 | 1430.50 | 1421.66 | 4.63 | 5.22 | 6.85 | 139.80 | 3.8 |
| 60% | 23.32 | -37.57 | 1408.70 | 1399.25 | 6.09 | 6.72 | 8.08 | 164.90 | 3.8 |
| 70% | 22.77 | -42.30 | 1375.30 | 1366.30 | 8.31 | 8.91 | 9.55 | 194.90 | 3.8 |

**Table B.6.** 2,3 short directly

| Load Level | Rotor Frequency (Hz) (20-30) | Amplitude (dB) (20-30) | Measured Speed (rpm) (from drives panel) | Computed speed (rpm) (from rotor peak) | % Slip (from measured speed) | % Slip (from computed speed) | Current (A) (measured by device) | % Current /Nominal (4.9 A) |
|---|---|---|---|---|---|---|---|---|
| noload | 24.92 | -26.05 | 1495.20 | 1495.09 | 0.32 | 0.33 | 3.55 | 72.45 |
| 10% | 24.72 | -40.26 | 1485.30 | 1483.20 | 0.98 | 1.12 | 3.86 | 78.78 |
| 20% | 24.51 | -32.21 | 1474.10 | 1470.86 | 1.73 | 1.94 | 4.38 | 89.39 |
| 30% | 24.27 | -31.95 | 1461.70 | 1456.33 | 2.55 | 2.91 | 5.18 | 105.71 |
| 40% | 24.00 | -33.89 | 1447.70 | 1439.87 | 3.49 | 4.01 | 6.40 | 130.61 |
| 50% | 23.68 | -34.14 | 1430.70 | 1420.99 | 4.62 | 5.27 | 7.25 | 147.96 |
| 60% | 23.30 | -37.88 | 1406.30 | 1397.74 | 6.25 | 6.82 | 8.48 | 173.06 |
| 70% | 22.77 | -41.03 | 1378.20 | 1366.31 | 8.12 | 8.91 | 9.95 | 203.06 |

**Table B.7.** 2,3 short with resistance

| Load Level | Rotor Frequency (Hz) (20-30) | Amplitude (dB) (20-30) | Measured Speed (rpm) (from drives panel) | Computed speed (rpm) (from rotor peak) | % Slip (from measured speed) | % Slip (from computed speed) | Current (A) (measured by device) | % Current /Nominal (4.9 A) | Voltage (V) |
|---|---|---|---|---|---|---|---|---|---|
| Base-line | 24.97 | -26.25 | | | | | 3.40 | 69.39 | 10.9 |
| noload | 24.94 | -24.77 | 1495.30 | 1496.27 | 0.31 | 0.25 | 3.40 | 69.39 | 10.5 |
| 10% | 24.72 | -23.52 | 1485.80 | 1483.43 | 0.95 | 1.10 | 3.62 | 73.88 | 10.5 |
| 20% | 24.52 | -25.88 | 1475.10 | 1471.09 | 1.66 | 1.93 | 4.13 | 84.29 | 10.5 |
| 30% | 24.28 | -26.42 | 1461.70 | 1457.00 | 2.55 | 2.87 | 4.88 | 99.59 | 10.5 |
| 40% | 24.02 | -29.87 | 1447.70 | 1441.21 | 3.49 | 3.92 | 5.79 | 118.16 | 10.5 |
| 50% | 23.72 | -32.95 | 1431.50 | 1423.07 | 4.57 | 5.13 | 6.86 | 140.00 | 10.5 |
| 60% | 23.35 | -36.52 | 1409.50 | 1400.70 | 6.03 | 6.62 | 8.08 | 164.90 | 10.5 |
| 70% | 22.85 | -38.46 | 1381.60 | 1370.97 | 7.89 | 8.60 | 9.47 | 193.27 | 10.5 |

**Table B.8.** 1,2,3 short directly

| Load Level | Rotor Frequency (Hz) (20-30) | Amplitude (dB) (20-30) | Measured Speed (rpm) (from drives panel) | Computed speed (rpm) (from rotor peak) | % Slip (from measured speed) | % Slip (from computed speed) | Current (A) (measured by device) | % Current /Nominal (4.9 A) |
|---|---|---|---|---|---|---|---|---|
| noload | 24.96 | -28.71 | 1495.30 | 1497.53 | 0.31 | 0.16 | 3.49 | 71.22 |
| 10% | 24.72 | -29.96 | 1485.70 | 1483.24 | 0.95 | 1.12 | 3.80 | 77.55 |
| 20% | 24.90 | -35.80 | 1474.90 | 1494.04 | 1.67 | 0.40 | 4.37 | 89.18 |
| 30% | 24.28 | -32.47 | 1462.30 | 1456.66 | 2.51 | 2.89 | 5.17 | 105.51 |
| 40% | 23.99 | -37.17 | 1447.60 | 1439.66 | 3.49 | 4.02 | 6.16 | 125.71 |
| 50% | 23.67 | -36.53 | 1428.20 | 1420.40 | 4.79 | 5.31 | 7.28 | 148.57 |
| 60% | 23.25 | -39.18 | 1403.70 | 1394.87 | 6.42 | 7.01 | 8.56 | 174.69 |
| 70% | 22.65 | -42.83 | 1368.10 | 1358.89 | 8.79 | 9.41 | 10.08 | 205.71 |

**Table B.9.** 1,2,3 short with resistance

| Load Level | Rotor Frequency (Hz) (20-30) | Amplitude (dB) (20-30) | Measured Speed (rpm) (from drives panel) | Computed speed (rpm) (from rotor peak) | % Slip (from measured speed) | % Slip (from computed speed) | Current (A) (measured by device) | % Current /Nominal (4.9 A) |
|---|---|---|---|---|---|---|---|---|
| Base-line | 24.97 | -18.39 | | | | | 3.40 | |
| noload | 24.93 | -19.75 | 1494.60 | 1495.52 | 0.36 | 0.30 | 3.38 | 68.98 |
| 10% | 24.73 | -33.08 | 1485.50 | 1483.75 | 0.97 | 1.08 | 3.61 | 73.67 |
| 20% | 24.53 | -26.41 | 1475.30 | 1471.69 | 1.65 | 1.89 | 4.12 | 84.08 |
| 30% | 24.29 | -27.20 | 1462.80 | 1457.46 | 2.48 | 2.84 | 4.86 | 99.18 |
| 40% | 24.03 | -29.99 | 1448.80 | 1441.90 | 3.41 | 3.87 | 5.80 | 118.37 |
| 50% | 23.72 | -32.76 | 1431.70 | 1423.49 | 4.55 | 5.10 | 6.88 | 140.41 |
| 60% | 23.34 | -35.73 | 1409.20 | 1400.21 | 6.05 | 6.65 | 8.11 | 165.51 |
| 70% | 22.80 | -39.35 | 1376.30 | 1368.10 | 8.25 | 8.79 | 9.55 | 194.90 |

**Table B.10.** B1-1,B2-1 short directly

| Load Level | Rotor Frequency (Hz) (20-30) | Amplitude (dB) (20-30) | Measured Speed (rpm) (from drives panel) | Computed speed (rpm) (from rotor peak) | % Slip (from measured speed) | % Slip (from computed speed) | Current (A) (measured by device) | % Current /Nominal (4.9 A) |
|---|---|---|---|---|---|---|---|---|
| noload | 24.93 | -28.23 | 1495.20 | 1496.07 | 0.32 | 0.26 | 3.61 | 73.67 |
| 10% | 24.73 | -29.88 | 1485.80 | 1483.61 | 0.95 | 1.09 | 3.90 | 79.59 |
| 20% | 24.52 | -33.50 | 1474.20 | 1470.92 | 1.72 | 1.94 | 4.46 | 91.02 |
| 30% | 24.28 | -31.69 | 1462.10 | 1456.51 | 2.53 | 2.90 | 5.26 | 107.35 |
| 40% | 24.01 | -39.02 | 1447.70 | 1440.57 | 3.49 | 3.96 | 6.20 | 126.53 |
| 50% | 23.69 | -35.21 | 1428.50 | 1421.11 | 4.77 | 5.26 | 7.27 | 148.37 |
| 60% | 23.28 | -38.53 | 1405.30 | 1396.75 | 6.31 | 6.88 | 8.51 | 173.67 |
| 70% | 22.76 | -41.43 | 1369.80 | 1365.72 | 8.68 | 8.95 | 9.98 | 203.67 |

**Table B.11.** B1-1,B2-1 short with resistance

| Load Level | Rotor Frequency (Hz) (20-30) | Amplitude (dB) (20-30) | Measured Speed (rpm) (from drives panel) | Computed speed (rpm) (from rotor peak) | % Slip (from measured speed) | % Slip (from computed speed) | Current (A) (measured by device) | % Current /Nominal (4.9 A) |
|---|---|---|---|---|---|---|---|---|
| Base-line | 24.97 | -18.72 | | | | | 3.34 | |
| noload | 24.94 | -18.49 | 1494.70 | 1496.59 | 0.35 | 0.23 | 3.35 | 68.37 |
| 10% | 24.73 | -20.96 | 1485.20 | 1483.84 | 0.99 | 1.08 | 3.61 | 73.67 |
| 20% | 24.53 | -27.14 | 1475.30 | 1471.66 | 1.65 | 1.89 | 4.17 | 85.10 |
| 30% | 24.30 | -27.55 | 1463.40 | 1457.97 | 2.44 | 2.80 | 4.94 | 100.82 |
| 40% | 24.04 | -30.66 | 1449.30 | 1442.16 | 3.38 | 3.86 | 5.89 | 120.20 |
| 50% | 23.73 | -33.85 | 1432.20 | 1423.95 | 4.52 | 5.07 | 6.97 | 142.24 |
| 60% | 23.35 | -37.62 | 1410.20 | 1400.95 | 5.99 | 6.60 | 8.22 | 167.76 |
| 70% | 22.77 | -40.63 | 1380.20 | 1366.25 | 7.99 | 8.92 | 9.68 | 197.55 |

**Table B.12.** B1-2,B2-1 short directly

| Load Level | Rotor Frequency (Hz) (20-30) | Amplitude (dB) (20-30) | Measured Speed (rpm) (from drives panel) | Computed speed (rpm) (from rotor peak) | % Slip (from measured speed) | % Slip (from computed speed) | Current (A) (measured by device) | % Current /Nominal (4.9 A) |
|---|---|---|---|---|---|---|---|---|
| noload | 24.95 | -27.37 | 1494.20 | 1497.10 | 0.39 | 0.19 | 3.68 | 75.10 |
| 10% | 24.73 | -29.26 | 1484.90 | 1483.71 | 1.01 | 1.09 | 3.99 | 81.43 |
| 20% | 25.49 | -35.31 | 1473.90 | 1529.47 | 1.74 | -1.96 | 4.60 | 93.88 |
| 30% | 25.01 | -43.18 | 1460.70 | 1500.44 | 2.62 | -0.03 | 5.41 | 110.41 |
| 40% | 23.98 | -38.63 | 1445.30 | 1438.86 | 3.65 | 4.08 | 6.38 | 130.20 |
| 50% | 23.64 | -40.82 | 1426.40 | 1418.26 | 4.91 | 5.45 | 7.50 | 153.06 |
| 60% | 23.21 | -41.02 | 1399.50 | 1392.50 | 6.70 | 7.17 | 8.81 | 179.80 |
| 70% | 22.52 | -43.91 | 1360.30 | 1350.97 | 9.31 | 9.94 | 10.40 | 212.24 |

**Table B.13.** B1-2,B2-1 short with resistance

| Load Level | Rotor Frequency (Hz) (20-30) | Amplitude (dB) (20-30) | Measured Speed (rpm) (from drives panel) | Computed speed (rpm) (from rotor peak) | % Slip (from measured speed) | % Slip (from computed speed) | Current (A) (measured by device) | % Current /Nominal (4.9 A) |
|---|---|---|---|---|---|---|---|---|
| Base-line | 24.97 | -18.46 | | | | | 3.34 | 68.16 |
| noload | 24.93 | -20.40 | 1495.50 | 1495.55 | 0.30 | 0.30 | 3.37 | 68.78 |
| 10% | 24.74 | -20.54 | 1486.70 | 1484.17 | 0.89 | 1.06 | 3.64 | 74.29 |
| 20% | 24.53 | -26.27 | 1476.20 | 1471.99 | 1.59 | 1.87 | 4.21 | 85.92 |
| 30% | 24.31 | -27.06 | 1464.50 | 1458.43 | 2.37 | 2.77 | 4.98 | 101.63 |
| 40% | 24.05 | -30.02 | 1451.50 | 1443.05 | 3.23 | 3.80 | 5.95 | 121.43 |
| 50% | 23.75 | -32.61 | 1434.10 | 1425.07 | 4.39 | 5.00 | 7.05 | 143.88 |
| 60% | 23.37 | -36.15 | 1411.80 | 1402.37 | 5.88 | 6.51 | 8.31 | 169.59 |
| 70% | 22.84 | -39.42 | 1379.30 | 1370.50 | 8.05 | 8.63 | 9.81 | 200.20 |

**Table B.14.** B1-3,B2-1 short directly

| Load Level | Rotor Frequency (Hz) (20-30) | Amplitude (dB) (20-30) | Measured Speed (rpm) (from drives panel) | Computed speed (rpm) (from rotor peak) | % Slip (from measured speed) | % Slip (from computed speed) | Current (A) (measured by device) | % Current /Nominal (4.9 A) |
|---|---|---|---|---|---|---|---|---|
| noload | 24.97 | -25.22 | 1495.10 | 1498.20 | 0.33 | 0.12 | 3.51 | 71.63 |
| 10% | 24.72 | -25.41 | 1485.50 | 1483.48 | 0.97 | 1.10 | 3.81 | 77.76 |
| 20% | 24.51 | -29.98 | 1475.10 | 1470.56 | 1.66 | 1.96 | 4.34 | 88.57 |
| 30% | 24.27 | -33.11 | 1461.20 | 1456.10 | 2.59 | 2.93 | 5.11 | 104.29 |
| 40% | 24.00 | -34.22 | 1446.70 | 1440.11 | 3.55 | 3.99 | 6.09 | 124.29 |
| 50% | 23.69 | -35.75 | 1429.50 | 1421.68 | 4.70 | 5.22 | 7.17 | 146.33 |
| 60% | 23.27 | -36.89 | 1405.70 | 1396.30 | 6.29 | 6.91 | 8.46 | 172.65 |
| 70% | 22.73 | -40.76 | 1370.70 | 1363.78 | 8.62 | 9.08 | 9.95 | 203.06 |

# Appendix C

# Test Results of Stator Short Faults after Misalignment Adjust

**Table C.1.** 1,2 short directly

| Load Level | Rotor Frequency (Hz) (20-30) | Amplitude (dB) (20-30) | Measured Speed (rpm) (from drives panel) | Computed speed (rpm) (from rotor peak) | % Slip (from measured speed) | % Slip (from computed speed) | Current (A) (measured by device) | % Current /Nominal (4.9 A) |
|---|---|---|---|---|---|---|---|---|
| noload | 24.97 | -25.52 | 1495.30 | 1498.23 | 0.31 | 0.12 | 3.31 | 67.55 |
| 10% | 24.73 | -23.36 | 1485.30 | 1483.51 | 0.98 | 1.10 | 3.63 | 74.08 |
| 20% | 24.51 | -28.77 | 1474.70 | 1470.80 | 1.69 | 1.95 | 4.20 | 85.71 |
| 30% | 24.27 | -31.13 | 1461.70 | 1456.22 | 2.55 | 2.92 | 5.01 | 102.24 |
| 40% | 24.00 | -30.68 | 1446.80 | 1440.14 | 3.55 | 3.99 | 5.99 | 122.24 |
| 50% | 23.67 | -33.45 | 1428.40 | 1420.27 | 4.77 | 5.32 | 7.11 | 145.10 |
| 60% | 23.26 | -35.06 | 1405.10 | 1395.58 | 6.33 | 6.96 | 8.38 | 171.02 |
| 70% | 22.73 | -37.77 | 1369.40 | 1363.61 | 8.71 | 9.09 | 9.91 | 202.24 |

**Table C.2.** 1,2 short with resistance

| Load Level | Rotor Frequency (Hz) (20-30) | Amplitude (dB) (20-30) | Measured Speed (rpm) (from drives panel) | Computed speed (rpm) (from rotor peak) | % Slip (from measured speed) | % Slip (from computed speed) | Current (A) (measured by device) | % Current /Nominal (4.9 A) |
|---|---|---|---|---|---|---|---|---|
| Base-line | 24.97 | -33.35 | | | | | 3.29 | |
| noload | 24.98 | -32.54 | 1495.30 | 1498.56 | 0.31 | 0.10 | 3.29 | 67.14 |
| 10% | 24.73 | -23.21 | 1486.20 | 1483.97 | 0.92 | 1.07 | 3.52 | 71.84 |
| 20% | 24.53 | -25.21 | 1475.70 | 1471.91 | 1.62 | 1.87 | 4.06 | 82.86 |
| 30% | 24.30 | -26.37 | 1463.70 | 1458.05 | 2.42 | 2.80 | 4.83 | 98.57 |
| 40% | 24.04 | -29.33 | 1449.70 | 1442.69 | 3.35 | 3.82 | 5.80 | 118.37 |
| 50% | 23.74 | -31.69 | 1432.50 | 1424.36 | 4.50 | 5.04 | 6.88 | 140.41 |
| 60% | 23.36 | -35.16 | 1410.90 | 1401.45 | 5.94 | 6.57 | 8.15 | 166.33 |
| 70% | 22.83 | -36.51 | 1377.80 | 1370.01 | 8.15 | 8.67 | 9.65 | 196.94 |

**Table C.3.** 1,3 short directly

| Load Level | Rotor Frequency (Hz) (20-30) | Amplitude (dB) (20-30) | Measured Speed (rpm) (from drives panel) | Computed speed (rpm) (from rotor peak) | % Slip (from measured speed) | % Slip (from computed speed) | Current (A) (measured by device) | % Current /Nominal (4.9 A) |
|---|---|---|---|---|---|---|---|---|
| noload | 24.97 | -29.54 | 1495.50 | 1498.10 | 0.30 | 0.13 | 3.26 | 66.53 |
| 10% | 24.73 | -24.14 | 1486.10 | 1483.83 | 0.93 | 1.08 | 3.55 | 72.45 |
| 20% | 24.52 | -26.57 | 1475.50 | 1471.38 | 1.63 | 1.91 | 4.11 | 83.88 |
| 30% | 24.29 | -27.84 | 1463.30 | 1457.28 | 2.45 | 2.85 | 4.92 | 100.41 |
| 40% | 24.03 | -30.20 | 1449.30 | 1441.51 | 3.38 | 3.90 | 5.87 | 119.80 |
| 50% | 23.71 | -32.75 | 1430.60 | 1422.46 | 4.63 | 5.17 | 7.01 | 143.06 |
| 60% | 23.32 | -35.18 | 1407.80 | 1399.09 | 6.15 | 6.73 | 8.29 | 169.18 |
| 70% | 22.76 | -38.13 | 1372.60 | 1365.70 | 8.49 | 8.95 | 9.83 | 200.61 |

**Table C.4.** 1,3 short with resistance

| Load Level | Rotor Frequency (Hz) (20-30) | Amplitude (dB) (20-30) | Measured Speed (rpm) (from drives panel) | Computed speed (rpm) (from rotor peak) | % Slip (from measured speed) | % Slip (from computed speed) | Current (A) (measured by device) | % Current /Nominal (4.9 A) |
|---|---|---|---|---|---|---|---|---|
| Base-line | 24.97 | -27.33 | | | | | 3.41 | |
| noload | 24.97 | -27.22 | 1495.60 | 1498.28 | 0.29 | 0.11 | 3.42 | 69.80 |
| 10% | 24.72 | -25.00 | 1485.90 | 1483.46 | 0.94 | 1.10 | 3.53 | 72.04 |
| 20% | 24.51 | -25.86 | 1474.80 | 1470.76 | 1.68 | 1.95 | 4.03 | 82.24 |
| 30% | 24.27 | -27.83 | 1462.50 | 1456.15 | 2.50 | 2.92 | 4.79 | 97.76 |
| 40% | 24.00 | -30.87 | 1447.60 | 1440.10 | 3.49 | 3.99 | 5.76 | 117.55 |
| 50% | 23.68 | -33.19 | 1429.30 | 1420.87 | 4.71 | 5.28 | 6.88 | 140.41 |
| 60% | 23.29 | -35.26 | 1406.40 | 1397.15 | 6.24 | 6.86 | 8.14 | 166.12 |
| 70% | 22.72 | -38.04 | 1371.20 | 1362.95 | 8.59 | 9.14 | 9.65 | 196.94 |

**Table C.5.** 2,3 short directly

| Load Level | Rotor Frequency (Hz) (20-30) | Amplitude (dB) (20-30) | Measured Speed (rpm) (from drives panel) | Computed speed (rpm) (from rotor peak) | % Slip (from measured speed) | % Slip (from computed speed) | Current (A) (measured by device) | % Current /Nominal (4.9 A) |
|---|---|---|---|---|---|---|---|---|
| noload | 24.96 | -29.83 | 1494.80 | 1497.74 | 0.35 | 0.15 | 3.43 | 70.00 |
| 10% | 24.72 | -32.58 | 1485.30 | 1482.99 | 0.98 | 1.13 | 3.74 | 76.33 |
| 20% | 25.50 | -34.54 | 1473.70 | 1529.91 | 1.75 | -1.99 | 4.34 | 88.57 |
| 30% | 24.26 | -33.89 | 1461.70 | 1455.52 | 2.55 | 2.97 | 5.14 | 104.90 |
| 40% | 23.98 | -34.00 | 1445.90 | 1438.75 | 3.61 | 4.08 | 6.11 | 124.69 |
| 50% | 23.66 | -36.37 | 1426.80 | 1419.37 | 4.88 | 5.38 | 7.24 | 147.76 |
| 60% | 23.25 | -35.70 | 1403.90 | 1394.85 | 6.41 | 7.01 | 8.51 | 173.67 |
| 70% | 22.71 | -37.42 | 1370.40 | 1362.38 | 8.64 | 9.17 | 10.04 | 204.90 |

**Table C.6.** 2,3 short with resistance

| Load Level | Rotor Frequency (Hz) (20-30) | Amplitude (dB) (20-30) | Measured Speed (rpm) (from drives panel) | Computed speed (rpm) (from rotor peak) | % Slip (from measured speed) | % Slip (from computed speed) | Current (A) (measured by device) | % Current /Nominal (4.9 A) |
|---|---|---|---|---|---|---|---|---|
| Base-line | 24.97 | -26.75 | | | | | 3.23 | |
| noload | 24.97 | -26.60 | 1495.60 | 1498.28 | 0.29 | 0.11 | 3.23 | 65.92 |
| 10% | 24.72 | -24.47 | 1485.30 | 1483.04 | 0.98 | 1.13 | 3.48 | 71.02 |
| 20% | 24.50 | -25.65 | 1474.70 | 1470.19 | 1.69 | 1.99 | 4.04 | 82.45 |
| 30% | 24.26 | -28.10 | 1462.20 | 1455.66 | 2.52 | 2.96 | 4.81 | 98.16 |
| 40% | 23.99 | -30.53 | 1447.30 | 1439.66 | 3.51 | 4.02 | 5.78 | 117.96 |
| 50% | 23.67 | -34.05 | 1429.40 | 1420.04 | 4.71 | 5.33 | 6.88 | 140.41 |
| 60% | 23.28 | -35.68 | 1405.20 | 1396.64 | 6.32 | 6.89 | 8.16 | 166.53 |
| 70% | 22.75 | -37.96 | 1372.40 | 1364.96 | 8.51 | 9.00 | 9.63 | 196.53 |

**Table C.7.** B1-1,B2-1 short directly

| Load Level | Rotor Frequency (Hz) (20-30) | Amplitude (dB) (20-30) | Measured Speed (rpm) (from drives panel) | Computed speed (rpm) (from rotor peak) | % Slip (from measured speed) | % Slip (from computed speed) | Current (A) (measured by device) | % Current /Nominal (4.9 A) |
|---|---|---|---|---|---|---|---|---|
| noload | 24.94 | -37.06 | 1494.80 | 1496.43 | 0.35 | 0.24 | 3.57 | 72.86 |
| 10% | 24.71 | -32.60 | 1484.70 | 1482.59 | 1.02 | 1.16 | 3.87 | 78.98 |
| 20% | 24.49 | -33.90 | 1473.20 | 1469.32 | 1.79 | 2.05 | 4.42 | 90.20 |
| 30% | 24.24 | -32.63 | 1460.70 | 1454.39 | 2.62 | 3.04 | 5.19 | 105.92 |
| 40% | 23.97 | -34.38 | 1444.80 | 1437.94 | 3.68 | 4.14 | 6.14 | 125.31 |
| 50% | 23.63 | -35.99 | 1426.10 | 1418.00 | 4.93 | 5.47 | 7.23 | 147.55 |
| 60% | 23.22 | -36.82 | 1402.40 | 1393.39 | 6.51 | 7.11 | 8.48 | 173.06 |
| 70% | 22.68 | -38.59 | 1368.50 | 1360.66 | 8.77 | 9.29 | 9.95 | 203.06 |

**Table C.8.** B1-1,B2-1 short with resistance

| Load Level | Rotor Frequency (Hz) (20-30) | Amplitude (dB) (20-30) | Measured Speed (rpm) (from drives panel) | Computed speed (rpm) (from rotor peak) | % Slip (from measured speed) | % Slip (from computed speed) | Current (A) (measured by device) | % Current /Nominal (4.9 A) |
|---|---|---|---|---|---|---|---|---|
| Base-line | 24.97 | -27.81 | | | | | 3.30 | |
| noload | 24.97 | -27.36 | 1494.50 | 1498.24 | 0.37 | 0.12 | 3.32 | 67.76 |
| 10% | 24.72 | -24.15 | 1484.70 | 1483.48 | 1.02 | 1.10 | 3.57 | 72.86 |
| 20% | 24.51 | -26.16 | 1479.60 | 1470.80 | 1.36 | 1.95 | 4.12 | 84.08 |
| 30% | 24.27 | -28.24 | 1462.30 | 1456.30 | 2.51 | 2.91 | 4.89 | 99.80 |
| 40% | 24.01 | -30.33 | 1447.50 | 1440.47 | 3.50 | 3.97 | 5.85 | 119.39 |
| 50% | 23.69 | -32.93 | 1430.40 | 1421.60 | 4.64 | 5.23 | 6.95 | 141.84 |
| 60% | 23.31 | -35.04 | 1406.30 | 1398.73 | 6.25 | 6.75 | 8.21 | 167.55 |
| 70% | 22.80 | -38.19 | 1376.50 | 1368.11 | 8.23 | 8.79 | 9.66 | 197.14 |

**Table C.9.** B1-2,B2-1 short directly

| Load Level | Rotor Frequency (Hz) (20-30) | Amplitude (dB) (20-30) | Measured Speed (rpm) (from drives panel) | Computed speed (rpm) (from rotor peak) | % Slip (from measured speed) | % Slip (from computed speed) | Current (A) (measured by device) | % Current /Nominal (4.9 A) |
|---|---|---|---|---|---|---|---|---|
| noload | 24.99 | -35.12 | 1494.70 | 1499.14 | 0.35 | 0.06 | 3.66 | 74.69 |
| 10% | 24.94 | -33.63 | 1485.10 | 1496.57 | 0.99 | 0.23 | 4.01 | 81.84 |
| 20% | 25.51 | -34.77 | 1472.80 | 1530.43 | 1.81 | -2.03 | 4.60 | 93.88 |
| 30% | 25.75 | -37.34 | 1460.20 | 1545.10 | 2.65 | -3.01 | 5.36 | 109.39 |
| 40% | 23.96 | -37.95 | 1443.80 | 1437.34 | 3.75 | 4.18 | 6.32 | 128.98 |
| 50% | 23.62 | -36.21 | 1424.60 | 1417.07 | 5.03 | 5.53 | 7.42 | 151.43 |
| 60% | 23.19 | -38.68 | 1399.60 | 1391.45 | 6.69 | 7.24 | 8.71 | 177.76 |
| 70% | 22.62 | -38.78 | 1364.20 | 1357.06 | 9.05 | 9.53 | 10.22 | 208.57 |

**Table C.10.** B1-2,B2-1 short with resistance

| Load Level | Rotor Frequency (Hz) (20-30) | Amplitude (dB) (20-30) | Measured Speed (rpm) (from drives panel) | Computed speed (rpm) (from rotor peak) | % Slip (from measured speed) | % Slip (from computed speed) | Current (A) (measured by device) | % Current /Nominal (4.9 A) |
|---|---|---|---|---|---|---|---|---|
| Base-line | 24.97 | -27.32 | | | | | 3.33 | |
| noload | 24.97 | -26.85 | 1495.10 | 1498.27 | 0.33 | 0.12 | 3.38 | 68.98 |
| 10% | 24.72 | -24.42 | 1484.30 | 1483.24 | 1.05 | 1.12 | 3.65 | 74.49 |
| 20% | 24.51 | -26.13 | 1473.40 | 1470.52 | 1.77 | 1.97 | 4.19 | 85.51 |
| 30% | 24.27 | -28.18 | 1461.30 | 1455.95 | 2.58 | 2.94 | 4.95 | 101.02 |
| 40% | 24.00 | -30.23 | 1446.40 | 1439.83 | 3.57 | 4.01 | 5.90 | 120.41 |
| 50% | 23.68 | -33.22 | 1429.20 | 1420.78 | 4.72 | 5.28 | 6.98 | 142.45 |
| 60% | 23.30 | -34.89 | 1406.80 | 1398.28 | 6.21 | 6.78 | 8.24 | 168.16 |
| 70% | 22.79 | -38.04 | 1375.20 | 1367.53 | 8.32 | 8.83 | 9.71 | 198.16 |

**Table C.11.** 1,2,3 short directly

| Load Level | Rotor Frequency (Hz) (20-30) | Amplitude (dB) (20-30) | Measured Speed (rpm) (from drives panel) | Computed speed (rpm) (from rotor peak) | % Slip (from measured speed) | % Slip (from computed speed) | Current (A) (measured by device) | % Current /Nominal (4.9 A) |
|---|---|---|---|---|---|---|---|---|
| noload | 24.95 | -34.92 | 1495.20 | 1497.11 | 0.32 | 0.19 | 3.43 | 70.00 |
| 10% | 24.73 | -36.99 | 1486.30 | 1483.76 | 0.91 | 1.08 | 3.76 | 76.73 |
| 20% | 24.83 | -34.11 | 1475.30 | 1490.08 | 1.65 | 0.66 | 4.36 | 88.98 |
| 30% | 24.29 | -31.93 | 1463.40 | 1457.36 | 2.44 | 2.84 | 5.19 | 105.92 |
| 40% | 24.02 | -33.14 | 1449.20 | 1441.44 | 3.39 | 3.90 | 6.12 | 124.90 |
| 50% | 23.70 | -32.77 | 1430.70 | 1422.04 | 4.62 | 5.20 | 7.24 | 147.76 |
| 60% | 23.29 | -34.76 | 1406.40 | 1397.52 | 6.24 | 6.83 | 8.52 | 173.88 |
| 70% | 22.76 | -37.98 | 1373.50 | 1365.53 | 8.43 | 8.96 | 10.04 | 204.90 |

**Table C.12.** 1,2,3 short with resistance

| Load Level | Rotor Frequency (Hz) (20-30) | Amplitude (dB) (20-30) | Measured Speed (rpm) (from drives panel) | Computed speed (rpm) (from rotor peak) | % Slip (from measured speed) | % Slip (from computed speed) | Current (A) (measured by device) | % Current /Nominal (4.9 A) |
|---|---|---|---|---|---|---|---|---|
| Base-line | 24.97 | -29.61 | | | | | 3.26 | |
| noload | 24.97 | -29.01 | 1494.70 | 1498.33 | 0.35 | 0.11 | 3.27 | 66.73 |
| 10% | 24.73 | -23.28 | 1485.70 | 1483.90 | 0.95 | 1.07 | 3.51 | 71.63 |
| 20% | 24.52 | -25.56 | 1475.10 | 1471.49 | 1.66 | 1.90 | 4.03 | 82.24 |
| 30% | 24.29 | -26.46 | 1463.50 | 1457.54 | 2.43 | 2.83 | 4.82 | 98.37 |
| 40% | 24.02 | -30.29 | 1448.70 | 1441.21 | 3.42 | 3.92 | 5.78 | 117.96 |
| 50% | 23.71 | -32.07 | 1430.40 | 1422.60 | 4.64 | 5.16 | 6.88 | 140.41 |
| 60% | 23.31 | -35.23 | 1408.30 | 1398.81 | 6.11 | 6.75 | 8.16 | 166.53 |
| 70% | 22.79 | -37.71 | 1376.10 | 1367.59 | 8.26 | 8.83 | 9.69 | 197.76 |

**Table C.13.** On line test with coupling gap

| Load Level | Rotor Frequency (Hz) (20-30) | Amplitude (dB) (20-30) | Measured Speed (rpm) (from drives panel) | Computed speed (rpm) (from rotor peak) | % Slip (from measured speed) | % Slip (from computed speed) | Current (A) (measured by device) | % Current /Nominal (4.9 A) |
|---|---|---|---|---|---|---|---|---|
| noload | 24.97 | -26.04 | 1494.90 | 1497.91 | 0.34 | 0.14 | 3.21 | 65.51 |
| 10% | 24.73 | -23.75 | 1485.20 | 1483.64 | 0.99 | 1.09 | 3.47 | 70.82 |
| 20% | 24.52 | -22.30 | 1474.90 | 1471.48 | 1.67 | 1.90 | 4.04 | 82.45 |
| 30% | 24.29 | -25.70 | 1463.10 | 1457.42 | 2.46 | 2.84 | 4.82 | 98.37 |
| 40% | 24.04 | -29.18 | 1449.20 | 1442.10 | 3.39 | 3.86 | 5.80 | 118.37 |
| 50% | 23.73 | -31.92 | 1432.40 | 1423.77 | 4.51 | 5.08 | 6.91 | 141.02 |
| 60% | 23.36 | -35.33 | 1410.30 | 1401.31 | 5.98 | 6.58 | 8.18 | 166.94 |
| 70% | 22.86 | -39.20 | 1380.50 | 1371.59 | 7.97 | 8.56 | 9.65 | 196.94 |

**Table C.14.** On line test without coupling gap

| Load Level | Rotor Frequency (Hz) (20-30) | Amplitude (dB) (20-30) | Measured Speed (rpm) (from drives panel) | Computed speed (rpm) (from rotor peak) | % Slip (from measured speed) | % Slip (from computed speed) | Current (A) (measured by device) | % Current /Nominal (4.9 A) |
|---|---|---|---|---|---|---|---|---|
| noload | 24.96 | -25.69 | 1494.30 | 1497.53 | 0.38 | 0.16 | 3.22 | 65.71 |
| 10% | 24.73 | -28.46 | 1485.60 | 1483.92 | 0.96 | 1.07 | 3.48 | 71.02 |
| 20% | 24.53 | -26.72 | 1475.70 | 1471.69 | 1.62 | 1.89 | 4.04 | 82.45 |
| 30% | 24.30 | -26.54 | 1464.10 | 1457.91 | 2.39 | 2.81 | 4.82 | 98.37 |
| 40% | 24.04 | -29.69 | 1449.70 | 1442.34 | 3.35 | 3.84 | 5.77 | 117.76 |
| 50% | 23.73 | -32.45 | 1432.20 | 1424.01 | 4.52 | 5.07 | 6.89 | 140.61 |
| 60% | 23.35 | -35.95 | 1410.50 | 1401.08 | 5.97 | 6.59 | 8.13 | 165.92 |
| 70% | 22.83 | -37.43 | 1377.50 | 1369.94 | 8.17 | 8.67 | 9.63 | 196.53 |

# Appendix D

# Induction motor parameters

## D.1 Data of the Motor Type SZJKe 14a

The following tables show the parameters of SZJKe 14a.

**Table D.1.** Ratings of motor SZJKe 14a

| Parameter | Value |
|---|---|
| Active power PN [kW] | 0.8 |
| Nominal voltage UN [V] | 380 |
| Nominal current [A] | 2.2 |
| Nominal power factor cosN [-] | 0.74 |
| Rotor speed [rpm] | 1400 |
| No load speed [rpm] | 1497 |
| Winding connection | Y |
| Number of poles per phase winding p[-] | 2 |
| Nominal frequency [Hz] | 50 |
| Number of rotor bars [-] | 22 |
| Number of stator slots [-] | 24 |
| Rotor inertia $[kg * m^2]$ | 0.0025 |
| Coil number per phase | 4 |
| Turn number of coil | 90 |

**Table D.2.** Equivalent circuit parameters

| Parameter | Value |
|---|---|
| Stator winding resistance Rs [Ohms] | 8.4 |
| Referred rotor winding resistance Rr[Ohm] | 8.2 |
| Stator winding reactance Xs [Ohms] | 10.3 |
| Referred rotor winding reactance Xr [Ohms] | 10.3 |
| Magnetizing reactance [Ohms] | 137.5 |
| Core loss component RFe [Ohms] | 2938 |

**Table D.3.** Data of bearing SKF type 6304 ZZ CXSQ

| Parameter | Value |
|---|---|
| Numbers of balls Nb [-] | 7 |
| Ball diameter Bd [mm] | 6 |
| Bearing pitch diameter Pd [mm] | 32 |
| Ball contact angle a [rad] | 0 |

## D.2 Data of the Motor Type Sg112M-4

The following tables show the parameters of Sg112M-4.

**Table D.4.** Ratings of motor Sg112M-4

| Parameter | Value |
|---|---|
| Active power PN [kW] | 1.33 |
| Nominal voltage UN [V] | 380 |
| Nominal current [A] | 2.867 |
| Nominal power factor cosN [-] | 0.84 |
| Rotor speed [rpm] | 1445 |
| No load speed [rpm] | 1492 |
| Winding connection | Y |
| Number of poles per phase winding p[-] | 2 |
| Nominal frequency [Hz] | 50 |
| Number of rotor bars [-] | 28 |
| Number of stator slots [-] | 24 |
| Rotor inertia $[kg * m^2]$ | 0.0197 |

**Table D.5.** Data of bearing 6306-2Z

| Parameter | Value |
|---|---|
| Numbers of balls Nb [-] | 8 |
| Ball diameter Bd [mm] | 12 |
| Bearing pitch diameter Pd [mm] | 52 |
| Ball contact angle a [rad] | 0 |

**Table D.6.** Equivalent circuit parameters

| Parameter | Value |
|---|---|
| Stator winding resistance Rs [Ohms] | 5.6 |
| Referred rotor winding resistance Rr[Ohm] | 2.24 |
| Stator winding reactance Xs [Ohms] | 6.45 |
| Referred rotor winding reactance Xr [Ohms] | 6.45 |
| Magnetizing reactance [Ohms] | 238 |
| Core loss component RFe [Ohms] | 2252 |

# Appendix E

# Test Results of Induction Motor Broken Rotor Bar Fault

Experiment Data Provided by the Cracow University of Technology

**Table E.1.** Symmetrical Motor I

| Measure-ment file name | Slip | Loading (%) | 2sf | Peak value (Hz) (Current) | Peak value (dB) (Current) | Peak value (Hz) Device | Peak value (dB) Device | Differ-ence with 50 Hz (dB) | Average rotor speed (rpm) | Load current (A) |
|---|---|---|---|---|---|---|---|---|---|---|
| S1_001.dat | 0.01 | 66.82 | 0.93 | 9.38 | -69.43 | 9.38 | -66.79 | | 1486.00 | 1.47 |
| S1_002.dat | 0.03 | 81.36 | 3.33 | 3.22 | -67.75 | 3.22 | -62.57 | 34.62 | 1450.00 | 1.79 |
| S1_003.dat | 0.04 | 90.91 | 4.33 | 4.39 | -66.55 | 4.25 | -58.82 | 37.45 | 1435.00 | 2.00 |
| S1_004.dat | 0.05 | 101.36 | 5.40 | 5.57 | -62.69 | 5.42 | -54.00 | 44.13 | 1419.00 | 2.23 |
| S1_005.dat | 0.07 | 112.73 | 6.60 | 6.45 | -60.42 | 6.59 | -51.69 | 48.77 | 1401.00 | 2.48 |

**Table E.2.** 1 broken rotor bar in Motor I

| Measure-ment file name | Slip | Loading (%) | 2sf | Peak value (Hz) (Current) | Peak value (dB) (Current) | Peak value (Hz) Device | Peak value (dB) Device | Differ-ence with 50 Hz (dB) | Average rotor speed (rpm) | Load current (A) |
|---|---|---|---|---|---|---|---|---|---|---|
| S1_006.dat | 0.01 | 68.64 | 0.93 | 9.38 | -76.70 | 9.96 | -49.44 | | 1486.00 | 1.51 |
| S1_007.dat | 0.03 | 82.27 | 3.27 | 3.22 | -56.42 | 6.45 | -49.91 | 37.05 | 1451.00 | 1.81 |
| S1_008.dat | 0.05 | 95.45 | 4.80 | 4.69 | -49.87 | 4.69 | -44.48 | 29.81 | 1428.00 | 2.10 |
| S1_009.dat | 0.06 | 105.00 | 5.80 | 5.86 | -47.61 | 5.86 | -40.69 | 35.54 | 1413.00 | 2.31 |
| S1_010.dat | 0.07 | 115.91 | 7.07 | 7.03 | -39.32 | 6.88 | -40.78 | 32.46 | 1394.00 | 2.55 |

**Table E.3.** 2 broken rotor bars in Motor I

| Measure-ment file name | Slip | Loading (%) | 2sf | Peak value (Hz) (Current) | Peak value (dB) (Current) | Peak value (Hz) Device | Peak value (dB) Device | Differ-ence with 50 Hz (dB) | Average rotor speed (rpm) | Load current (A) |
|---|---|---|---|---|---|---|---|---|---|---|
| S1_011.dat | 0.01 | 69.55 | 1.07 | 9.38 | -62.40 | 10.69 | -58.95 | | 1484.00 | 1.53 |
| S1_012.dat | 0.03 | 85.00 | 3.47 | 3.52 | -53.23 | 3.37 | -44.44 | 28.59 | 1448.00 | 1.87 |
| S1_013.dat | 0.05 | 95.00 | 4.60 | 4.39 | -48.69 | 4.54 | -38.40 | 29.17 | 1431.00 | 2.09 |
| S1_014.dat | 0.06 | 105.00 | 5.67 | 5.57 | -40.94 | 5.57 | -36.43 | 28.80 | 1415.00 | 2.31 |
| S1_015.dat | 0.07 | 115.91 | 6.80 | 6.74 | -38.01 | 6.74 | -33.24 | 36.07 | 1398.00 | 2.55 |

**Table E.4.** 3 broken rotor bars in Motor I

| Measure-ment file name | Slip | Loading (%) | 2sf | Peak value (Hz) (Current) | Peak value (dB) (Current) | Peak value (Hz) Device | Peak value (dB) Device | Differ-ence with 50 Hz (dB) | Average rotor speed (rpm) | Load current (A) |
|---|---|---|---|---|---|---|---|---|---|---|
| S1_016.dat | 0.02 | 68.64 | 1.53 | 0.29 | -71.68 | 10.55 | -58.01 | | 1477.00 | 1.51 |
| S1_017.dat | 0.04 | 82.27 | 3.60 | 3.52 | -54.53 | 3.52 | -50.33 | 35.53 | 1446.00 | 1.81 |
| S1_018.dat | 0.05 | 95.00 | 5.07 | 4.98 | -44.55 | 4.98 | -41.96 | 37.71 | 1424.00 | 2.09 |
| S1_019.dat | 0.06 | 103.18 | 6.00 | 5.86 | -46.70 | 6.01 | -40.87 | 40.91 | 1410.00 | 2.27 |
| S1_020.dat | 0.07 | 114.09 | 7.27 | 7.32 | -45.50 | 7.18 | -36.70 | 36.28 | 1391.00 | 2.51 |

**Table E.5.** Symmetrical Motor II

| Measure-ment file name | Slip | Loading (%) | 2sf | Peak value (Hz) (Current) | Peak value (dB) (Current) | Peak value (Hz) Device | Peak value (dB) Device | Differ-ence with 50 Hz (dB) | Average rotor speed (rpm) | Load current (A) |
|---|---|---|---|---|---|---|---|---|---|---|
| S1_001.dat | 0.01 | 51.36 | 0.50 | 0.29 | -75.10 | 4.25 | -22.47 | | 1492.44 | 1.13 |
| S1_002.dat | 0.02 | 92.27 | 2.15 | 8.79 | -72.31 | 10.69 | -49.49 | | 1467.69 | 2.03 |
| S1_003.dat | 0.04 | 145.45 | 4.04 | 8.20 | -63.68 | 8.06 | -56.61 | | 1439.34 | 3.20 |
| S1_004.dat | 0.05 | 184.55 | 5.49 | 5.57 | -65.71 | 10.84 | -57.97 | 40.77 | 1417.59 | 4.06 |
| S1_005.dat | 0.08 | 240.91 | 7.79 | 7.91 | -62.68 | 7.76 | -58.88 | 45.20 | 1383.14 | 5.30 |

**Table E.6.** 1 broken rotor bar in Motor II

| Measure-ment file name | Slip | Loading (%) | 2sf | Peak value (Hz) (Current) | Peak value (dB) (Current) | Peak value (Hz) Device | Peak value (dB) Device | Differ-ence with 50 Hz (dB) | Average rotor speed (rpm) | Load current (A) |
|---|---|---|---|---|---|---|---|---|---|---|
| S2_006.dat | 0.00 | 38.72 | 0.48 | 8.50 | -71.70 | 9.96 | -58.38 | | 1492.74 | 1.11 |
| S2_007.dat | 0.02 | 71.85 | 2.31 | 2.34 | -55.52 | 2.34 | -49.28 | | 1465.34 | 2.06 |
| S2_008.dat | 0.04 | 110.57 | 4.04 | 4.10 | -50.03 | 4.10 | -44.15 | 34.05 | 1439.34 | 3.17 |
| S2_009.dat | 0.06 | 142.31 | 5.64 | 5.57 | -48.04 | 5.57 | -44.44 | 35.00 | 1415.44 | 4.08 |
| S2_010.dat | 0.08 | 184.86 | 8.04 | 7.91 | -47.13 | 8.06 | -37.02 | 31.41 | 1379.34 | 5.30 |

**Table E.7.** 2 broken rotor bars in Motor II

| Measure-ment file name | Slip | Loading (%) | 2sf | Peak value (Hz) (Current) | Peak value (dB) (Current) | Peak value (Hz) Device | Peak value (dB) Device | Differ-ence with 50 Hz (dB) | Average rotor speed (rpm) | Load current (A) |
|---|---|---|---|---|---|---|---|---|---|---|
| S2_011.dat | 0.00 | 39.07 | 0.39 | 8.50 | -68.43 | 7.76 | -60.42 | | 1494.14 | 1.12 |
| S2_012.dat | 0.02 | 70.46 | 2.15 | 2.05 | -58.49 | 2.20 | -54.47 | | 1467.74 | 2.02 |
| S2_013.dat | 0.04 | 109.52 | 4.01 | 3.81 | -54.37 | 3.96 | -45.30 | 29.17 | 1439.89 | 3.14 |
| S2_014.dat | 0.06 | 147.19 | 5.80 | 5.86 | -48.54 | 6.01 | -22.44 | 34.66 | 1412.99 | 4.22 |
| S2_015.dat | 0.08 | 184.51 | 7.82 | 7.91 | -45.82 | 7.76 | -39.58 | 28.77 | 1382.64 | 5.29 |

**Table E.8.** 3 broken rotor bars in Motor II

| Measure-ment file name | Slip | Loading (%) | 2sf | Peak value (Hz) (Current) | Peak value (dB) (Current) | Peak value (Hz) Device | Peak value (dB) Device | Differ-ence with 50 Hz (dB) | Average rotor speed (rpm) | Load current (A) |
|---|---|---|---|---|---|---|---|---|---|---|
| S2_016.dat | 0.01 | 38.72 | 0.51 | 9.67 | -69.75 | 6.88 | -66.81 | | 1492.39 | 1.11 |
| S2_017.dat | 0.02 | 69.76 | 2.25 | 2.34 | -54.94 | 2.20 | -48.94 | | 1466.29 | 2.00 |
| S2_018.dat | 0.04 | 109.52 | 4.03 | 4.10 | -46.87 | 4.10 | -42.10 | 29.75 | 1439.54 | 3.14 |
| S2_019.dat | 0.06 | 148.59 | 5.93 | 5.86 | -44.13 | 6.01 | -40.53 | 33.59 | 1410.99 | 4.26 |
| S2_020.dat | 0.07 | 178.93 | 7.42 | 7.32 | -44.84 | 7.47 | -34.72 | 26.82 | 1388.74 | 5.13 |